ADAPTOR PROTEIN COMPLEX 5-RELATED HEREDITARY SPASTIC PARAPLEGIAS

Dissertation

in partial fulfillment of the requirements for the degree of

doctor rerum naturalium (Dr. rer. nat)

submitted to the Faculty Council of the School of Medicine

at Friedrich-Schiller-University of Jena

by M.Sc. Molecular Medicine Federico Ribaudo

born on 11.02.1992 in Monza, Italy

Table of contents

1. List of abbreviations

AIM	ATG8-interacting motif
ALR	Autophagic lysosome reformation
ALS	Amyotrophic lateral sclerosis
AP	Adaptor protein complex
ATG	Autophagy related gene
BECN1	Beclin1
BFP	Blue fluorescent protein
CNS	Central nervous system
dKO	Double Knockout
Dyn2	Dynamin2
EBSS	Earle's balanced salt solution
ER	Endoplasmic reticulum
ERES	ER exit sites
FBA	Foot based angle
FIP200	FAK family kinase-interacting protein of 200kD
GFP	Green fluorescent protein
HSP	Hereditary spastic paraplegia
IM	Isolation membrane
KD	Knockdown
KI	Knockin
KO	Knockout
LAMP1	Lysosome-associated membrane glycoprotein 1
LC3	Microtubule-associated protein 1A/1B-light chain 3
LIR	LC3-interacting region
M6PR	Mannose 6-Phosphate Receptor
MEFs	Mouse embryonic fibroblasts

mTOR	Inhibitory mechanistic Target of Rapamycin
PdtIns	Phosphatidylinositol
PdtIns(3)P / PI3P	Phosphatidylinositol-3 phosphate
PdtIns(4)P / PI4P	Phosphatidylinositol-4 phosphate
PdtIns(4,5)P$_2$ / PI(4,5)P2	Phosphatidylinositol-4,5 biphosphate
PE	Phosphatidylethanolamine
PI4K	Phosphatidylinositol-4 phosphate kinase
PI4K2A	Phosphatidylinositol 4-kinase type 2 alpha
PIs	Phosphoinositides
PM	Plasma membrane
p-S6K	Phosphorylated p70S6 Kinase
PtdIns(3,5)P$_2$ / PI3,5P2	Phosphatidylinositol-3,5 biphosphate
PtdIns(5)P / PI5P	Phosphatidylinositol-5 phosphate
qRT-PCR	Qualitative real-time PCR
RFP	Red fluorescent protein
ROS	Reactive oxygen species
SPG	Spastic paraplegia gene
SPIN	Spinster
SQSTM1/p62	Sequestosome 1
STX17	Syntaxin17
TFEB	Transcription factor EB
TGN	*trans*Golgi network
UBA	Ubiquitin-binding domain
WT	Wild type

2. German summary (Zusammenfassung)

Die hereditäre spastische Paraplegie (HSP) umfasst eine Gruppe heterogener neurodegenerativer Erkrankungen, die durch die Degeneration kortikospinaler Nervenfasern gekennzeichnet ist. Im Zusammenhang mit HSP wurden bereits mehr als 80 mutierte Gene (SPG) beschrieben. SPG11 und SPG15 gemeinsam machen die häufigste autosomal-rezessive erbliche HSP-Form aus. SPG11 und SPG15 sind außerdem mit SPG48, einer weiteren Form der autosomal-rezessiv vererbbaren HSP, assoziiert. SPG48 Patienten zeigen Mutationen in der zeta-Untereinheit des neu beschriebenen Adaptorproteinkomplexes-5 (AP-5). Verschiedene Hinweise sprechen für eine gemeinsame Rolle der Proteine SPG11, SPG15/ZFYVE26 und AP-5 zeta.

In dieser Studie wurde die Rolle von SPG11, ZFYVE26 und AP-5 für die Pathogenese der HSP untersucht. Es wurde ein SPG48 Mausmodell (*Ap5z* KO) generiert und charakterisiert. Mithilfe dieses Modells wurden strukturelle Veränderungen des *trans*Golgi Netzwerkes (TGN), ein gestörter Transport von Endosomen zum TGN sowie eine Beeinträchtigung der Rückgewinnung von Lysosomen aus Autolysosomen (ALR) entdeckt. Außerdem wurde analysiert, ob der gleichzeitige Verlust von *Spg11* und *Zyfve26* zu einem schwerwiegenderen Krankheitsbild im Mausmodell führt. Im Einklang mit der Annahme, dass beide Proteine eine gemeinsame Funktion für Autophagie und ALR haben, wurde kein schwerwiegenderer Phänotyp im Doppel Knockout (KO) im Vergleich zu den Einzel-KO's beobachtet. Zusätzlich wurde gezeigt, dass sich PI4K2A, eine Kinase, welche für die Produktion von Phosphatidylinositol-4 Phosphat (PdtIns(4)P) aus PdtIns zuständig ist, in Lipofuszin-ähnlichem Material in Neuronen von *Spg11* KO und *Zfyve26* KO-Mäusen anhäuft.

Zusammengefasst zeigen die Ergebnisse, dass der Verlust von SPG11 oder ZFYVE26 zu einer Fehllokalisation von PI4K2A führt. Dies wiederum verändert lokal die Konzentration von PdtIns(4)P und PdtIns(4,5)P$_2$. Dadurch kann es zu einer gestörten Rekrutierung von Effektoren wie Clathrin und Dynamin2 und einem ALR-Defekt kommen. Dies wiederum führt zu einer gestörten Autophagie und langfristig zur Neurodegeneration.

3. Summary

Hereditary spastic paraplegia (HSP) denotes a group of heterogeneous neurodegenerative disorders caused by the degeneration of upper motor neurons. More than 80 associated genes (SPG) have been described so far. SPG11 and SPG15 together are among the most common forms of autosomal-recessive HSP. Clinically, SPG11 and SPG15 cannot be distinguished. Hence, it was proposed that both proteins are pathogenetically linked. Moreover, SPG11 and SPG15 are closely related with SPG48, another form of autosomal-recessive HSP. SPG48 patients show mutations in the zeta subunit of the newly described adaptor protein complex-5 (AP-5). Clinically, these patients present a similar but milder phenotype compared with SPG11 and SPG15.

In this study, we used *Spg11*, *Zfyve26* and *Spg48* Knockout (KO) mice to evaluate the role of SPG11, ZFYVE26 and AP-5 in the pathogenesis of HSP. We found structural alterations of the *trans*Golgi network (TGN), an impairment of the retrieval of proteins from late endosomes to the TGN as well as an impairment of autophagic lysosome reformation (ALR) and autophagy. Moreover, we evaluated whether the simultaneous loss of *Spg11* and *Zfyve26* aggravates the phenotype in mice. Supporting a common role of these proteins in autophagy and ALR we did not observe any aggravation of the phenotype by simultaneous disruption of Spg11 and Zfve26. Furthermore, we were able to show that PI4K2A accumulates in autofluorescent intraneuronal deposits of *Spg11* KO and *Zfyve26* KO mice. PI4K2A, one of the four kinases responsible for the production of phosphatidylinositol-4 phosphate (PdtIns(4)P) from PdtIns, was found to be increased in mouse embryonic fibroblasts (MEFs) and brain samples of both KO mice.

Taken together, the results show that the loss of SPG11 and ZFYVE26 leads to an increased accumulation of PI4K2A in autofluorescent material. The accumulation of this kinase resulted in the increase of its product PdtIns(4)P. This may also lead to altered levels of PdtIns(4,5)P$_2$ and thus to a dysregulated recruitment of the ALR effectors Clathrin and Dynamin 2. This in turn can result in impaired autophagy and neurodegeneration. Further analyses should be performed to clarify the role of these proteins in autophagy and ALR.

1. Introduction

1.1 Hereditary Spastic Paraplegia (HSP)

Hereditary Spastic Paraplegia (HSP) is a group of neurodegenerative disorders characterized by a prominent lower-extremity spasticity due to degeneration of corticospinal tract fibers (Blackstone 2012). First symptoms can arise during the infancy, childhood, adolescence or adulthood (Shribman et al. 2019). Advances in DNA sequencing technologies allowed to identify more than 80 distinct genetic loci mutated in HSPs with all modes of inheritance: autosomal-dominant, autosomal-recessive and X-linked (Klebe et al. 2015). Few mitochondrial DNA mutations have also been described (Mignarri et al. 2016; Verny et al. 2011; Sánchez-Ferrero et al. 2012) (Figure 1).

HSPs are present in populations worldwide with a pooled global average prevalence of about 1.8:100,000 with geographic variances (Ruano et al. 2014). For example, a study in southeast Norway revealed a total prevalence of 7.4:100.000 (Erichsen et al. 2009), while in Portugal the prevalence is 4.1:100.000 (Coutinho et al. 2013). Interestingly, some forms of HSPs are more frequent in certain continents compared to others. Autosomal-dominant forms of HSP prevail in Northern Europe and North America (Ruano et al. 2014; Finsterer et al. 2012; Blackstone 2018). Autosomal-recessive HSPs have been mostly observed in populations with high consanguinity, like in the middle East and North Africa (Coutinho et al. 1999; Boukhris et al. 2009).

In the past, HSPs have been divided into pure and complex forms (Harding 1983). Generally, patients affected by pure HSP show a slow progression of the disease with a prominent spasticity of the lower limbs, often associated with hypertonia, corticospinal tract signs, reduction of proprioception and vibration sense of lower extremities (Harding 1983). In some cases voiding dysfunction has been described (Fourtassi et al. 2012). Complex forms are associated with additional features including neuropathy, parkinsonism, cognitive impairment, epilepsy, dementia, aphasia, amyotrophy and visual abnormalities (Harding 1983; Blackstone 2018). Moreover, some cases show clinical overlap with other disorders like lower motor neuron disease, cerebellar ataxia or leukodystrophy (Blackstone 2018). Most of the patients, especially in the case of pure forms, have a normal lifespan.

Many of the autosomal-dominant forms of HSP (around 70-80 % of patients) are pure forms. The most common one is SPG4, covering 40% of the cases, with mutations in *SPAST* encoding the protein Spastin (Beetz et al. 2006; Hazan et al. 1999).

Autosomal-recessive HSPs, like the SPG11 or the SPG15 subtypes, are often defined as complex due to various clinical manifestations (Ruano et al. 2014) (chapter 1.1.2). Unfortunately, so far, no specific treatment is available. Therapy is mainly symptomatic in order to maintain the mobility and avoid complications due to falls or inactivity with the use of physiotherapy (Blackstone 2018).
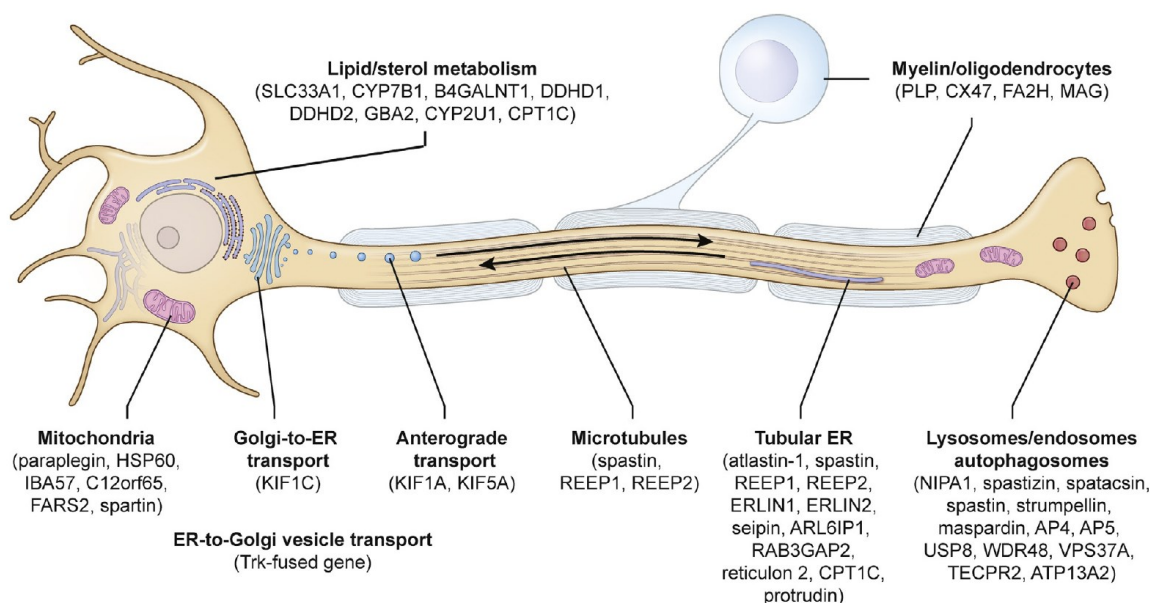
Figure 1. Scheme of HSP genes involved in the pathogenesis. HSP is a heterogeneous group of neurodegenerative disorders affecting the corticospinal motor neurons. Different genes have been described to cause HSP. Their products have been shown or proposed to act in different compartments and processes. ER: Endoplasmic reticulum (Blackstone 2018).

1.1.2. SPG11, SPG15 and SPG48

SPG11 is the most common subtype of autosomal-recessive HSPs. It is characterized by a slow progression of the disease and cognitive decline. Usually the first symptoms arise in childhood or at early teenager years, before the second decade of life (Kara et al. 2016). Canonical SPG11 symptoms include difficulties in walking and spasticity of distal extremities, ataxia, severe bladder problems, parkinsonism and neuropathy (Guidubaldi et al. 2011; Kara et al. 2016). The major hallmark is the thinning of the corpus callosum, which can vary based on the severity of the disease (Stevanin et al. 2008; Kara et al. 2016). Indeed, patients with a mild to moderate disease show a small reduction of the corpus callosum compared to a severe disease development where the thinning is more pronounced (Kara et al. 2016).

SPG15 is another common autosomal-recessive HSP subtype. Its clinical course cannot be distinguished from SPG11 and, thus, the diagnosis is exclusively molecular (Kara et al. 2016).

SPG11 and *SPG15* encode for Spatacsin/SPG11 and Spastizin/ZFYVE26, respectively, which are known to interact (Chang et al. 2014; Słabicki et al. 2010).

The human *SPG11* gene is located on chromosome 15q21.1 and encompasses 40 exons (Pozner et al. 2020). More than 100 mutations, mostly non-sense or frameshift mutations, have been described so far, but no *"hot spots"* have been found (Denora et al. 2016). The encoded protein is a large protein ($\approx$ 280 kDa) which is ubiquitously expressed in the central nervous system (CNS) during embryonic development in rodents (Stevanin et al. 2008). In humans, *SPG11* mRNA is highly expressed in the cerebral cortex and cerebellum (Stevanin et al. 2008).

Spastizin, also known as ZFYVE26, is encoded by *SPG15*/*ZFYVE26* located on chromosome 14q24.1 which includes 42 exons (Hanein et al. 2008). Truncating mutations of this gene have been described to cause HSP (Hanein et al. 2008). In humans, the *ZFYVE26* mRNA is mostly expressed in the bone marrow, the adrenal gland, lungs, skeletal muscles and in the adult and fetal brain (Hanein et al. 2008). In rodents, a high expression has been observed in the granular layer of the cerebellum, the spinal cord and the hippocampus with a stronger expression at embryonic stages as compared to adult brains (Hanein et al. 2008).

It has been shown that both proteins localize to different cellular compartments suggesting different roles inside the cell. A localization of SPG11 and ZFYVE26 to the endosomes and lysosomes has been shown (Murmu et al. 2011; Khundadze et al. 2013; Hirst et al. 2013). Different roles of Spatacsin and Spastizin in the process of autophagy have been reported (Vantaggiato et al. 2019). Both proteins have been linked to the recycling of lysosomes from autolysosomes (autophagic lysosome reformation/ALR) (Varga et al. 2015; Chang et al. 2014). Indeed, even though both SPG11 and SPG15 have been found to interact with proteins involved in endosomal trafficking and maturation, only loss of Spastizin leads to a defect of endosome-autophagosome fusion (Vantaggiato et al. 2019).

Besides, Spatacsin and Spastizin interact within a complex with proteins that have later been identified as subunits of the adaptor complex-5 (Hirst et al. 2012; Hirst et al. 2013). Notably, its zeta subunit is associated with another HSP entity, i.e. SPG48. Adaptor protein complexes (AP) are a family of heterotetrameric protein complexes that facilitate the transport of cargo proteins into vesicular carriers from one membrane compartment to another one inside the cell (Sanger et al. 2019). Several adaptor protein complexes have been described and characterized (AP1-5), each with a specific localization and function (Sanger et al. 2019) (Figure 2). Only the function of AP-5 remains unclear. Mutations in *AP5Z1*/*SPG48*, a relatively newly discovered heterotetrameric adaptor protein complex (Hirst et al. 2012), are associated with another subtype of autosomal-recessive HSP (Słabicki et al. 2010). Few cases have been described so

far (Słabicki et al. 2010; Hirst et al. 2016; Pensato et al. 2014). All patients recapitulate the classical phenotype of a complex HSP with spasticity of the lower limbs, parkinsonism, cognitive impairment, thinning of corpus callosum etc. (Hirst et al. 2016). In contrast to SPG11 and 15, the onset is at middle- or late-adulthood (Słabicki et al. 2010; Hirst et al. 2016). Only one case with early onset in a 7-year-old boy has been described (Pensato et al. 2014).

The *AP5Z1* gene is located on chromosome 7p22 and encompasses 17 exons. Two isoforms have been described with two different functions. Initially, AP5Z1, also known as KIAA0415, was described as an helicase involved in DNA double-strand break repair (Słabicki et al. 2010). This function seems to be associated with the shorter isoform, which is predominantly nuclear (Słabicki et al. 2010). The longer isoform is mostly cytoplasmatic and a subunit of the adaptor protein complex-5 (Hirst et al. 2012).

As for Spatacsin and Spastizin, a role for AP-5 in autophagy has been suggested (Hirst et al. 2013). Moreover, as support for this hypothesis, accumulations of abnormal multilamellar structures, positive for the endolysosomal marker lysosome-associated membrane glycoprotein 1 (LAMP1) were reported in SPG11, SPG15 and SPG48 patient fibroblasts (Renvoisé et al. 2014; Hirst et al. 2015).

A novel function of AP-5 was recently described by Hirst et al. 2018. In this study, it was shown that AP-5 acts as a backup system for the retrieval of proteins from late endosomes to the *trans*Golgi network (TGN) (Hirst et al. 2018). Additionally, it has been proposed that AP-5 together with Spatacsin and Spastizin is involved in protein sorting. An hypothetical model suggests that ZFYVE26 facilitates the docking on membranes due to its interaction with Phosphatidylinositol 3-phosphate (PtdIns(3)P) while SPG11 forms the scaffold around the vesicles (Hirst et al. 2013; Pensato et al. 2014).

This interaction would explain the clinical overlap of patients carrying mutations in either one of these genes.
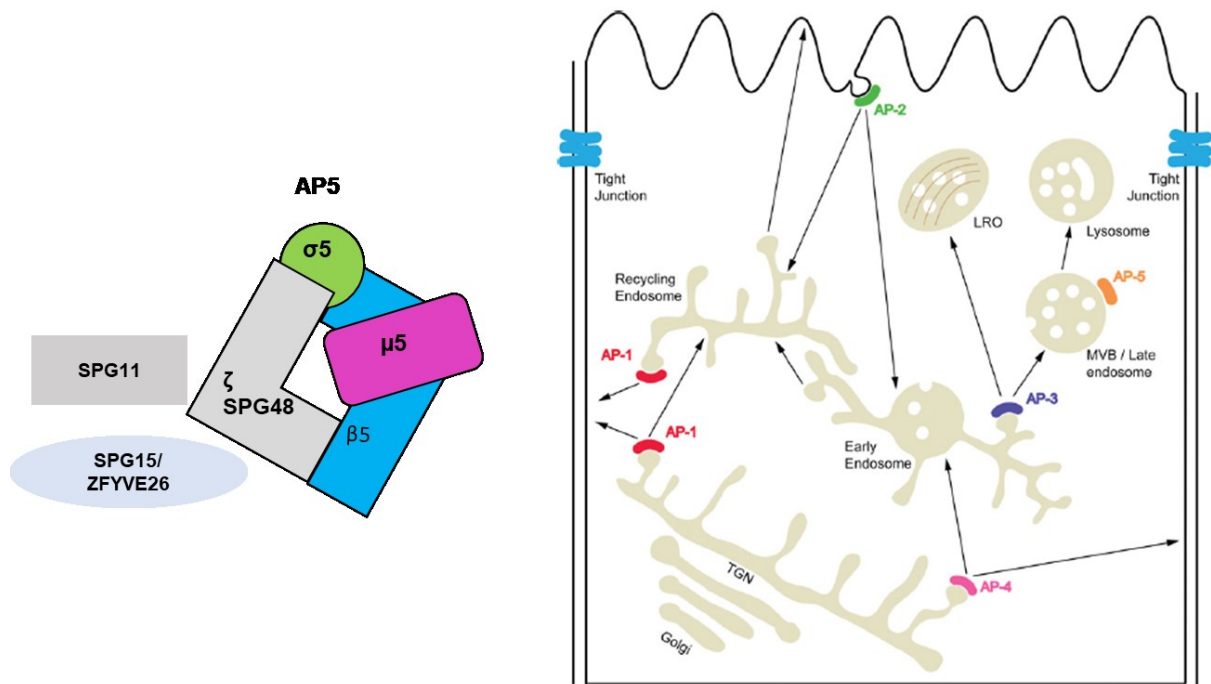
Figure 2. Adaptor protein complexes and HSP. Adaptor protein complexes facilitate the transport of cargo proteins into vesicular carriers from one membrane compartment to another one inside the cell. Four of the five AP complexes have been extensively studied and characterized (AP 1-4). AP-5 is the newly discovered adaptor protein complex and comprises 4 subunits, Beta (β), Sigma (σ), Mu (μ) and Zeta (ζ). Mutations in the zeta subunit of AP-5 have been associated with one of the autosomal-recessive forms of HSP (SPG48). Moreover, it has been shown that AP-5 interacts with two other proteins involved in HSP, Spatacsin (SPG11) and Spastizin (SPG15/ZFYVE26) (Park and Guo 2014)

1.2 Autophagy

Autophagy is a highly conserved cellular process, which facilitates the recycling of nutrients and the degradation of potentially harmful entities.

In literature, three different types of autophagy have been described: macroautophagy, microautophagy and chaperone-mediated autophagy (Parzych and Klionsky 2014).

Macroautophagy, often referred to as autophagy, is the best characterized process and is tightly regulated by different autophagy related genes (ATGs) (Nishimura and Tooze 2020). The encoded proteins were first described in yeast and sequentially several orthologues were described in mammalians as a proof of a conserved process (Takeshige et al. 1992; Mizushima et al. 1998).

Autophagy can be divided into six steps (Figure 3):

1. Initiation
2. Phagophore formation (Nucleation)
3. Autophagosome formation (Elongation and Completion)
4. Fusion with lysosomes (Docking and Fusion)

5. Cargo degradation

6. Autophagic lysosome reformation (ALR)
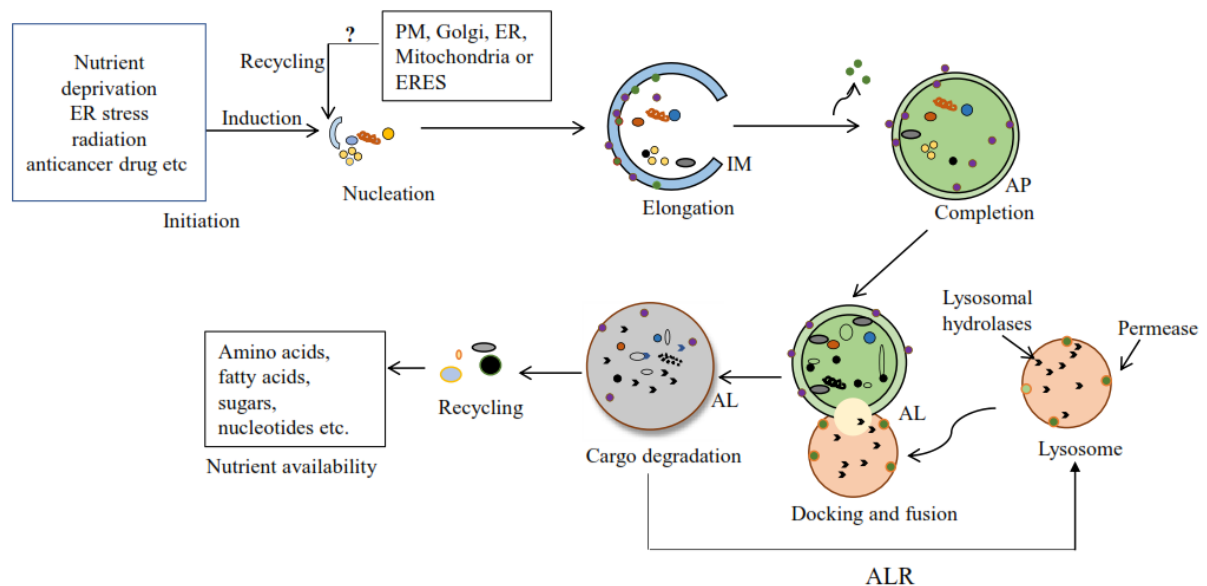
Figure 3. Macroautophagy. Macroautophagy/Autophagy is sensitive to different intracellular or environmental stimuli. It starts with the recruitment of several protein complexes, leading to the formation of the autophagosome. Autophagosomes incorporate different cargos that are degraded after fusion with lysosomes. The pool of lysosomes is maintained with the help of autophagic lysosome reformation (ALR). ER: endoplasmic reticulum; PM: plasma membrane; ERES: ER exit sites; IM: isolated membrane; AP: autophagosome; AL: autolysosome (Al-Bari 2020).

Under normal conditions, autophagy occurs at a low level but can be induced in response to different stimuli including cell stress like nutrient or energy deprivation, pathogen infection and hypoxia (Parzych and Klionsky 2014). In mammals, initiation of autophagy starts with the formation of an isolation membrane (IM). It derives from different organelles, e.g. the endoplasmic reticulum (ER), and is enriched with PtdIns(3)P -rich subdomains (omegasome) due to the recruitment of the kinases ULK1 and PI3KC3 (Axe et al. 2008; Abada and Elazar 2014; Backer 2016).

The ULK1 complex consists of a combination of different proteins: ULK1 itself, the FAK family kinase-interacting protein of 200kD (FIP200), ATG13 and ATG101 (Suzuki et al. 2015). PI3KC3 is a lipid kinase responsible for the generation of PtdIns(3)P and essential for the initiation (Backer 2016). In particular, PI3KC3 forms two complexes, PI3KC3-C1 and PI3KC3-C2, both containing VPS34, p150 and Beclin1 (BECN1) (Itakura et al. 2008).

During starvation-induced autophagy, complex-I is translocated to the initiation site on the ER due to the interaction with the ATG14L subunit (Itakura et al. 2008). Here, ULK1

phosphorylates BECN1 and promotes the generation of PtdIns(3)P in omegasomes (Hurley and Young 2017). This leads to the subsequent interaction and recruitment of WIPI1/2 scaffold proteins which are essential for the elongation and formation of LC3-positive autophagosomes (Proikas-Cezanne et al. 2015).

Complex-II interacts with UVRAG and is involved in the endocytic pathway (Itakura et al. 2008).

For the elongation of the IM, two ubiquitin-like conjugation systems, ATG12 (ATG12-ATG5-ATG16 complex) and LC3 (microtubule-associated protein 1A/1B-light chain 3), are required (Al-Bari 2020). The first system coordinates the insertion of LC3-phosphatidylethanolamine (PE), known also as LC3-II, into the membrane for the autophagosome generation. The second system is involved in the cleavage and lipidation of MAP1-LC3 (Tanida et al. 2004). In mammalian cells, LC3 is cleaved by ATG4 near the C-terminal glycine to form the cytosolic soluble LC3-I, which is activated by ATG7 and delivered to the E2-like ATG3. Here, LC3-I is cleaved and converted to LC3-II (lipidation), forming the membrane-associated form (Al-Bari 2020). Thus, LC3-II is specifically inserted into the inner and outer membrane of the elongating autophagosome where it regulates the autophagosomal size due to the ability to determine the membrane curvature (Kraft et al. 2016; Jin and Klionsky 2014).

At this point, autophagy can be divided into non-selective or selective autophagy. In the first case, cytoplasmatic material is targeted inside the autophagosomes in a non-selective manner. Selective autophagy instead requires specific receptors which bind specific cargos that need to be degraded. All these receptors contain a specific domain, the LC3-interacting region (LIR) or the ATG8-interacting motif (AIM), which allow to bind specifically to proteins of the ATG8/LC3/GABARAP family (Zientara-Rytter and Subramani 2018).

In total, more than twenty different receptors have been described in mammalian cells. The best characterized and most common receptor involved in selective autophagy is p62, also known as SQSTM1 (Deng et al. 2017). It has been shown that p62 is able to promote the degradation of selective cargoes in three different ways: direct interaction with LC3 via its LIR motif, association with early autophagosomes (due to the recruitment of the ATG protein via its PB1 domain) and binding of ubiquitinated proteins via its ubiquitin-binding domain (UBA) (Dikic and Elazar 2018).

After selection, cargos are retained inside these double membrane vesicles known as autophagosomes and transported along microtubules for the fusion with lysosomes.

RAB7, a member of the small GTPase family, is important for the coordination of membrane trafficking (Hyttinen et al. 2013). RAB7 can interact with both, dynein and kinesin motor

proteins (Hyttinen et al. 2013; Jordens et al. 2001). Upon starvation, kinesin interacts with RAB7, LC3 and PtdIns(3)P transporting early autophagosomes to the minus-end of microtubules in the cell periphery (Pankiv et al. 2010). At the periphery, RAB7 interacts with dynein which allows the transport of late autophagosomes to the perinuclear region where the lysosomes are enriched. This enrichment is triggered by an increase of intracellular pH (Nakamura and Yoshimori 2017).

The fusion between autophagosomes and lysosomes is coordinated by the tethering complex HOPS RAB GTPase and SNARE proteins (Nakamura and Yoshimori 2017). Other important players are PI4K2A and INPP5E. They mediate the generation of PtdIns(4)P and PtdIns(3)P, respectively, on autophagosomes which are essential for autophagosome-lysosome fusion (Wang et al. 2015).

Upon starvation Syntaxin17 (STX17), a member of SNARE proteins, is recruited on mature autophagosomes where it interacts with the HOPS complex and SNAP29, forming an heterocomplex. This complex interacts with R-SNARE and VAMP8 leading to the formation of a high energetically favorable complex. This allows the fusion and generation of single membrane vesicles called autolysosomes (Itakura et al. 2012).

In autolysosomes, the material is degraded and the products released for recycling. The release of nutrients from autolysosomes stops the autophagy by activating the regeneration of lysosomes via the autophagic lysosome reformation (ALR) (Chen and Yu 2017).

1.2.1 Autophagic lysosome reformation (ALR)

During autophagy, lysosomes are consumed for the generation of autolysosomes. ALR is the final step of autophagy and essential for the recovery of the lysosomal pool (Yu et al. 2010).

During this process tubular structures, which are pH neutral, extrude from the autolysosomal membrane and are later cut to generate small vesicles called proto-lysosomes (Yu et al. 2010). These vesicles mature into functional lysosomes, thereby maintaining lysosomal homeostasis. This process is still not well known, but some key molecular players have been described: PtdIns(4,5)P_2, AP-2, Clathrin, KIF5B and Dynamin2 (Chen and Yu 2017, 2018).

During prolonged starvation, PtdIns(4,5)P_2 enriched-microdomains are generated on the surface of autolysosomes due to the conversion of PtdIns(4)P by the PIP5K1B (Rong et al. 2012). AP-2 then links Clathrin to PtdIns(4,5)P_2 molecules. One molecule of Clathrin recruits two AP-2 which then recruit two PtdIns(4,5)P_2 molecules generating the lattice on the membrane of autolysosomes (Chen and Yu 2017, 2018). The motor protein KIF5B is able to bind directly to PtdIns(4,5)P_2 and mediates the generation of reformation tubules at the sites of

Clathrin buds (Du et al. 2016). These reforming tubules are initially pH neutral, positive for LAMP1 but negative for LC3. The lumen does not contain any lysosomal proteins (Yu et al. 2010). The retention of the proteins from reformation tubules is mediated by the production of PtdIns(4)P by PI4K3B (Sridhar et al. 2013).

Another important player in ALR is Dynamin2, which is recruited at the tip of reformation tubules where microdomains of PtdIns(4,5)P_2 by PI5K1A are generated (Schulze et al. 2013; Rong et al. 2012). Once recruited to the membrane, the large GTPase Dynamin2 mediates the scission of the proto-lysosomes (Chen and Yu 2015).

Like other processes, also ALR is tightly regulated and under the control of mTOR (inhibitory mechanistic Target of Rapamycin) (Zhang et al. 2016). During starvation, mTOR is inhibited and autophagy can take place (Jung et al. 2010). After prolonged starvation, nutrients are released from autolysosomes, reactivating mTOR which provides a negative feedback signal in order to avoid excessive degradation and thus triggering ALR (Chen and Yu 2017, 2018). Spinster (SPIN), a sugar transporter and lysosomal efflux permease, has been described to be also involved in the initiation of ALR together with mTOR (Rong et al. 2011). Interestingly, it has been shown that mTOR regulates the generation of PtdIns(3)P in lysosomes via the PI3KC3 complex which in turn regulates the scission of tubules (Munson et al. 2015). PtdIns(3)P seems to be also involved in the initiation of ALR due to the interaction with two proteins involved in HSP, SPG11and SPG15 (Chang et al. 2014). The detailed mechanisms, however, are still poorly understood.

It has been shown that ALR has clinical importance, since it has been described to be involved in several diseases like Parkinson disease, HSP and skeletal muscles diseases (Magalhaes et al. 2016; Varga et al. 2015; McGrath et al. 2021). Therefore, further investigations of ALR for alternative and more effective therapeutic strategies are still needed.
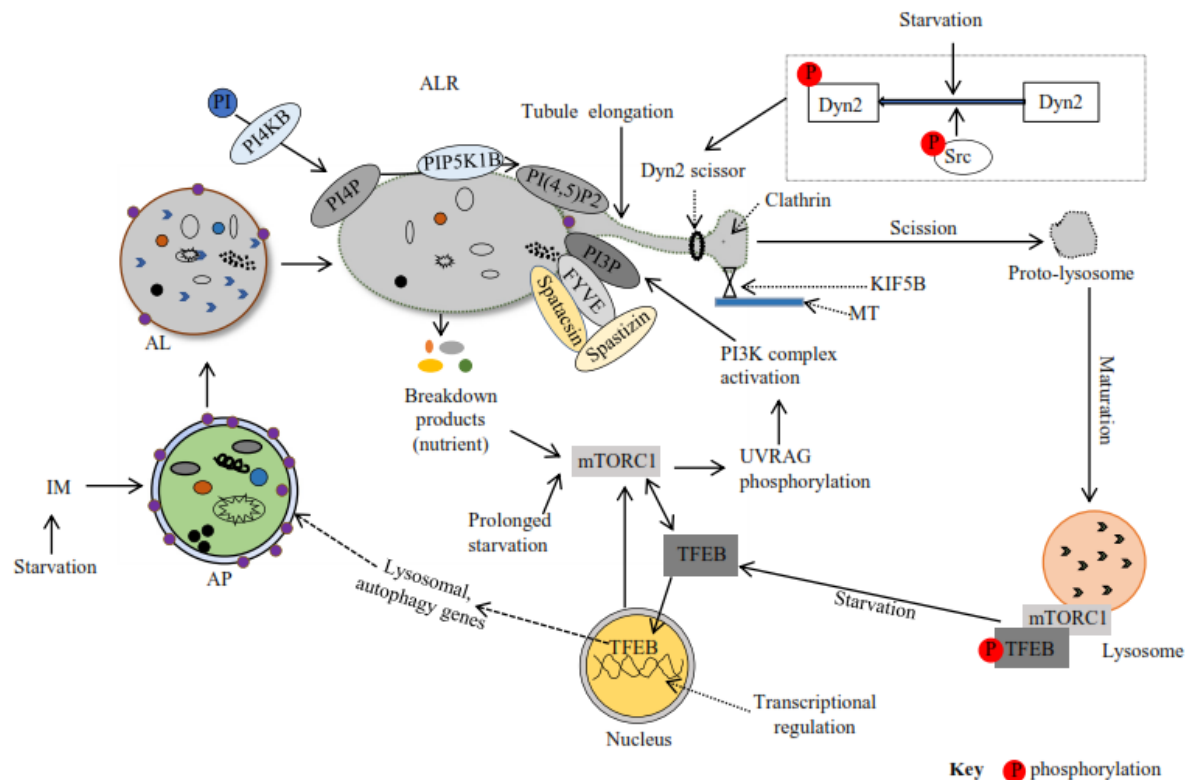
Figure 4. Autophagic lysosome reformation and its regulation. ALR is an important process essential for the regeneration of the lysosomal pool. Different players take part in this process, such as PtdIns(3)P, PtdIns(4)P, PtdIns(4,5)P$_2$, Spastizin, Spatacsin, Clathrin, KIF5B and Dynamin2. On the surface of autolysosomes, Clathrin is recruited via its interaction with PtdIns(4,5)P$_2$, leading to the generation of buds which are pulled by KIF5b. The reformation tubules undergo scission mediated by Dynamin 2, which generates proto-lysosomes. These structures will then generate new functional lysosomes. ALR is mainly regulated by mTORC1. After prolonged starvation, the release of nutrients from AL reactivates mTORC1, which subsequentially triggers ALR. mTORC1 is also involved in the biogenesis of lysosomes via its interaction with the TFEB-dependent pathway. During starvation, mTORC1 is inactivated, TFEB dephosphorylated and converted into its active form. Thus, TFEB translocates to the nucleus where it activates the transcription of lysosomal and autophagy genes. PI3P: Phosphatidylinositol 3 Phosphate; PI4P: Phosphatidylinositol 4 Phosphate; PI(4,5)P2: Phosphatidylinositol 4,5 biphosphate; Dyn2: Dynamin2; IM: isolated membrane; AP: autophagosome; AL: autolysosome; TFEB: transcription factor EB (Al-Bari 2020).

1.2.2 Autophagy regulation

Autophagy is important for the maintenance of the homeostasis in cells and therefore, a tight regulation is needed.

The main regulator of autophagy is mTOR, which is inactivated in response to different intracellular and environmental stressors, such as nutrient starvation, growth factors, hypoxia and ER stress (Saxton and Sabatini 2017).

mTOR and in particular mTORC1 comprises five components: the catalytic subunit mTOR, the regulatory associated protein Raptor, its inhibitor protein PRAS40 and DEPTOR (Saxton and Sabatini 2017).

mTORC1 can regulate autophagy in different ways. One of them is the interaction with the initiation complex ULK1 (He and Klionsky 2009). When mTORC1 is active under nutrient conditions it phosphorylates ATG13 preventing its association with ULK1 and therefore inhibiting autophagy initiation (Al-Bari and Xu 2020; Abada and Elazar 2014).

The ULK1 complex can also be activated in response to energy deficiency via AMPK signaling (Al-Bari 2020). In this condition, AMPK signaling directly phosphorylates Raptor and ULK1, leading to inhibition of mTORC1 and enhancement of autophagy (Gwinn et al. 2008; Kim et al. 2011). Interestingly, mTORC1 is sensitive to growth factors and nutrients. The presence of amino acids regulates mTORC1 positively via RAG proteins and the RAS-related GTPase (He and Klionsky 2009; Kim et al. 2008). mTOR then translocates to the surface of lysosomes, thereby gets activated and inhibits autophagy (Saxton and Sabatini 2017). Under starvation conditions, mTORC1 is inhibited and ULK1 active leading to the induction of autophagy (Hosokawa et al. 2009).

Moreover, mTORC1 is involved in lysosome biogenesis via its interaction with the transcription factor EB (TFEB)-dependent pathway (Martina et al. 2012), a member of the transcription factor MiTF/TFE family. Under nutrient conditions, mTORC1 phosphorylates TFEB on the surface of lysosomes, leading to its inactivation (Martina et al. 2012) (Figure 4). mTORC1 also promotes the release of phosphorylated TFEB to the cytoplasm and its interaction with chaperones which prevents the nuclear translocation of TFEB (Martina et al. 2012).

During starvation, mTORC1 is inhibited and dissociates from lysosomes. Thus, mTORC1 is no longer able to inhibit TFEB which diffuses from lysosomes to the nucleus where it then induces the expression of lysosomal-autophagy related genes (Martina et al. 2012) (Figure 4).

Finally, autophagy can also be regulated via mTOR independent pathways such as levels of Ca^{2+}, reactive oxygen species (ROS), HIF-1α, or MAPK/JNK signaling (Al-Bari and Xu 2020). Dysregulation of autophagy has been shown to be involved in several neurodegenerative diseases, including HSPs. Therefore, a better understanding of SPG11, 15 and 48 in this process might open new therapeutic strategies.

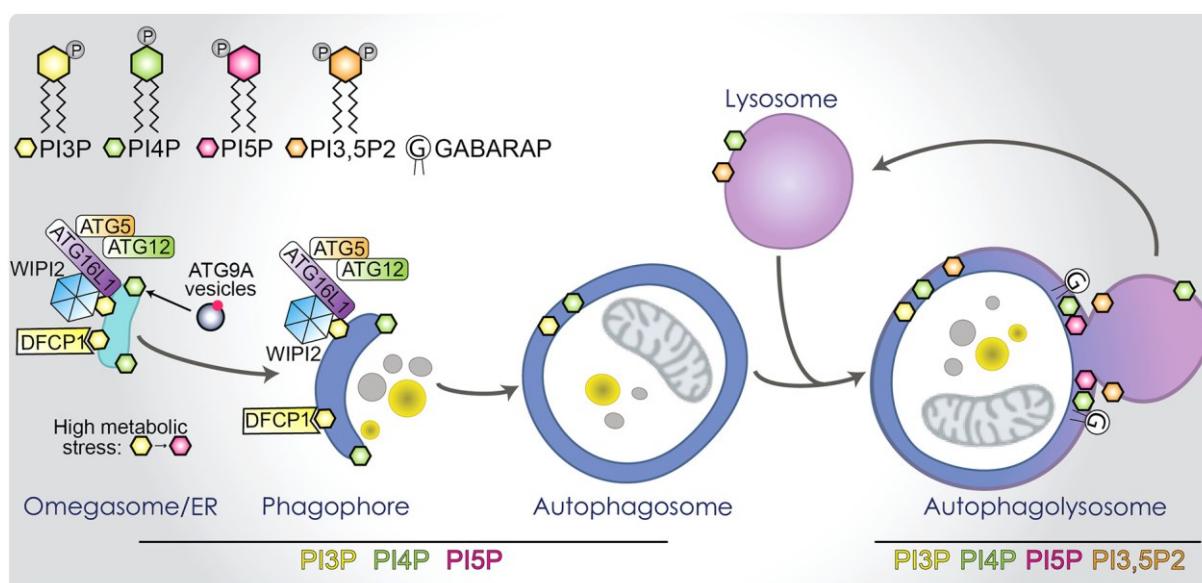1.3 Phosphoinositides and Autophagy

Phosphoinositides (PIs) are a family of key lipids in eukaryotes that are involved in the regulation of several processes. The synthesis and turnover of these lipids are regulated by phosphorylation/dephosphorylation on positions 3, 4 or 5 of phosphatidylinositol by specific lipid kinases or phosphatases (Dickson and Hille 2019). Phosphoinositides and therefore their

kinases/phosphatases have been described to be involved in several processes like cytoskeleton dynamics, signaling cascades and membrane trafficking which are important for the maintenance of the cellular homeostasis (Hammond and Burke 2020). Mutations in the enzymes involved in the generation of phosphoinositides have been described in several human diseases (Pendaries et al. 2003; Hammond and Burke 2020; Falasca 2012).

Phosphatidylinositol (PtdIns) is synthesized only at the ER membrane, while the associated phosphoinositides are present on different endomembranes at the cytoplasmatic side, like the plasma membrane (PM), ER, Golgi apparatus, endosomes and lysosomes (Craene et al. 2017; Hammond and Burke 2020). In particular, PtdIns(4,5)P$_2$ and PtdIns(3,4,5)P$_3$ are mainly found in the PM, PtdIns(4)P mainly in the Golgi apparatus, PtdIns(3)P and PtdIns(3,5)P$_2$ at endosomes and lysosomes (Craene et al. 2017).

Interestingly, PtdIns(3)P, PtdIns(3,5)P$_2$, PtdIns(4)P, PtdIns(4,5)P$_2$ and PtdIns(5)P have been described to be involved in autophagy-associated membrane events (Claude-Taupin and Morel 2021) (Figure 5).

Figure 5. Function and localization of phosphoinositides during autophagy. Phosphoinositides play an important role in different steps of autophagy. PtdIns(3)P and PtdIns(4)P are important for the initiation of autophagy, autophagosome formation and maturation. During glucose starvation, PtdIns(5)P is involved in autophagosome maturation or during metabolic stress in autophagosome-lysosome fusion. PtdIns(4)P and PtdIns(3,5)P2 are important for the generation of autolysosomes. PI3P: Phosphatidylinositol 3 Phosphate; PI4P: Phosphatidylinositol 4 Phosphate; PI5P: Phosphatidylinositol 5 Phosphate; PI3,5P2: Phosphatidylinositol 3,5 biphosphate; ER: endoplasmic reticulum (Claude-Taupin and Morel 2021)

1.3.1 PtdIns(3)P

As already mentioned, autophagy is characterized by different steps which are well regulated due to the involvement of different players. The *de novo* biogenesis of autophagosomes is one of the most important steps of this process where the materials which need to be degraded are engulfed inside these structures. During this process, PtdIns(3)P plays an important role. Indeed, the accumulation of PtdIns(3)P is essential for the recruitment of protein complexes involved in the generation and maturation of autophagosomes (Axe et al. 2008). Moreover, PtdIns(3)P has been described to be involved in autophagy-cargo selection to target ubiquitinated aggregates into autophagosomes (Filimonenko et al. 2010) and in ALR (Munson et al. 2015; Chang et al. 2014).

1.3.2 PtdIns(5)P and PtdIns(3,5)P$_2$

PtdIns(5)P is a rare phosphoinositide in mammalian cells. Its production is mediated by PIKFYVE, which transforms PtdIns into PtdIns(5)P (Shisheva 2012).

This rare phosphoinositide has been found in the PM of early endosomes and autophagosomes (Shisheva 2012). Indeed, during glucose starvation, PtdIns(5)P regulates the formation of autophagosomes by recruiting WIPI2 and DFCP1 which then allows LC3 lipidation independently of the presence of PtdIns(3)P (Vicinanza et al. 2015). A more recent study showed that PtdIns(5)P is also involved in autophagosome-lysosome fusion under high metabolic stress conditions (Lundquist et al. 2018).

Like PtdIns(5)P, PtdIns(3,5)P$_2$ is another low abundant phosphoinositide. PIKfyve kinase is not only involved in the generation of PtdIns(5)P, but also in the phosphorylation of PtdIns(3)P to PtdIns(3,5)P$_2$ (Zolov et al. 2012). The turnover of PtdIns(3,5)P$_2$ is dependent on the phosphatase FIG4, which generates PtdIns(3)P via dephosphorylation, therefore maintaining the correct levels of PtdIns(3,5)P$_2$ (Rudge et al. 2004).

PtdIns(3,5)P$_2$ is involved in the regulation of the two main regulators of autophagy, mTORC1 and AMPK, by controlling their subcellular localization (Bridges et al. 2012; Fernandez-Mosquera et al. 2019). Additionally, a role of PtdIns(3,5)P$_2$ in autophagosome-lysosome fusion depending on the function of INPP5E phosphatase has been described in neuronal cells (Hasegawa et al. 2016). Since INPP5E catalyzes the formation of PtdIns(3)P from PtdIns(3,5)P$_2$, mutations in this enzyme lead to high levels of PtdIns(3,5)P$_2$ which negatively regulates the fusion of autophagosomes and lysosomes (Hasegawa et al. 2016).

1.3.3 PtdIns(4)P and PI4Ks

PtdIns(4)P is another important phosphoinositide, which is mainly detected in the Golgi under nutrient conditions (Wang et al. 2003). Its generation is mediated by four different phosphatidylinositol-4 phosphate kinases (PI4Ks), which are involved in different processes: PI4K2A, PI4K2B, PI4K3A and PI4K3B (Boura and Nencka 2015).

The pool of PtdIns(4)P is associated with endocytosis (Jović et al. 2014), the protein transport to the Golgi and the formation of the *trans*Golgi vesicles, which promote the transport of specific cargos to late endosomes or to the PM (Guo et al. 2014). A role of PtdIns(4)P in autophagy and in particular the pool produced from PI4K2A has been described more recently (Wang et al. 2015). Under normal conditions, this kinase and its product are mainly accumulated in the TGN (Barylko et al. 2009). Upon starvation, PI4K2A is redistributed to autophagic structures, in particular to autophagosomes, via its interaction with GABARAP proteins (Wang et al. 2015). At this site, the production of PtdIns(4)P allows the autophagosome-lysosome fusion (Wang et al. 2015).

Mutations in this kinase have been associated with Gaucher disease (Jović et al. 2012), Hermansky-Pudlak Syndrome (Salazar et al. 2009), spastic paraplegia (Alkhater et al. 2018) and cancer (Li et al. 2010).

PI4K3B, another kinase, is responsible for the production of PtdIns(4)P on lysosomes. It has been shown to be involved in ALR (Sridhar et al. 2013). Around 20 % of this kinase associates with lysosomes and its presence controls the correct sorting of lysosomal substrates and prevents their incorporation into reformation tubules (Sridhar et al. 2013).

PtdIns(4)P also plays an indirect role in ALR due to its possible conversion to PtdIns(4,5)P_2 by PIP5K1A and B. It has been shown that PtdIns(4,5)P_2 plays a key role in the recruitment of Clathrin, KIF5B and Dynamin2 during ALR (Rong et al. 2012).

Furthermore, the balance between PtdIns(4)P and PtdIns(4,5)P_2 must be maintained for a proper ALR. A recent study has shown that mutations in the phosphatase INPP5K, involved in the generation of PtdIns(4)P from PtdIns(4,5)P_2, lead to ALR impairment causing skeletal muscle diseases (McGrath et al. 2021).

A balance between different forms of phosphoinositides appears to be crucial for several processes inside the cell. Small changes in the amount of these lipids can lead to severe consequences.

2. Aim of the study

HSP is a heterogeneous group of neurodegenerative disorders characterized by degeneration of the upper motoneuron axons leading to weakness and spastic gait (Fink 2014). More than 80 genetic loci have been described to cause different types of HSP (Klebe et al. 2015). Our group focuses on the most predominant autosomal-recessive HSP forms SPG11, SPG15 and the rare form SPG48, which are characterized by mutations in Spatacsin, Spastizin and the AP5 zeta subunit, respectively. Except SPG48, which shows milder symptoms, these forms share an identical clinical phenotype (Kara et al. 2016). It has been shown that Spatacsin, Spastizin and the subunits of AP-5 co-precipitate and thus, likely act together (Hirst et al. 2013). The role of these proteins is still poorly understood.

Our main objective was to investigate the pathophysiology of the AP-5-related proteins Spatacsin, Spastizin and AP-5 in autophagy and ALR.

Recently, AP-5 was described to act as a back-up system of the retromer for the retrieval of proteins from late endosomes to the TGN (Hirst et al. 2018). We aimed to investigate a role of AP-5 in this process in our mouse model and evaluate possible consequences on the TGN structure and the correct sorting of lysosomal proteins.

Another aim of this study was to evaluate whether a simultaneous disruption of SPG11 and SPG15 might aggravate the phenotype, thereby contributing to the identification of the role of these proteins. Because *Spg11* KO and *Zfyve26* KO as well as *AP5-zeta* KO mice accumulate undegraded autolysosomal material, we aimed to characterize these deposits by mass spectrometry to possibly identify misrouted cargoes. The accumulation of PI4K2A in deposits of *Spg11* KO and *Spg15* KO mice neurons, a kinase which is already known to be involved in autophagy (Wang et al. 2015), motivated us to evaluate whether it might also be involved in ALR. In particular we aimed to evaluate whether different levels of PI4K2A and its product, PtdIns(4)P, affect ALR as well as the recruitment of its key players.

3. Overview of the manuscripts

A mouse model for SPG48 reveals a block of autophagic flux upon disruption of adaptor protein complex five

Mukhran Khundadze*, Federico Ribaudo, Adeela Hussain, Jan Rosentreter, Sandor Nietzsche, Melanie Thelen, Dominic Winter, Birgit Hoffmann, Muhammad Awais Afzal, Tanja Hermann, Cecilia de Heus, Eva-Maria Piskor, Patricia Franzka, Lisa von Kleist, Tobias Stauber, Judith Klumperman, Christian Kosan, Markus Damme, Tassula Proikas-Cezanne, Christian A. Hübner. Published in the journal **Neurobiology of Disease** 127 (2019) 419–431

(* first authorship)

This study described for the first time a KO mouse for a subunit of the AP-5 complex which recapitulates the human phenotype. We confirmed the impairment of the retrieval from late endosomes to the TGN and revealed structural alterations of the Golgi Apparatus upon disruption of AP-5. Moreover, this study demonstrated that the absence of AP-5 leads to a block of autophagy with accumulation of undigested material, increased amount of autophagosomes and autolysosomes and impairment of ALR, resulting in axon degeneration.

My contribution to this work was the planning and execution of the following experimental work: preparation of cells for different experimental procedures, transfection, immunocytochemistry, microscope image optimization and acquisition, live cell imaging establishment and image acquisition, quantification of confocal images and time lapses, data collection, statistical analyses as well as participation in the preparation of the manuscript.

Mouse models for hereditary spastic paraplegia uncover a role of PI4K2A in autophagic lysosome reformation

Khundadze M*, Ribaudo F*, Hussain A, Stahlberg H, Brocke-Ahmadinejad N, Franzka P, Varga RE, Zarkovic M, Pungsrinont T, Kokal M, Ganley IG, Beetz C, Sylvester M, Hübner CA. Published in the journal **Autophagy**, 2021 Mar 9:1-17 8 (* first authorship)

In this study we demonstrated that the simultaneous disruption of *Spg11* and *Zfyve26* in mice does not aggravate the phenotype confirming a common role in the pathophysiology of HSP. The disruption of Spatacsin and Spastizin increased the amount of undigested material in neurons and led to ALR impairment. No impairment of the autophagosome-lysosome fusion process was observed in contrast to previous data. Moreover, we reported a new function of PI4K2A in ALR. It plays an important role in the recruitment of key players like Clathrin and Dynamin2 on reformation tubules. Finally, we proposed that increased levels of PI4K2A as
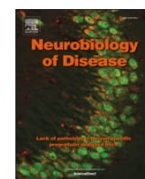
well as its product PtdIns(4)P in *Spg11* and *Zfyve26* KO mice contribute to the pathophysiology of SPG11 and SPG15.

My contribution to this work was the planning and execution of the following experimental work: preparation of cells for different experimental procedures, transfection, immunocytochemistry, microscope image optimization and acquisition, live cell imaging establishment and image acquisition, quantification of confocal images and time lapses, western blotting, RNA isolation and quantitative RT-PCR, flow cytometry, data collection, statistical analyses as well as participation in the preparation of the manuscript.

3.1 Manuscript I

A mouse model for SPG48 reveals a block of autophagic flux upon disruption of adaptor protein complex five

Mukhran Khundadze[a,*], Federico Ribaudo[a], Adeela Hussain[a], Jan Rosentreter[a], Sandor Nietzsche[b], Melanie Thelen[c], Dominic Winter[c], Birgit Hoffmann[d], Muhammad Awais Afzal[a], Tanja Hermann[a], Cecilia de Heus[e], Eva-Maria Piskor[f], Christian Kosan[f], Patricia Franzka[a], Lisa von Kleist[g], Tobias Stauber[g], Judith Klumperman[e], Markus Damme[h], Tassula Proikas-Cezanne[i], Christian A. Hübner[a,*]

[a] Institute of Human Genetics, University Hospital Jena, Friedrich-Schiller-University Jena, Jena 07747, Germany
[b] Electron Microscopy Center, University Hospital Jena, Friedrich-Schiller-University Jena, Jena 07743, Germany
[c] Institute for Biochemistry and Molecular Biology, University of Bonn, Bonn 53115, Germany
[d] Biomolecular Photonics Group, University Hospital Jena, Friedrich-Schiller-University Jena, Jena 07743, Germany
[e] Department of Cell Biology, Center for Molecular Medicine, University Medical Center Utrecht, Utrecht 3584, Netherlands
[f] Institute of Biochemistry and Biophysics, Friedrich-Schiller-University Jena, Jena 07743, Germany
[g] Institute of Chemistry and Biochemistry, Freie Universität Berlin, Berlin 14195, Germany
[h] Institute of Biochemistry, Christian-Albrechts-University Kiel, Kiel 24118, Germany
[i] Department of Molecular Biology, Eberhard Karls University Tübingen, Tübingen 72076, Germany

ARTICLE INFO

ABSTRACT

Hereditary spastic paraplegia is a spastic gait disorder that arises from degeneration of corticospinal axons. The subtype SPG48 is associated with mutations in the zeta subunit of the adaptor protein complex five (AP5). AP5 function and the pathophysiology of SPG48 are only poorly understood. Here, we report an AP5 zeta knockout mouse, which shows an age-dependent degeneration of corticospinal axons. Our analysis of knockout fibroblasts supports a trafficking defect from late endosomes to the *trans*Golgi network and reveals a structural defect of the Golgi. We further show that both autophagic flux and the recycling of lysosomes from autolysosomes were impaired in knockout cells. *In vivo*, we observe an increase of autophagosomes and autolysosomes and, at later stages, the accumulation of intracellular waste in neurons. Taken together, we propose that loss of AP5 function blocks autophagy and thus leads to the aberrant accumulation of autophagic cargo, which finally results in axon degeneration.

1. Introduction

Hereditary spastic paraplegia (HSP) is characterized as a progressive spastic gait disorder that arises from a length-dependent dying back degeneration of corticospinal tract fibers (Fink, 2014; Blackstone, 2018). More than 80 genetically distinct forms of HSP (SPGs) can be distinguished. SPG48 is transmitted as an autosomal recessive trait and is clinically highly variable with features such as sensory and motor neuropathy, ataxia, dystonia, myoclonus, and Parkinsonism in addition to spastic paraplegia. Because of the clinical overlap with lysosomal storage disorders and accumulation of multilamellar structures in

patient derived skin fibroblasts, it was proposed that SPG48 may represent a new type of lysosomal storage disorder (Hirst et al., 2016).

Initially the gene mutated in SPG48 was identified in a screen for DNA double strand break repair. It encodes the protein KIAA0415, which co-precipitates in a complex with five other proteins (Slabicki et al., 2010), two of which being associated with HSP as well, *i.e.* Spatacsin mutated in SPG11 and Spastizin mutated in SPG15. Because of the difficulties to reliably detect the endogenous proteins, the functional interplay between KIAA0415, Spastizin and Spatacsin is still not fully resolved. It has been proposed that Spastizin and Spatacsin play a role in cell division (Sagona et al., 2010), autophagy (Vantaggiato et al.,

2014), and endolysosomal trafficking (Hirst et al., 2013). Both proteins are involved in the recycling of lysosomes from autolysosomes (autophagic lysosome reformation) (Chang et al., 2014). This process is characterized by the formation of empty Lamp1-positive protrusions, which are finally pinched off from autolysosomes (Yu et al., 2010). Upon disruption of either Spastizin or Spatacsin, autophagosomes and autolysosomes increase in number, less of these autolysosomal tubules are formed and undegraded material accumulates over time (Khundadze et al., 2013; Vantaggiato et al., 2013; Chang et al., 2014; Varga et al., 2015).

Some years ago KIAA0415 and the other three proteins of the complex of unknown function were identified as the fifth adaptor protein complex because of the homology to other adaptor protein complexes with KIAA0415 being its zeta subunit (Hirst et al., 2011). Adaptor protein complexes are heterotetrameric protein complexes, which recognize and concentrate cargo proteins into vesicular carriers that mediate transport from a donor membrane to a target organelle. Although the cargo of AP5 is still largely unclear, elegant knockdown studies in HeLa cells suggest that AP5 is involved in the retrieval from the *trans*Golgi network to late endosomes (Hirst et al., 2018). Studies with patient iPSC-derived neurons from SPG48 patients further reported mitochondrial alterations (Denton et al., 2018).

Here, we describe a mouse model for SPG48, which is the first reported knockout mouse for a subunit of the AP5 complex. These mice accumulate autofluorescent material in neurons and develop late onset progressive gait abnormalities thus recapitulating the human phenotype. In agreement with a role of AP5 for the retrieval from late endosomes to the *trans*Golgi network, several Golgi-related proteins were enriched in lysosomal fractions of knockout mouse embryonic fibroblasts. Moreover, the Golgi apparatus was structurally altered. Analysis of autophagic flux and autophagic lysosome reformation upon starvation *in vitro* pointed to a defect of autophagic flux. This assumption was supported by the accumulation of autophagosomes and autolysosomes and the accumulation of undegraded autophagic cargo *in vivo*.

2. Materials and methods

2.1. Animals

Mice were housed with a 12 h light/dark cycle and fed on a regular diet *ad libitum*. All animal experiments were approved by the "Thüringer Landesamt für Lebensmittelsicherheit und Verbraucherschutz" (TLLV) in Germany (Approval number: 02-034-14).

The Ap5z1 knockout mouse strain used for this study was created from the embryonic stem cell clone EPD0587_5_A05 obtained from the KOMP Repository (www.komp.org) and generated by the Wellcome Trust Sanger Institute. Methods used on the CSD targeted alleles have been reported in (Skarnes et al., 2011). For genotyping DNA was isolated from tail biopsies. Genotyping primers were used in a single PCR reaction: f: GGAGCAA-CAGAACAAAGCTGTACG, KO-r: CGCCGGAACC GAAGTTCCTATTCC, WT-r: CAGGGCTGCTCACTCACCTACG. The primer pair f/WT-r amplified a 364 bp fragment for the wild-type allele and the primer pair f/KO-r a 250 bp fragment for the trapped allele. Experiments were conducted on mice with a mixed 129SVJ/C57BL/6 background.

2.2. Cell culture, mass spectrometry and immunoblot analyses

Mouse embryonic fibroblasts (MEFs) were prepared from E13.5 mouse pups and cultured in Dulbecco's Modified Eagle medium (DMEM) 1X with GlutaMAX-I supplemented with 10% FBS (Fetal Bovine Serum) and 1% penicillin/streptomycin (100×) in a humidified atmosphere with 5% CO_2 and 37 °C.

Hippocampal neurons were isolated from newborn pups and cultured as described previously (Sinning et al., 2011). Before transfection

cells were plated on coverslips and after 24 h transfected with 1 μg DNA/well in 24-well plates with lipofectamine 3000 reagent (Invitrogen, Germany). 24 to 48 h post-transfection cells were fixed with 4% formaldehyde for 15 min at room temperature. Immunocytochemistry was performed as described (Sinning et al., 2011). The M6PR retrieval assay was performed as described in (Hirst et al., 2018). Images were acquired with a confocal scanning fluorescence microscope (Zeiss LSM 880, Germany) with Airyscan using a Plan-Apochromat 63×/1.4 oil DIC M27 objective and analyzed with the ZenBlue co-localization plugin (Zeiss, Germany). Quantitative measurements of the lysosomal proteome were carried out as described (Thelen et al., 2017). Protein enrichment analysis has been carried out by using of the cellular compartment tool from the Genome Ontology Consortium (GO) website (http://www.geneontology.org) (Ashburner et al., 2000; The Gene Ontology, 2017). Lysosomal pH measurements were performed as described previously (Weinert et al., 2010). For overexpression of the 103Q-HTT-GFP fusion protein, the variant cDNA was cut with *Kpn*I and *Xba*I from the pYES2/103Q plasmid of Michael Sherman (Addgene plasmid # 1385) (Meriin et al., 2002), and cloned into the pEGFP-N1 vector (Clontech laboratories, USA). To detect Zfyve26 and Spatacsin brain tissue was homogenized in a buffer containing 300 mM Tris-HCl pH 8.8, 5 mM EDTA, 3 mM NaF, 10% (*v/v*) glycerol, 3% (*w/v*) SDS, complete protease inhibitor cocktail (Roche, Switzerland) as described (Varga et al., 2015).

### 2.3. Time-lapse imaging for ALR

For detection of lysosomal tubules, MEFs were plated on 42 mm coverslips (PeCon, Germany) in 6 cm plates and transfected after 24 h with 3 μg of Lamp1-GFP plasmid DNA using Lipofectamine 3000 (Invitrogen, Germany). The Lamp1-GFP plasmid was a gift from Esteban Dell'Angelica (Addgene plasmid # 34831) (Falcon-Perez et al., 2005). To induce autophagy, cells were incubated with EBSS medium (Gibco, Germany) for 8–9 h. Tubulation events were visualized with a fluorescence microscope (CellObserver Z1, Zeiss, Germany) equipped with an incubation chamber (37 °C, 5% CO_2). Time-lapse images were acquired every 2 s for 3 min with an exposure time of 200 ms using the ApoTome mode and the 40×/1.2 W objective. Number and length of tubules were evaluated for 30 cells of each genotype in three independent experiments using ImageJ (National Institutes of Health, Bethesda, USA).

2.4. Histological analysis

Immunohistochemistry was done on formalin fixed, free floating sections as described previously (Sinning et al., 2011). Purkinje cell numbers were quantified on 40 μm sagittal brain sections after staining of brain sections with an antibody directed against Calbindin. For statistical analysis the number of Purkinje cells per 1,000 μm distance along the Purkinje cell layer was counted from three different cerebellar sections from three mice per genotype. Images of the sagittal sections of wild-type and knockout brains were taken with a confocal scanning fluorescence microscope (Zeiss LSM 880, Germany) with Airyscan using a Plan-Apochromat 63×/1.4 oil DIC M27 objective. Neurons were quantified with the cell counter plugin and the area measurement tool of ImageJ.

2.5. Ultrastructural analysis and morphometry

For semi- and ultrathin sectioning of brain samples, four animals per genotype were perfused with 50 ml fixative (4% formaldehyde, 2.5% glutaraldehyde in phosphate buffer). Brain and spinal cord were removed and post fixed overnight at 4 °C. 150 μm sagittal and coronal sections were cut with a vibratome (Leica Microsystems, Germany) and processed as described (Beetz et al., 2013).
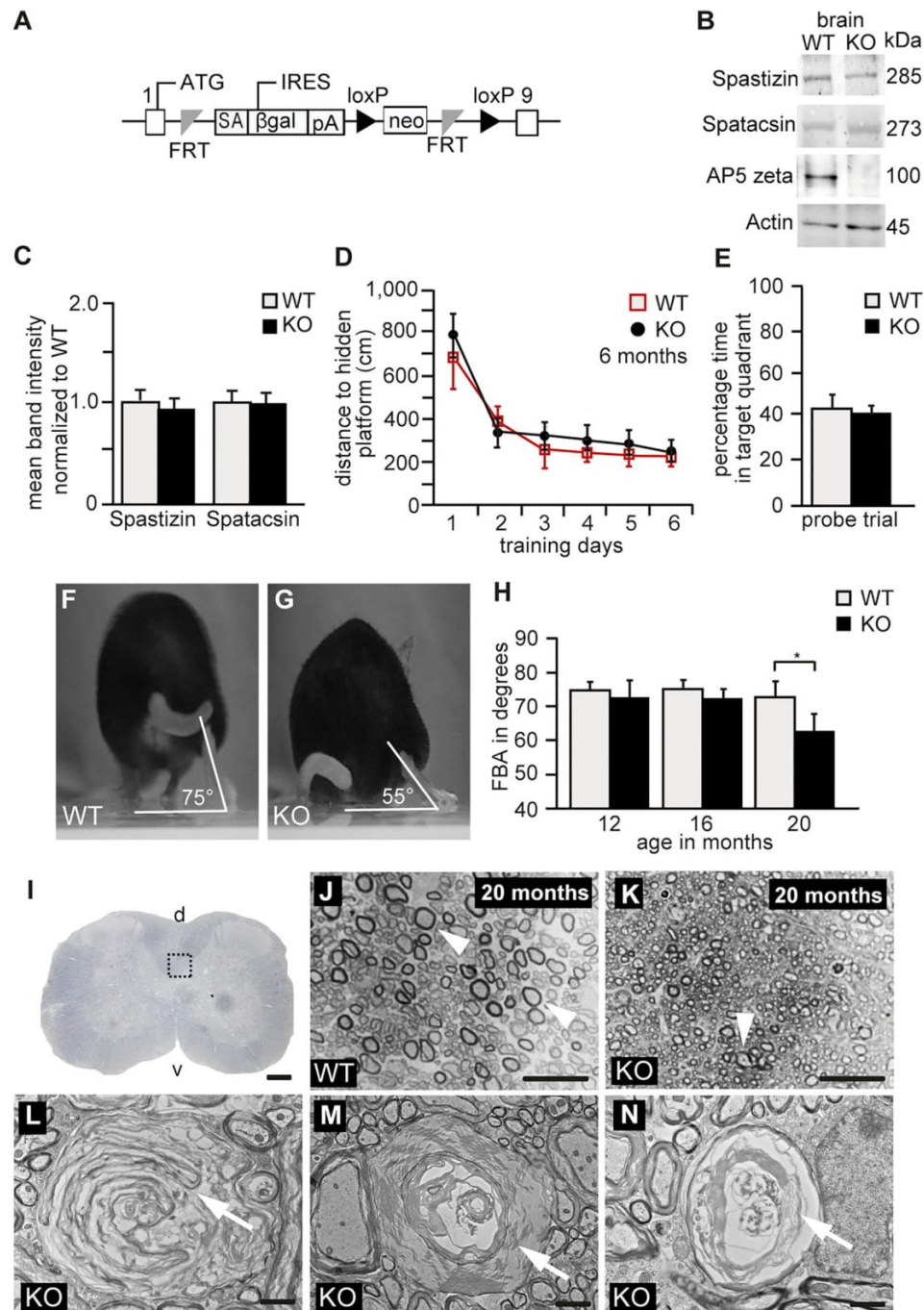
Fig. 1. Axon degeneration in AP5 zeta knockout mice. (A) Targeting strategy. Exons 2-8 of the *Ap5z1* gene are replaced by a gene trap cassette, which includes a splice acceptor (SA), internal ribosomal entry site (IRES), the β-galactosidase cassette (βgal) followed by a polyadenylation signal (pA) and a neomycin cassette (neo) flanked by loxP sites (black arrowheads). Both the βgal and neo cassette are flanked by frt sites (grey triangles). (B) Western Blot analysis of brain lysates with a polyclonal antibody directed against AP5 zeta detects a band of the predicted size in wild-type (WT) brain lysates, which is absent in homozygous trapped mice. Thus homozygous trapped mice represent AP5 zeta knockout mice (KO). Actin served as a loading control. (B,C) Spastizin and Spatacsin levels are not changed in total brain protein lysates of AP5 zeta KO mice (4 mice per genotype). (D-E) At six months of age no learning or memory deficits were noted in the Morris water maze (KO, $n = 8$; WT, $n = 7$; two-way ANOVA followed by Bonferroni test; $p > 0.05$). (F-G) Single video frames of a WT and a KO mouse walking on a beam at toe-off-position. The foot-base-angle (FBA) is indicated. (H) Compared to WT mice ($n = 9$) the FBA is decreased in 20 month-old AP5 zeta KO mice ($n = 10$) (two-way ANOVA followed by Bonferroni test; * $p < 0.05$). (I) Transversal semi-thin section of lumbar spinal cord to illustrate the regions shown in J and K. v: ventral; d: dorsal. Scale bar: 250 μm. (J, K) In comparison to controls large diameter axons (white arrowheads) are almost absent in the lumbar corticospinal tract of 20-month-old KO mice. Scale bars: 20 μm. (L-N) Transmission electron microscopy of lumbar corticospinal tract fibers illustrating different axonal pathologies including abnormal membranous material (white arrows) in AP5 zeta KO mice. Scale bars: 1.25 μm for L and N; 2.4 μm for M. Error bars in (C, D, E, H) represent mean ± SEM.

3. Results

3.1. Late onset corticospinal tract degeneration in AP5 zeta knockout mice

To generate AP5 deficient mice we injected the trapped embryonic stem cell clone EPD0587_5_A05 from the KOMP Repository (Fig. 1A) into donor blastocysts, which were transferred into foster mice. The resulting chimeric mice were mated to obtain heterozygous trapped mice. Mating of heterozygous offspring resulted in homozygous trapped mice at the expected Mendelian ratio. Validating that these represent AP5 zeta knockout mice, immunoblot analysis of brain lysates confirmed the absence of the AP5 zeta subunit (Fig. 1B). The abundance of Spatacsin and Spastizin, which are known to co-precipitate and interact with AP5 subunits (Slabicki et al., 2010; Hirst et al., 2011; Hirst et al., 2013), was not changed in brain lysates of AP5 zeta knockout mice (Fig. 1B, C).

Young knockout mice did not show any obvious abnormalities such as reduced body weight, motor deficits or increased mortality. In the Morris water maze paradigm the distance travelled to the hidden survival platform during the learning test (Fig. 1D) and the time spent in the target quadrant after removal of the survival platform in the memory test (Fig. 1E) did not differ between genotypes excluding a relevant spatial learning deficit at six months of age. To assess whether the AP5 zeta deficient mice develop a progressive gait abnormality we measured the foot base angle at toe-off position, when mice traversed a beam directing to the home cage as described previously (Beetz et al., 2013). In accordance with a rather mild motor phenotype in patients, we observed a significant flattening of this angle only at 20 months of age (Fig. 1F-H). At this time-point the morphological analysis of the lumbar corticospinal tract revealed a reduction of large diameter axons (Fig. 1I-K) and different signs of axon degeneration in knockout (Fig. 1L-N) but not in wild-type mice.

Taken together these findings are in agreement with late onset degeneration of the corticospinal tract, which results in a mild gait disturbance.

3.2. Accumulation of autofluorescent material in Purkinje neurons of AP5 zeta knockout mice

Starting around two months of age, neurons of different brain regions such as principal cells in the motor cortex and Purkinje cells accumulated autofluorescent deposits in both Spastizin and Spatacsin knockout mice (Khundadze et al., 2013; Varga et al., 2015). Although at a later time-point, an increase of autofluorescent material (emission wavelength 460–630 nm) was also evident in pyramidal neurons of layer V of the motor cortex (Fig. 2A, B) and in Purkinje neurons (Fig. 2E, F) in AP5 zeta knockout mice at eight months of age. At 20 months of age, only few dispersed and small autofluorescent spots were noted in wild-type mice (Fig. 2C, G), while larger clusters of autofluorescent material were a frequent finding in knockout mice (Fig. 2D, H). By ultrastructural analysis we observed larger clusters of membrane-associated electron-dense deposits of irregular shape in samples of aged knockout mice, which likely correspond with the autofluorescent material observed by light microscopy, but only some small particles resembling lipofuscin in aged control mice (Fig. 2I-J').

Because neurodegeneration frequently triggers the activation of astrocytes, we stained brain sections of 20-month-old mice for GFAP. Indeed, a strongly increased GFAP immunoreactivity was observed in knockout mice in different brain areas such as the Purkinje and granular cell layer of the cerebellum, while the molecular layer was spared (Fig. 2K, L). Labeling of Purkinje cells with Calbindin allowed us to quantify these cells. In contrast to Spastizin and Spatacsin knockout mice, where Purkinje cells were mostly lost at later stages, Purkinje cell bodies were preserved upon disruption of AP5 zeta (Fig. 2M).

In conclusion, morphological alterations in AP5 zeta knockout mice closely resemble findings in Spastizin and Spatacsin knockout mice but are less severe and occur later without overt Purkinje cell loss.

3.3. Accumulation of Lamp1-positive vesicles in axons of AP5 zeta knockout mice

It has been reported that AP5 localizes to the endolysosomal system (Hirst et al., 2013) and that SPG48 patient skin fibroblasts display abnormal endolysosomes (Hirst et al., 2015). To find an *in vivo* correlate in mice, we stained brain and spinal cord sections for the lysosomal membrane protein Lamp1. Notably, we found large Lamp1-positive spheroids with a diameter of up to 15 μm within the corticospinal tract of AP5 zeta knockout tissue, which were absent in control samples (Fig. 3A, B, B'). Electron microscopy suggested that these structures likely correspond with densely packed organelles such as mitochondria and vesicular structures (Fig. 3C) resembling lysosomes and autolysosomes (Fig. 3C', C''). Similar Lamp1-positive structures were also found in the granular layer of the cerebellum (Fig. 3D). Because they co-labeled with Calbindin (Fig. 3D', D''), which labels Purkinje cells, and the axonal marker protein Neurofilament 200 (Fig. 3E-E''), they likely represent swellings of Purkinje cell axons.

Taken together, clustering of organelles and Lamp1-positive vesicles underlies axonal swellings in AP5 zeta knockout mice.

3.4. Alterations of the transGolgi network in AP5 zeta knockout mouse embryonic fibroblasts

It has been reported that the morphology of mitochondria is changed in iPSC-derived neurons from SPG48 patients and upon knockdown of AP5 zeta in hEPCs (Denton et al., 2018). However, the morphology of Purkinje cell mitochondria at the ultrastructural level and the quantification of signal intensities for the mitochondrial marker protein Mtc02 in Purkinje cell bodies did not support gross changes of the mitochondrial pool in AP5 zeta knockout mice at 20 months of age (Fig. S1A-E).

We considered that AP5 may play a role for the sorting of lysosomal proteins. Therefore, we labeled control and AP5 zeta deficient mouse embryonic fibroblasts (MEFs) with either 'light' or 'heavy' isotope labeled-amino acids and isolated lysosomes with magnetic particles as reported previously (Thelen et al., 2017). Surprisingly, we did not find any striking alterations of typical lysosomal proteins, but rather an increase in several Golgi related proteins such as the Golgi glycoprotein one (Glg1) in the lysosomal fraction of knockout MEFs (Fig. 4A and Table S1), which is consistent with a defect in the trafficking between endolysosomea and Golgi.

To confirm that AP5 might act as a backup pathway for the retromer for the retrieval from late endosomes back to the Golgi apparatus (Hirst et al., 2018), we incubated MEFs from both genotypes with a M6PR antibody and chased the antibody for 60 min. Then cells were fixed and stained with a secondary antibody directed against the M6PR antibody and co-stained for TGN38 to label the *trans*Golgi network. In agreement with previous findings (Hirst et al., 2018), there was increased signal of the M6PR outside of the *trans*Golgi network area in AP5 zeta deficient MEFs (Fig. S2A-D). In addition, we noted a clear reduction of TGN38-signals in knockout MEFs, while the *cis*Golgi marker Giantin appeared unaltered (Fig. 4B-D). As judged from the ultrastructural analysis, there was an increase of cells with a more vesiculated Golgi apparatus and a significant decrease of the size of Golgi stacks in AP5 zeta knockout MEFs (Fig. 4E-H).

To get an idea whether these changes also apply *in vivo*, we stained sections of the cerebellum of two- and 20-month-old mice and quantified the TGN38- and Glg1-signals of individual Purkinje cell bodies. Interestingly, the TGN38- and Glg1-labeling did not differ between genotypes at two months, but was clearly reduced in AP5 zeta knockout mice at 20 months of age (Fig. 4I-Q). A decrease of Glg1 levels in AP5 zeta knockout mice was also confirmed by immunoblot analysis of brain lysates from 20-month-old mice (Fig. 4R), while protein abundance did
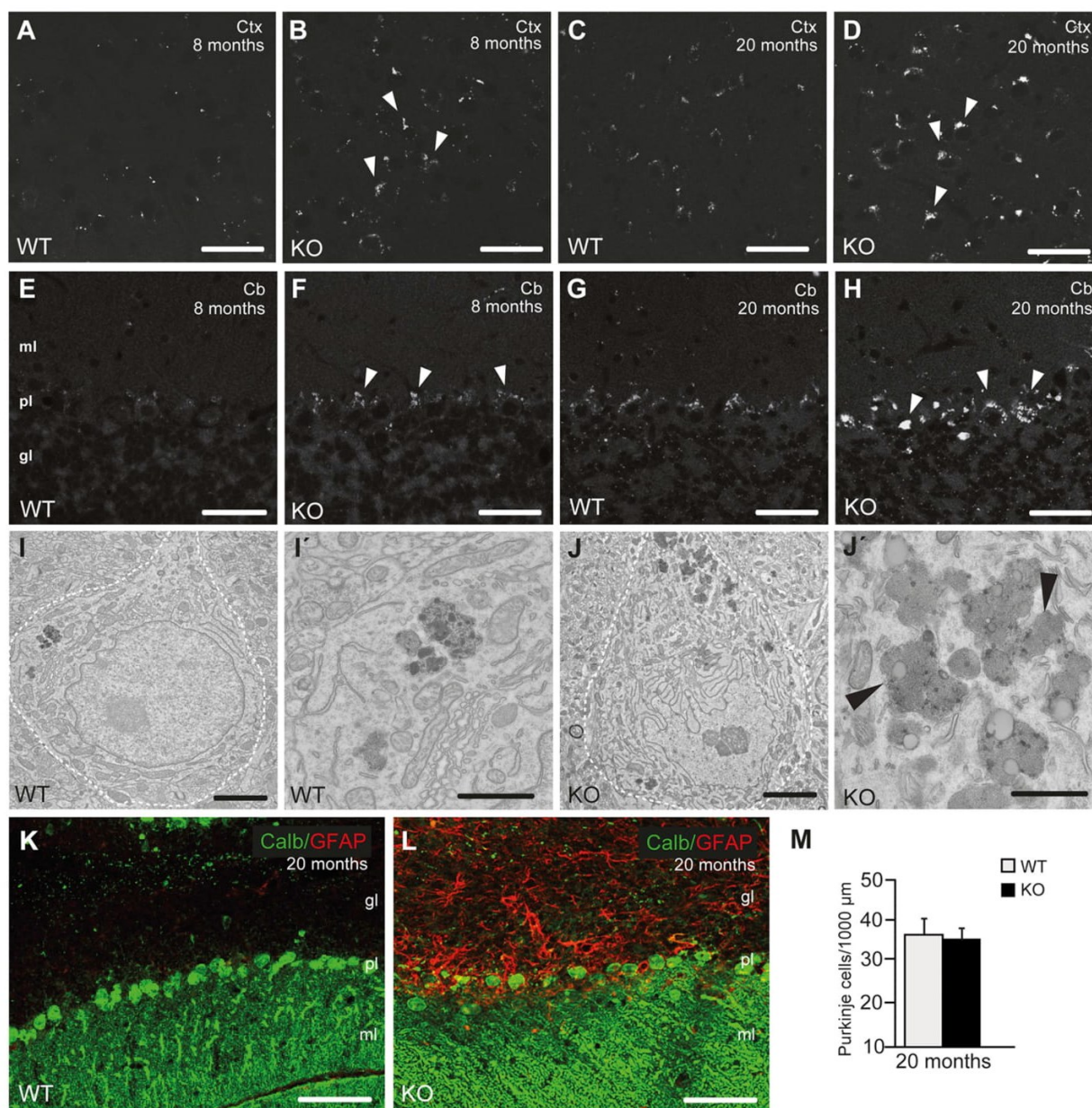
Fig. 2. Accumulation of autofluorescent material in AP5 zeta knockout neurons. (A-H) A substantial age-dependent increase of autofluorescent material was observed in pyramidal neurons in layer V of the motor cortex (A-D) and in Purkinje neurons (*E*-H) of knockout (B, D, F, H) compared to control mice (A, C, E, G) (excited at 488 nm, shown in white). Ctx: cortex; Cb: cerebellum; ml: molecular layer; pl: Purkinje cell layer; gl: granule cell layer. Scale bars: 50 μm. (I-J´) At the ultrastructural level electron dense material particles were more abundant in KO (J, J´) compared to WT Purkinje cells (I, I´) at 20 months of age. The cell bodies of Purkinje cells are indicated by a dashed line. The magnification of the highlighted regions in (I) and (J) are shown in (I´) and (J´), respectively. Black arrowheads indicate membranes associated with the electron dense material. Scale bars: 2.5 μm for (I, J); 1.2 μm for (I´, J´). (K, L) Co-stainings for GFAP and Calbindin, which labels Purkinje cells, show a strong activation of astrocytes in the granular and Purkinje cell layer of KO mice at 20 months of age (L), while Purkinje cell bodies are preserved. Scale bars: 50 μm. (M) Quantification of Purkinje cells (three mice per genotype, Student's *t*-test; p > 0.05). Error bars represent mean ± SEM.

not differ at six months of age (Fig. S2E).

Thus, the disruption of AP5 zeta causes a redistribution of some Golgi related proteins to lysosomes and structural alterations of the Golgi apparatus in MEFs. Correlates of which were only detected in Purkinje neurons of aged knockout mice.

3.5. Impaired autophagy and autophagic lysosome reformation in AP5 zeta deficient MEFs

Western blot analysis did not reveal alterations of Lamp1 levels and the ratio between the mature and the precursor forms of the lysosomal protease Cathepsin D was unchanged in KO MEFs (Fig. 5A). Lysosomal
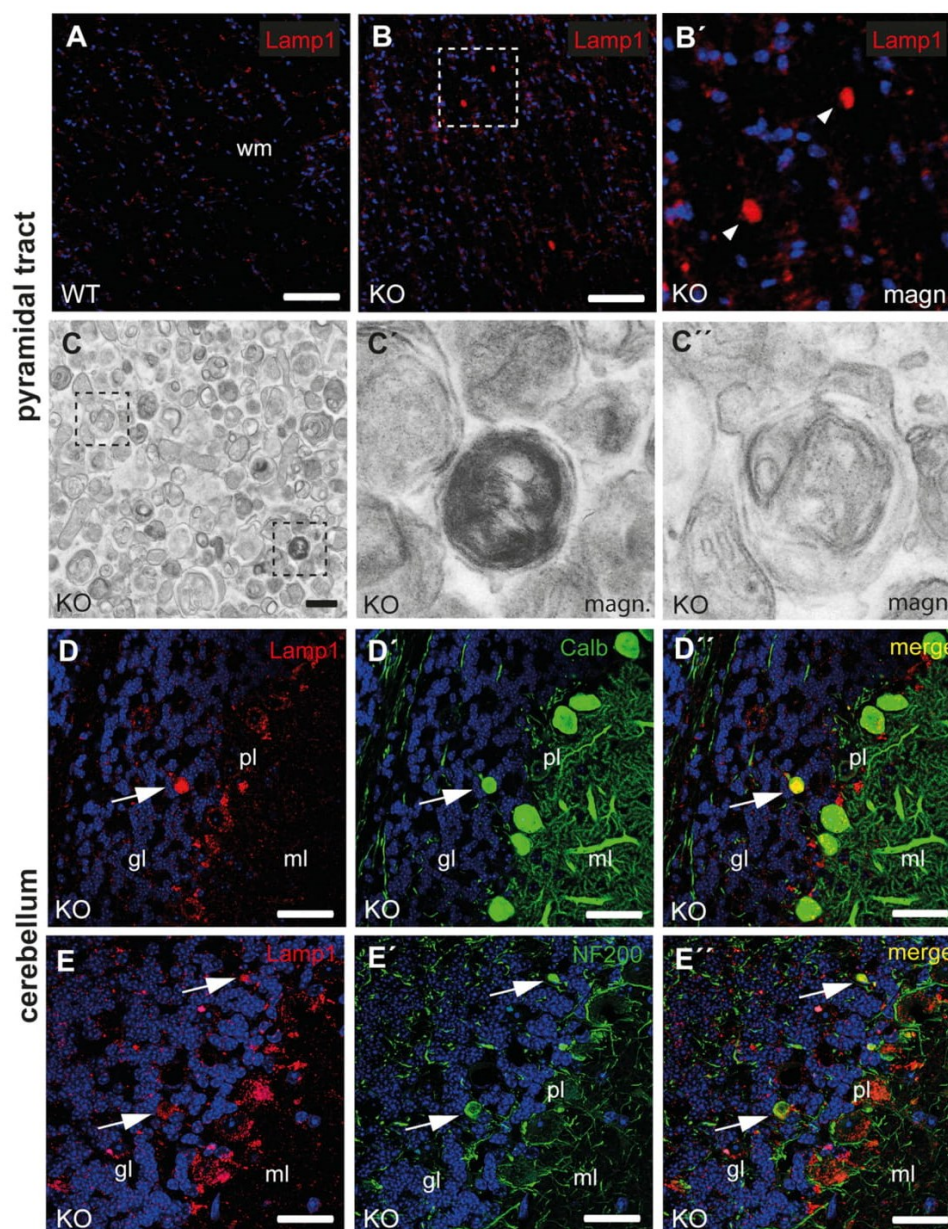
Fig. 3. Lamp1-positive axonal swellings in AP5 zeta knockout mice. (A-B′) At 20 months of age Lamp1-positive spheroids (Lamp1: red; blue: nuclei) are present in the corticospinal tract of the lumbar spinal cord of AP5 zeta KO mice (B) but not in controls (A). (B′) is a magnification of the region indicated in (B). Scale bars: 100 μm. (C-C″) The ultrastructural analysis identified clustered vesicles in some corticospinal tract axons (C). Magnifications of the regions indicated in (C) are consistent with lysosomes (C′) and autolysosomes (C″). Scale bar in C: 500 nm. (D-E″) Lamp1-positive spheroids are also detected in the cerebellar granule cell layer of 20-month-old KO mice (D, E), which also label for the Purkinje cell marker Calbindin (D′) and the axonal marker Neurofilament 200 (E′). The overlays are shown in (D″) and (E″). wm: white matter; pl: Purkinje cell layer, ml: molecular cell layer, gl: granule cell layer. Scale bars: 50 μm. (For interpretation of the references to colour in this figure legend, the reader is referred to the web version of this article.)

pH as an important determinant for the activity of lysosomal proteases also did not differ between genotypes (WT: 4.29, SE: ± 0.09; KO: 4.41, SE: ± 0.14) suggesting that the acidification of the lysosomal compartment is not compromised.

Further, we addressed whether autophagy may be impaired upon functional disruption of AP5 zeta. During the process of autophagy cytosolic LC3 (LC3-I) becomes conjugated to phosphatidylethanolamine at the nascent autophagosome, and is then referred to as LC3-II as it migrates faster in SDS-PAGE. Autophagosomes represent LC3-positive but Lamp1-negative double-membrane bound vesicles that sequester cytoplasmic material destined for degradation. Autophagosomes then fuse with lysosomes resulting in acidic Lamp1- and LC3-positive autolysosomes, in which the degradation of the engulfed material and LC3 by lysosomal enzymes takes place. Here, in basal autophagy conditions, both LC3-I and LC3-II abundances did not differ between genotypes (Fig. 5B, baseline). This result suggests that basal autophagy is not

27
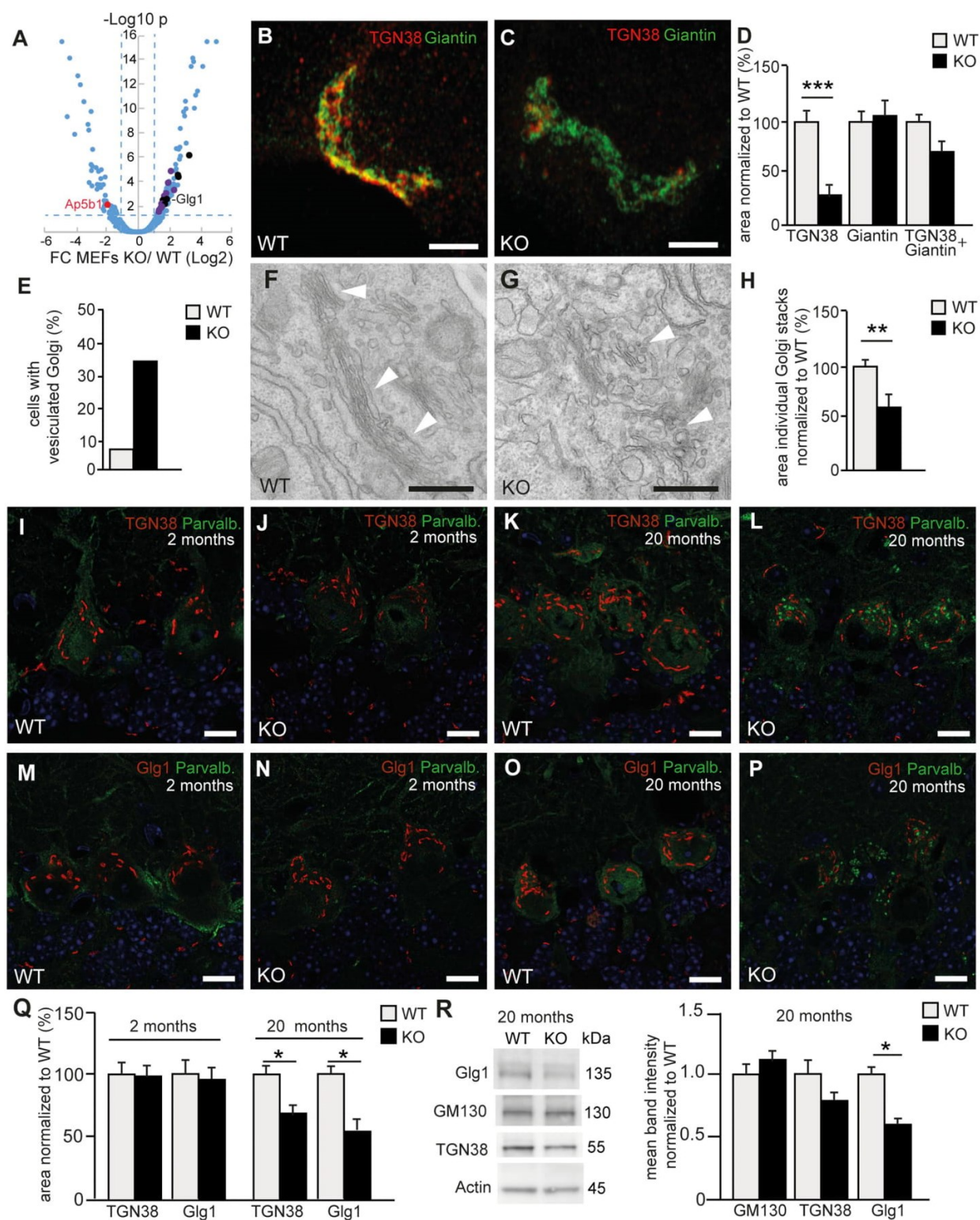
(caption on next page)

Fig. 4. Alterations of the Golgi apparatus upon disruption of AP5 zeta. (A) SILAC-based quantification of the proteome of lysosome enriched fractions from WT and KO mouse embryonic fibroblasts (MEFs) from four replica each. The complete list of differentially regulated proteins is shown in Table S1. The x-axis shows the log2-fold change (the fold change threshold > 1.0 is shown by blue dashed line) and the y-axis the respective -log10 p-value of significance analyzed by Student's t-test (significance threshold $p < 0.05$,). Differentially expressed endolysosome-associated proteins are shown as lilac colored dots; differentially expressed Golgi-associated proteins are shown as black colored dots. The spot representing the AP5 beta subunit is shown in red. (B-D) The relative area of TGN38-positive structures (*trans*Golgi) but not Giantin-positive structures (*cis*Golgi) are reduced in AP5 zeta KO MEFs. Scale bar: 1 μm. (E-H) The ultrastructural analysis of Golgi stacks revealed an increased number of MEFs with a vesiculated Golgi apparatus (E). Exemplary images are shown in (F) and (G). The Golgi complex is indicated by white arrowheads. (H) Overall the mean size of individual Golgi stacks was decreased. Student's t-test (40 cells per genotype; ** $p < 0.01$). Scale bars: 500 nm. (I-Q) Signals for the *trans*Golgi proteins TGN38 and Glg1 were reduced in Purkinje cells in brain sections of 20- but not two-month-old KO mice. Student's t-test (over 30 cells from three mice per genotype; * $p < 0.05$). Scale bars: 10 μm. (R) A reduction of Glg1 abundance was confirmed by immunoblot analysis of total brain lysates of 20-month-old mice. Actin served as a loading control. Student's t-test (three mice per genotype; * $p < 0.05$). Error bars in (D, H, Q, R) represent mean ± SEM. (For interpretation of the references to colour in this figure legend, the reader is referred to the web version of this article.)

affected in AP5 zeta KO MEFs. In contrast, under conditions were we induced autophagy by starvation with EBSS we observed that the abundance of LC3-II was significantly increased in AP5 zeta knockout MEFs (Fig. 5B, EBSS and EBSS + Torin1). However, when we starved the cells with EBSS while inhibiting lysosomal function by Bafilomycin A1 administration, we did not observe a significant increase of LC3-II in AP5 KO MEFs compared to WT (Fig. 5B, EBSS + BafA), suggesting a block in the autophagic flux in the absence of AP5. In order to challenge this assumption, we starved WT and AP5 zeta KO MEFs for 4 h and co-stained endogenous LC3 and Lamp1 to assess co-localizing LC3/Lamp1 puncta, indicative for autolysosomes (Fig. 5C-H). In line with our western blot results (Fig. 5B) we were unable to observe a difference in

the numbers of autolysosomes (AL, LC3/LAMP1-positive yellow puncta) in basal autophagy conditions (Fig. 5C-E). Consistently, we also did not observe an increase of autophagosomes (AP, LC3-positive green puncta) and the numbers of lysosomes also did not change (Lys, Lamp1-positive red puncta) (Fig. 5C-E). However, upon starvation-induced autophagy (Fig. 5F-H), we detected a significant increase in the numbers of autophagosomes (AP, LC3, green puncta), as well as a significant decrease in the numbers of autolysosomes (AL, LC3/Lamp1, yellow puncta). Taken together, our results strongly indicate that in the absence of AP5 zeta the autophagic flux is blocked under stressed conditions, such as starvation.

Based on this observation we hypothesized that blocked autophagy
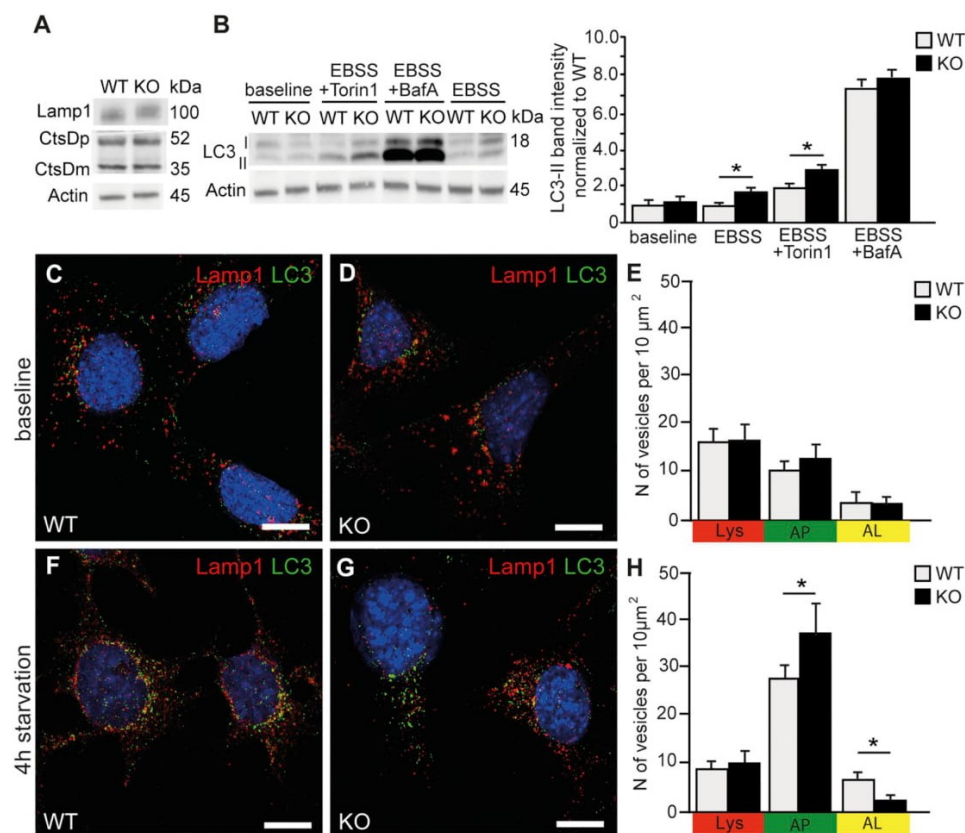
Fig. 5. Impaired autophagy upon disruption of AP5 zeta. (A) Lamp1 protein abundance and the lysosomal processing of the lysosomal protease Cathepsin D precursor (CtsDp) into the mature enzyme (CtsDm) were unchanged in KO MEFs. (B) LC3-I and LC3-II levels at baseline and upon induction of autophagy by EBSS starvation, EBSS starvation plus Torin1, and EBSS after blocking lysosomal degradation by Bafilomycin A (BafA). Actin served as a loading control. Student's t-test (three experiments; * $p < 0.05$). (C-H) Quantification of lysosomes (Lys, Lamp1-positive and LC3-negative red puncta), autophagosomes (AP, Lamp1-negative, LC3-positive green puncta), and autolysosomes (AL, Lamp1-positive and LC3-positive yellow puncta) in MEFs at baseline and upon induction of autophagy by starvation supports a defect of autophagic flux. Scale bars: 10 μm. Student's t-test (30 cells from three experiments; * $p < 0.05$). Error bars in (B, E, H) represent mean ± SEM. (For interpretation of the references to colour in this figure legend, the reader is referred to the web version of this article.)
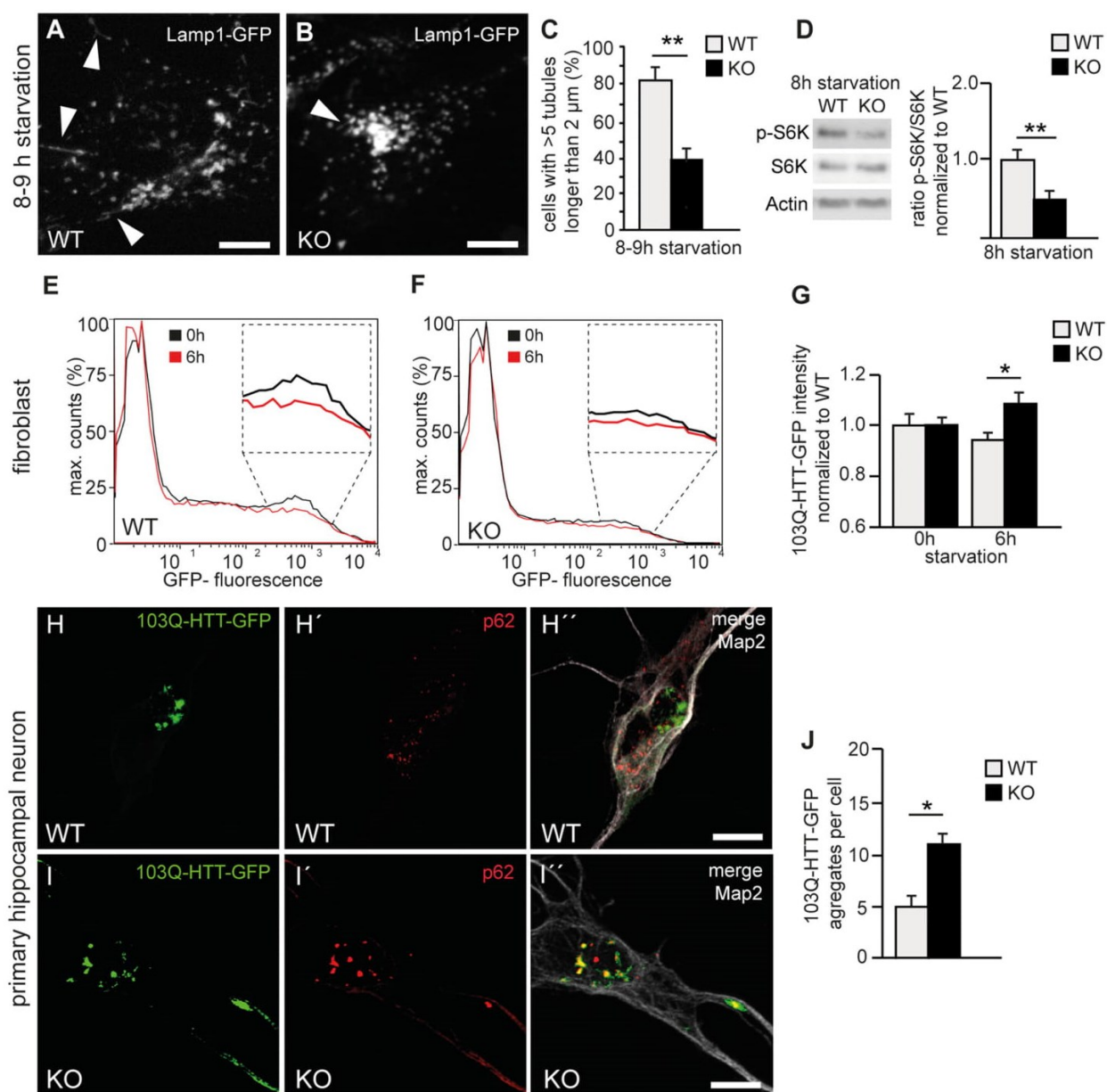
Fig. 6. Impaired autophagic lysosome reformation and increased accumulation of mutant huntingtin aggregates upon disruption of AP5 zeta. (A-C) Autophagic lysosome reformation is impaired in AP5 zeta KO. Cells with more than five Lamp1-positive tubules longer than 2 μm were counted by live cell imaging between eight and nine h of starvation. Student's *t*-test (over 30 cells from three experiments; ** p < 0.01). Scale bars: 10 μm. (D) Analysis of the abundance of phosphorylated S6K (p-S6K) compared to total S6K levels in MEFs upon 8 h of starvation. Actin served as a loading control. Student's *t*-test (*n* = 3 experiments; ** p < .01). (E-G) Median fluorescence intensity of GFP at 0 h and after 6 h of starvation in MEFs transfected with the aggregation prone 103Q huntingtin (HTT) variant. Student's *t*-test (200,000 cells from three experiments; * p < 0.05) (H-J) Number of GFP-positive aggregates per cell in primary hippocampal neurons at day five, 24 h after transfection. Neurons were stained by Map2 (shown in grey). Scale bars: 5 μm. Student's *t*-test (over 10 cells from three experiments; * p < 0.05). Error bars in (C, D, G, J) represent mean ± SEM.

in AP5 zeta knockout MEFs may be related to a defect in autophagic lysosome reformation (ALR), occurring upon prolonged starvation (Yu et al., 2010). Therefore, we assessed the extent of protolysosomal tubules forming from autolysosomes by live cell imaging of cells transfected with Lamp1-GFP upon prolonged starvation periods between 8 and 9 h (Fig. 6A, B; Video S1, S2). Strikingly, when compared to WT MEFs, the number of cells with more than five Lamp1-GFP-positive tubules that were longer than 2 μm was significantly reduced in AP5

zeta knockout MEFs (Fig. 6C). Because the recycling of lysosomes from autolysosomes was reported to be regulated by mTOR activity (Yu et al., 2010), we quantified the phosphorylation of its *bona fide* substrate p70S6 Kinase (p-S6K) in MEF lysates under prolonged starvation (eight hours) (Fig. 6D). Interestingly, we detected a significant decrease of S6K phosphorylation in starved AP5 zeta KO MEFs. This result reveals that AP5 zeta should play a role in lysosomal function under challenging conditions, such as starvation. Of note, a decrease of S6K

phosphorylation in cells compromised in ALR has been previously reported (Magalhaes et al., 2016) and is in line with our finding here.

3.6. Impaired degradation of aggregation prone Huntingtin in AP5 zeta knockout MEFs and neurons

To address our assumption that AP5 KO MEFs display a block in the autophagic flux, we transfected wild-type and AP5 zeta knockout MEFs with a GFP-labeled aggregation-prone N-terminal fragment of Huntingtin (103Q-HTT-GFP), which is largely degraded *via* selective autophagy (Ravikumar et al., 2004), and measured GFP fluorescence intensity by flow cytometry over time as an indicator for the autophagic flux. Upon starvation of AP5 KO MEFs a significant increase in GFP fluorescence was found which suggests that less 103Q-HTT-GFP was degraded under these conditions (Fig. 6E-G). This finding goes in line with our previously described results. We also addressed this question in primary neurons derived from WT and AP5 zeta KO mice. Confirming a defect in the degradative capacity of AP5 zeta KO neurons, the number of 103Q-HTT-GFP and p62-positive aggregates per neuron was significantly increased at day five *in vitro* (Fig. 6H-J).

Taken together, we provide evidence that AP5 should be a critical factor for lysosomal function and autophagic degradation in stress conditions.

3.7. Accumulation of autophagic material in vivo in AP5 zeta knockout mice

We asked whether the results obtained in MEFs and cultured neurons also apply *in vivo*. As in cultured MEFs overall Lamp1 abundance was not changed in brain lysates of 20-month-old mice and the lysosomal processing of cathepsin D was intact (Fig. 7A-C). Moreover, levels of mTOR, the key regulator of autophagy, and Beclin 1, which is involved in the control of autophagosome formation (Wirawan et al., 2012), did not differ between genotypes. Notably, however, levels of the autophagic cargo receptor p62 (Danieli and Martens, 2018), which recognizes toxic cellular waste and is then scavenged by autophagy, were significantly increased in Triton X-100 insoluble brain fractions of 20-month-old knockout mice. Moreover, the p62 signal localized to autofluorescent deposits in brain sections of 20-month-old knockout mice (Fig. 7D-D″), which also labeled for Lamp1 (Fig. 7E-E″).

In analogy to our experiments with MEFs we also quantified lysosomes, autophagosomes, and autolysosomes in Purkinje cell bodies in brain sections of two-month-old mice, a time-point before we detected autofluorescent material. While Lamp1-positive but p62-negative lysosomes (red puncta) did not differ between genotypes, p62-positive but Lamp1-negative autophagosomes (green puncta) and Lamp1- and p62-positive autolysosomes (yellow puncta) were significantly increased (Fig. 7F-H).

Thus, our *in vivo* data strongly support our previous results achieved *in vitro* (Fig. 5), demonstrating an accumulation of autophagic vesicles through a block in the autophagic flux in neurons of AP5 zeta KO mice (Fig. 6).

4. Discussion

4.1. AP5 zeta knockout mice are a valid model for SPG48

SPG11, SPG15, and SPG48 are closely related disorders with overlapping symptoms such as intellectual disability, sensorimotor neuropathy, hereditary spastic paraplegia, ataxia, and Parkinsonism. The majority of SPG48 genotypes, however, manifest with a later age at onset and intellectual disability is less frequent and rather mild compared with SPG11 and SPG15 patients (Pensato et al., 2014; Schlipf et al., 2014; Hirst et al., 2016), which often present with learning difficulties in childhood as the first symptom before the spasticity manifests during the second or third decades. In agreement with the clinical

presentation, AP5 zeta knockout mice are less severely affected than the mouse models for SPG11 and SPG15 (Khundadze et al., 2013; Varga et al., 2015) and do not develop cognitive deficits up to six months of age. While Spatacsin and Spastizin knockout mice are almost paralyzed at 20 months of age and display severe brain atrophy with neuronal loss, this does not apply to AP5 zeta knockout mice. Nevertheless, a loss of large diameter axons in the lumbar corticospinal tract as a typical hallmark of HSP (Fink, 2014) was clearly observed.

4.2. Accumulation of lysosome-related material in AP5 zeta knockout mice

Axonal loss was further associated with the occurrence of axonal swellings, which have also been reported in other mouse models of HSP such as *e.g.* SPG2 (Edgar et al., 2004), SPG4 (Tarrade et al., 2006), SPG7 (Ferreirinha et al., 2004) and, more recently, SPG51 (De Pace et al., 2018). Notably, the latter is caused by mutations in the gene encoding the epsilon subunit of the adaptor protein 4 complex (AP4) (Abou Jamra et al., 2011). Similar to results obtained for AP4 epsilon knockout mice (De Pace et al., 2018), axonal swellings are also Lamp1-positive upon disruption of AP5 zeta. From our ultrastructural analysis these swellings correspond with clusters of organelles and vesicles resembling lysosomes, autolysosomes or autophagic vesicles. Focal axonal swellings are encountered in several neurodegenerative disorders, including multiple sclerosis, motor neuron disease, spastic paraplegia, and Alzheimer's disease. Although there is growing evidence that deficits in axonal transport such as observed in SPG10 (Blackstone et al., 2011) may contribute to axonal swellings, it is yet unclear whether this also applies to AP5 knockout mice.

Lamp1-positive material also accumulates in Purkinje cell bodies of AP5 zeta knockout mice and is characterized by a strong autofluorescence and likely correlates with clusters of electron dense material of irregular shape, which are bordered by membranes, resembling residual bodies filled with indigestible materials, which are considered as nondegradable intralysosomal material (Terman and Brunk, 2004). In any case, it is conceivable that at some point these intracellular deposits impair intracellular transport and thus contribute to the cellular pathology.

4.3. Disruption of AP5 zeta results in a fragmentation of the Golgi apparatus

Previous findings suggested that AP5 is involved as a backup system for the retrieval from late endosomes to the *trans*Golgi network (TGN) based on subcellular fractionation profiling and quantitative mass spectrometry, which identified some Golgi proteins to be mis-localized (Hirst et al., 2018). Since we considered that AP5 might play a role for lysosome homeostasis, we chose a similar approach and compared the proteome of lysosomes from wild-type and knockout MEFs. Similar to the previous report (Hirst et al., 2018), we also found a number of usually Golgi resident proteins including Glg1 to be increased in the lysosomal fraction, but no obviously meaningful changes of lysosomal proteins. While the function of Glg1 is still elusive, our findings are in agreement with the idea that AP5 may play a role for the retrieval of proteins from late endosomes to the TGN, which is also supported by our data that the transport of M6PR towards the TGN was impaired in knockout MEFs. However, we also noted a robust decrease of TGN38 signals in knockout MEFs and a smaller and more vesiculated Golgi apparatus by ultrastructural analysis. Notably, similar alterations were found upon disruption of the Golgi protein GM130, which also develop Purkinje cell pathologies (Liu et al., 2017). Such alterations of the Golgi are a quite frequent finding in neurodegenerative disorders including Alzheimer's disease, Parkinson's disease, amyotrophic lateral sclerosis (ALS) and spinocerebellar ataxia (Gonatas et al., 1992; Stieber et al., 1996; Mizuno et al., 2001; Huynh et al., 2003; Nakagomi et al., 2008). Still it is tempting to speculate that the structural changes might be a consequence of a defect in the retrieval of Golgi proteins from late
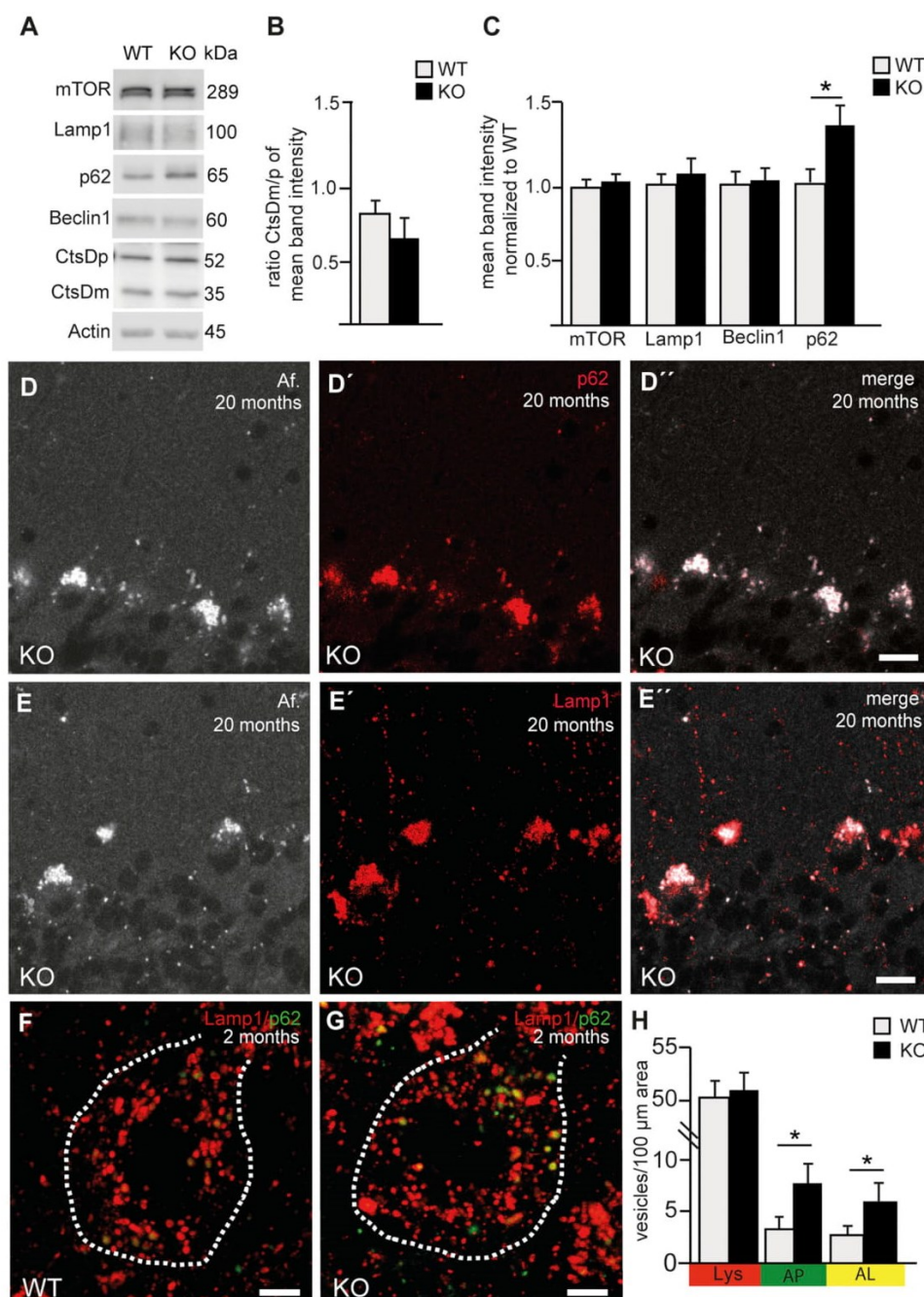
Fig. 7. Impaired autophagy in AP5 zeta knockout mice. (A-C) mTOR, Lamp1, Beclin1 abundance and lysosomal processing of the lysosomal protease Cathepsin D precursor (CtsDp) into the mature enzyme (CtsDm) are not changed in brain lysates from 20-month-old knockout mice, while p62 levels (Triton X insoluble fraction) are increased. Actin served as a loading control. Student's *t*-test (three mice per genotype; * p < 0.05). (D-E″) Autofluorescent deposits in AP5 zeta knockout brains are positive for both Lamp1 and p62. Scale bars: 10 μm. Af: Autofluorescence. (F-H) Quantification of lysosomes (Lys, Lamp1-positive and p62-negative red puncta), autophagosomes (AP, Lamp1-negative and p62-positive green puncta), and autolysosomes (AL, Lamp1-positive and p62-positive yellow puncta) in Purkinje cells in brain sections of three-month-old mice before accumulation of autofluorescent material are in agreement with a defect in autophagy. Scale bars: 5 μm. Student's *t*-test (over 30 cells from three mice per genotype; * p < 0.05). Error bars in (B, C, H) represent mean ± SEM. (For interpretation of the references to colour in this figure legend, the reader is referred to the web version of this article.)

endosomes. Our data that changes in Golgi proteins in immuno-fluorescence stainings were only observed at 20 months, but not at two months of age, rather argue for a minor role of AP5 for the retrieval from late endosomes to the TGN.

4.4. Dysfunctional autophagy upon disruption of AP5 zeta

As a first hint that autophagy under stressed conditions is compromised upon disruption of AP5 zeta, the number of autophagosomes was increased in starved knockout MEFs while the number of lysosomes was reduced. Increased autophagosome numbers were also observed in fibroblasts of SPG15 patients as well as in Spastizin knockdown studies in primary mouse neurons (Vantaggiato et al., 2013; Vantaggiato et al., 2018) and in HeLa cells upon knockdown of either Spastizin or Spatacsin (Chang et al., 2014). As also shown for Spastizin and Spatacsin (Chang et al., 2014), the extent of protolysosomal tubules forming from autolysosomes upon prolonged starvation periods was reduced in the absence of AP5 zeta. The defect in ALR in AP5 zeta deficient cells does not occur as a secondary effect of reduced Spastizin and Spatacsin protein abundance, but we cannot rule out that it is caused by a wrong localization of Spastizin and Spatacsin upon disruption of AP5 zeta. Notably, a trend towards enlargement of autolysosomes was reported after knock-down of the beta subunit of AP5, but tubulation itself was not analyzed (Chang et al., 2014). Further supporting a defect in ALR, the abundance of p-S6K was reduced in AP5 knockout MEFs and did not recover upon prolonged starvation, similar to cells lacking functional glucocerebrosidase, in which autophagic lysosome reformation is impaired (Magalhaes et al., 2016). Whether blocked autophagy in AP5 zeta knockout MEFs is a consequence of defective autophagic lysosome reformation (ALR) or *vice versa* we cannot answer for the time being.

Because lysosomes are organelles critical for terminating autophagy *via* their fusion with mature autophagosomes to generate autolysosomes that degrade autophagic materials, impairment of autophagic lysosome reformation will have consequences on the clearance of cellular components *via* autophagy. This includes the degradation of abnormal proteins, which is also largely mediated *via* autophagy (Hara et al., 2006; Komatsu et al., 2006; Mizushima, 2007) and a common cause of neuronal degeneration (Williams et al., 2006; Martini-Stoica et al., 2016). Indeed, the degradation of an aggregation prone GFP-tagged Huntingtin variant was impaired in both MEFs and primary neurons of AP5 zeta knockout mice. In the long term, defective autophagy will thus lead to the accumulation of undegraded material as observed in aged knockout mice.

In summary, we show that disruption of AP5 results in defective autophagy upon challenged conditions, which reduces the degradative capacity and causes the accumulation of autophagic cargo and possibly toxic proteins. This scenario may be aggravated by alterations of the Golgi apparatus. Future studies will hopefully help to resolve how AP5, Spastizin and Spatacsin interact to regulate autophagy and the recycling of lysosomes from autolysosomes.

Supplementary data to this article can be found online at https://doi.org/10.1016/j.nbd.2019.03.026.

Competing interests

The authors report no competing interests.

Funding

Acknowledgements

References

Abou Jamra, R., Philippe, O., Raas-Rothschild, A., Eck, S.H., Graf, E., Buchert, R., et al., 2011. Adaptor protein complex 4 deficiency causes severe autosomal-recessive intellectual disability, progressive spastic paraplegia, shy character, and short stature. Am. J. Hum. Genet. 88 (6), 788–795.

Ashburner, M., Ball, C.A., Blake, J.A., Botstein, D., Butler, H., Cherry, J.M., et al., 2000. Gene ontology: tool for the unification of biology. The Gene Ontology Consortium. Nat. Genet. 25 (1), 25–29.

Beetz, C., Koch, N., Khundadze, M., Zimmer, G., Nietzsche, S., Hertel, N., et al., 2013. A spastic paraplegia mouse model reveals REEP1-dependent ER shaping. J. Clin. Invest. 123 (10), 4273–4282.

Blackstone, C., 2018. Hereditary spastic paraplegia. Handb. Clin. Neurol. 148, 633–652.

Blackstone, C., Kane, C.J., Reid, E., 2011. Hereditary spastic paraplegias: membrane traffic and the motor pathway. Nat. Rev. Neurosci. 12, 31–42.

Chang, J., Lee, S., Blackstone, C., 2014. Spastic paraplegia proteins spastizin and spatacsin mediate autophagic lysosome reformation. J. Clin. Invest. 124 (12), 5249–5262.

Danieli, A., Martens, S., 2018. p62-mediated phase separation at the intersection of the ubiquitin-proteasome system and autophagy. J. Cell Sci. 131 (19).

De Pace, R., Skirzewski, M., Damme, M., Mattera, R., Mercurio, J., Foster, A.M., et al., 2018. Altered distribution of ATG9A and accumulation of axonal aggregates in neurons from a mouse model of AP-4 deficiency syndrome. PLoS Genet. 14 (4), e1007363.

Denton, K., Mou, Y., Xu, C.C., Shah, D., Chang, J., Blackstone, C., et al., 2018. Impaired mitochondrial dynamics underlie axonal defects in hereditary spastic paraplegias. Hum. Mol. Genet. 27 (14), 2517–2530.

Edgar, J.M., McLaughlin, M., Barrie, J.A., McCulloch, M.C., Garbern, J., Griffiths, I.R., 2004. Age-related axonal and myelin changes in the rumpshaker mutation of the Plp gene. Acta Neuropathol. 107 (4), 331–335.

Falcon-Perez, J.M., Nazarian, R., Sabatti, C., Dell'Angelica, E.C., 2005. Distribution and dynamics of Lamp1-containing endocytic organelles in fibroblasts deficient in BLOC-3. J. Cell Sci. 118 (Pt 22), 5243–5255.

Ferreirinha, F., Quattrini, A., Pirozzi, M., Valsecchi, V., Dina, G., Broccoli, V., et al., 2004. Axonal degeneration in paraplegin-deficient mice is associated with abnormal mitochondria and impairment of axonal transport. J. Clin. Invest. 113 (2), 231–242.

Fink, J.K., 2014. Hereditary spastic paraplegia: clinical principles and genetic advances. Semin. Neurol. 34 (3), 293–305.

Gonatas, N.K., Stieber, A., Mourelatos, Z., Chen, Y., Gonatas, J.O., Appel, S.H., et al., 1992. Fragmentation of the Golgi apparatus of motor neurons in amyotrophic lateral sclerosis. Am. J. Pathol. 140 (3), 731–737.

Hara, T., Nakamura, K., Matsui, M., Yamamoto, A., Nakahara, Y., Suzuki-Migishima, R., et al., 2006. Suppression of basal autophagy in neural cells causes neurodegenerative disease in mice. Nature 441 (7095), 885–889.

Hirst, J., Barlow, L.D., Francisco, G.C., Sahlender, D.A., Seaman, M.N., Dacks, J.B., et al., 2011. The fifth adaptor protein complex. PLoS Biol. 9 (10), e1001170.

Hirst, J., Borner, G.H., Edgar, J., Hein, M.Y., Mann, M., Buchholz, F., et al., 2013. Interaction between AP-5 and the hereditary spastic paraplegia proteins SPG11 and SPG15. Mol. Biol. Cell 24 (16), 2558–2569.

Hirst, J., Edgar, J.R., Esteves, T., Darios, F., Madeo, M., Chang, J., et al., 2015. Loss of AP-5 results in accumulation of aberrant endolysosomes: defining a new type of lysosomal storage disease. Hum. Mol. Genet. 24 (17), 4984–4996.

Hirst, J., Madeo, M., Smets, K., Edgar, J.R., Schols, L., Li, J., et al., 2016. Complicated spastic paraplegia in patients with AP5Z1 mutations (SPG48). Neurol. Genet. 2 (5), e98.

Hirst, J., Itzhak, D.N., Antrobus, R., Borner, G.H.H., Robinson, M.S., 2018. Role of the AP-5 adaptor protein complex in late endosome-to-Golgi retrieval. PLoS Biol. 16 (1), e2004411.

Huynh, D.P., Yang, H.T., Vakharia, H., Nguyen, D., Pulst, S.M., 2003. Expansion of the polyQ repeat in ataxin-2 alters its Golgi localization, disrupts the Golgi complex and causes cell death. Hum. Mol. Genet. 12 (13), 1485–1496.

Khundadze, M., Kollmann, K., Koch, N., Biskup, C., Nietzsche, S., Zimmer, G., et al., 2013. A hereditary spastic paraplegia mouse model supports a role of ZFYVE26/SPASTIZIN for the endolysosomal system. PLoS Genet. 9 (12), e1003988.

Komatsu, M., Waguri, S., Chiba, T., Murata, S., Iwata, J., Tanida, I., et al., 2006. Loss of autophagy in the central nervous system causes neurodegeneration in mice. Nature 441 (7095), 880–884.

Liu, C., Mei, M., Li, Q., Roboti, P., Pang, Q., Ying, Z., et al., 2017. Loss of the golgin GM130 causes Golgi disruption, Purkinje neuron loss, and ataxia in mice. Proc. Natl. Acad. Sci. U. S. A. 114 (2), 346–351.

Magalhaes, J., Gegg, M.E., Migdalska-Richards, A., Doherty, M.K., Whitfield, P.D., Schapira, A.H., 2016. Autophagic lysosome reformation dysfunction in glucocerebrosidase deficient cells: relevance to Parkinson disease. Hum. Mol. Genet. 25 (16), 3432–3445.

Martini-Stoica, H., Xu, Y., Ballabio, A., Zheng, H., 2016. The autophagy-Lysosomal pathway in Neurodegeneration: a TFEB perspective. Trends Neurosci. 39 (4), 221–234.

Meriin, A.B., Zhang, X., He, X., Newnam, G.P., Chernoff, Y.O., Sherman, M.Y., 2002. Huntington toxicity in yeast model depends on polyglutamine aggregation mediated by a prion-like protein Rnq1. J. Cell Biol. 157 (6), 997–1004.

Mizuno, Y., Hattori, N., Kitada, T., Matsumine, H., Mori, H., Shimura, H., et al., 2001. Familial Parkinson's disease. Alpha-synuclein and parkin. Adv. Neurol. 86, 13–21.

Mizushima, N., 2007. Autophagy: process and function. Genes Dev. 21 (22), 2861–2873.

Nakagomi, S., Barsoum, M.J., Bossy-Wetzel, E., Sutterlin, C., Malhotra, V., Lipton, S.A., 2008. A Golgi fragmentation pathway in neurodegeneration. Neurobiol. Dis. 29 (2), 221–231.

Pensato, V., Castellotti, B., Gellera, C., Pareyson, D., Ciano, C., Nanetti, L., et al., 2014. Overlapping phenotypes in complex spastic paraplegias SPG11, SPG15, SPG35 and SPG48. Brain 137 (Pt 7), 1907–1920.

Ravikumar, B., Vacher, C., Berger, Z., Davies, J.E., Luo, S., Oroz, L.G., et al., 2004. Inhibition of mTOR induces autophagy and reduces toxicity of polyglutamine expansions in fly and mouse models of Huntington disease. Nat. Genet. 36 (6), 585–595.

Sagona, A.P., Nezis, I.P., Pedersen, N.M., Liestol, K., Poulton, J., Rusten, T.E., et al., 2010. PtdIns(3)P controls cytokinesis through KIF13A-mediated recruitment of FYVE-CENT to the midbody. Nat. Cell Biol. 12 (4), 362–371.

Schlipf, N.A., Schule, R., Klimpe, S., Karle, K.N., Synofzik, M., Wolf, J., et al., 2014. AP5Z1/SPG48 frequency in autosomal recessive and sporadic spastic paraplegia. Mol. Genet. Genomic Med. 2 (5), 379–382.

Sinning, A., Liebmann, L., Kougioumtzes, A., Westermann, M., Bruehl, C., Hubner, C.A., 2011. Synaptic glutamate release is modulated by the Na$^+$-driven Cl$^-$/HCO$_3^-$ exchanger Slc4a8. J. Neurosci. 31 (20), 7300–7311.

Skarnes, W.C., Rosen, B., West, A.P., Koutsourakis, M., Bushell, W., Iyer, V., et al., 2011. A conditional knockout resource for the genome-wide study of mouse gene function. Nature 474 (7351), 337–342.

Slabicki, M., Theis, M., Krastev, D.B., Samsonov, S., Mundwiller, E., Junqueira, M., et al., 2010. A genome-scale DNA repair RNAi screen identifies SPG48 as a novel gene associated with hereditary spastic paraplegia. PLoS Biol. 8 (6), e1000408.

Stieber, A., Mourelatos, Z., Gonatas, N.K., 1996. In Alzheimer's disease the Golgi apparatus of a population of neurons without neurofibrillary tangles is fragmented and atrophic. Am. J. Pathol. 148 (2), 415–426.

Tarrade, A., Fassier, C., Courageot, S., Charvin, D., Vitte, J., Peris, L., et al., 2006. A mutation of spastin is responsible for swellings and impairment of transport in a region of axon characterized by changes in microtubule composition. Hum. Mol. Genet. 15 (24), 3544–3558.

Terman, A., Brunk, U.T., 2004. Lipofuscin. Int. J. Biochem. Cell Biol. 36 (8), 1400–1404.

The Gene Ontology C, 2017. Expansion of the gene ontology knowledgebase and resources. Nucleic Acids Res. 45 (D1), D331–D338.

Thelen, M., Winter, D., Braulke, T., Gieselmann, V., 2017. SILAC-based comparative proteomic analysis of lysosomes from mammalian cells using LC-MS/MS. Methods Mol. Biol. 1594, 1–18.

Vantaggiato, C., Crimella, C., Airoldi, G., Polishchuk, R., Bonato, S., Brighina, E., et al., 2013. Defective autophagy in spastizin mutated patients with hereditary spastic paraparesis type 15. Brain 136, 3119–3139 Pt 10.

Vantaggiato, C., Clementi, E., Bassi, M.T., 2014. ZFYVE26/SPASTIZIN: a close link between complicated hereditary spastic paraparesis and autophagy. Autophagy 10 (2), 374–375.

Vantaggiato, C., Panzeri, E., Castelli, M., Citterio, A., Arnoldi, A., Santorelli, F.M., et al., 2018. ZFYVE26/SPASTIZIN and SPG11/SPATACSIN mutations in hereditary spastic paraplegia types AR-SPG15 and AR-SPG11 have different effects on autophagy and endocytosis. Autophagy 1–24.

Varga, R.E., Khundadze, M., Damme, M., Nietzsche, S., Hoffmann, B., Stauber, T., et al., 2015. In vivo evidence for lysosome depletion and impaired Autophagic clearance in hereditary spastic paraplegia type SPG11. PLoS Genet. 11 (8), e1005454.

Weinert, S., Jabs, S., Supanchart, C., Schweizer, M., Gimber, N., Richter, M., et al., 2010. Lysosomal pathology and osteopetrosis upon loss of H$^+$-driven lysosomal Cl$^-$ accumulation. Science 328 (5984), 1401–1403.

Williams, A., Jahreiss, L., Sarkar, S., Saiki, S., Menzies, F.M., Ravikumar, B., et al., 2006. Aggregate-prone proteins are cleared from the cytosol by autophagy: therapeutic implications. Curr. Top. Dev. Biol. 76, 89–101.

Wirawan, E., Lippens, S., Vanden Berghe, T., Romagnoli, A., Fimia, G.M., Piacentini, M., et al., 2012. Beclin1: a role in membrane dynamics and beyond. Autophagy 8 (1), 6–17.

Yu, L., McPhee, C.K., Zheng, L., Mardones, G.A., Rong, Y., Peng, J., et al., 2010. Termination of autophagy and reformation of lysosomes regulated by mTOR. Nature 465 (7300), 942–946.

34

3.1.1 Supplementary Material

Extended experimental procedures

Behavioral analysis

Spatial memory was assessed in a Morris water maze, consisting of a circular tank (diameter 120 cm, depth 60 cm) filled with water at 23±1 °C at a depth of 30 cm as described in (Khundadze et al., 2013).

For gait analysis mice were trained to walk on a horizontal 20 cm elevated plastic beam (1,000 mm long, either 38 mm broad for cohorts between 8 and 12 months of age or 48 mm broad for mice with an age between 16 and 20 months of age) leading to their home cage. After the initial learning phase, the foot-base-angle at toe-off positions of the hind-paws was measured in ImageJ using single video frames from recordings of beam walking mice.

Immunoblot analyses

For immunoblot analysis, brain samples were homogenized in a buffer containing 25 mM sucrose, 50 mM Tris-HCl pH 7.4, 1 mM EDTA, completed with protease inhibitor mix. The homogenates were centrifuged at 500 g at 4°C for 10 min. The supernatants were collected and mixed with a buffer containing 25 mM sucrose, 50 mM Tris-HCl pH 7.4, 1 mM EDTA, 1% TritonX-100 completed with proteinase inhibitors and gently rotated for 1 h at 4°C (i.e: triton X-100 soluble fraction). After centrifugation at 13,000 g and 4°C for 15 minutes the pellets were dissolved in 1% (w/v) SDS/PBS buffer (i.e: triton X-100 insoluble fraction). The samples were denatured at 95°C in Lämmli buffer and separated in 4-20% pre-cast gradient gels (BioRad, Germany). After transfer on a PVDF membrane (Roche, Switzerland), 2.5% (w/v) milk powder with 2.5% (w/v) BSA in TBS-T buffer (Tris-buffered saline with Tween 20, Sigma-Aldrich, Germany) was used in order to block the membrane. Primary and secondary antibodies were incubated in blocking solution. For detection of proteins ECL Western Blotting Detection System (GE Healthcare Amersham, USA) was used. For autophagy studies mouse embryonic fibroblasts (MEFs) were either incubated for 6 h with 1 µM Torin 1 (Merck, Germany) to initiate or 100 nM Bafilomycin A (Santa Cruz, USA) to block autophagy and subsequently lysed in a buffer containing 50 mM Tris-HCl pH 8.0, 120 mM NaCl, 0.5% NP40, 2 mM EDTA completed with protease inhibitor mix and PhosSTOP (Roche, Switzerland). The lysates were rotated for 30 minutes and centrifuged at 10,000 g at 4°C. The resulting supernatant was denatured in sample buffer for 5 minutes at 95°C and separated in 8-15% polyacrylamide pre-cast gradient gels. 5% BSA in TBS-T served as blocking solution. Antibodies used for this study are available as Supplementary information.

Antibodies

For immunoblotting a polyclonal affinity purified rabbit anti-Zfyve26 antibody (Khundadze etal., 2013) was used diluted 1:50. The following commercially obtained antibodies were used: rabbit anti-AP5Z1, 1:500 (Atlas antibodies, USA); rabbit anti-SPATACSIN, 1:500, (Protein Tech, UK); mouse anti-M6PR (Cation-independent mannose 6-phosphate receptor), 1:100 for the retrieval assay (Abcam, UK); rabbit anti-Glg1, 1:500 for immunofluorescence studies and 1:1,000 for immunoblot analysis (Abcam, UK); mouse anti-NF200, 1:50 (Sigma-Aldrich, Germany); mouse anti-Parvalbumin, 1:5,000 (Swant, Switzerland); mouse anti-Calnexin, 1:1,000 (BD Biosciences, USA); mouse anti-Giantin, 1:1,000 (Enzo Life Sciences, Germany); rabbit anti-GM130, 1:500 (Sigma Aldrich, Germany); rat anti-Lamp1, 1:200 for immunofluorescence and 1:500 for immunoblot studies (BD Pharmigen, USA); mouse anti-p62, 1:500 for immunofluorescence and 1:1,000 for immunoblot analysis (Abcam, UK); rabbit anti-TGN38, 1:250 for immunofluorescence studies and 1:1,000 for immunoblot analysis (Santa Cruz, USA); rabbit anti-Beclin-1, 1:1,000 and mouse anti-CtsD, 1:500 (Santa Cruz, USA); guinea pig anti-MAP2, 1:1,000 (Synaptic Systems, Germany); mouse anti–β-actin, 1:5,000 (Abcam, UK); rabbit anti-LC3, 1:250 for immunofluorescence and 1:500 for immunoblot analysis; rabbit anti-mTOR, 1:1,000; rabbit anti-70S6-kinase, 1:500 and rabbit anti-phospho-70S6-kinase, 1:500 (Cell Signaling, USA). Mouse anti-Mtc02, 1:500 (Abcam, UK). Horseradish peroxidase–labelled secondary antibodies for Western blotting: goat anti-rabbit and goat anti-mouse, both 1:4,000 (Amersham Bioscience, UK); goat anti-rat, 1:1,000 (Santa Cruz; USA).

Fluorescently labelled secondary antibodies: goat anti-guinea pig-Alexa Fluor 546; goat anti-mouse-Alexa Fluor 488 and 546, goat anti-rabbit Alexa Fluor 488 and 546, 1:1,000 (Invitrogen, Germany). Goat anti-rabbit, goat anti-mouse and goat anti-rat Cy5, 1:1,000 (Invitrogen, Germany). Nuclei were stained with Hoechst-33258, 1:10,000 (Molecular Probes, Germany).

Flow cytometry

Flow cytometric measurements were performed with an LSR Fortessa system (BD Biosciences, USA). Data were acquired with the BD FACSDIVA V8.0.1 software (BD Biosciences, USA). In addition to GFP fluorescence, FSC (forward scatter) and SSC (side scatter) signals were acquired. For analysis of HTT degradation, MEF cells were transfected with 103Q-HTT-GFP, pretreated with MG-132 (1μM, Merck Millipore, Germany) and Cycloheximide (10 μg/ml, Sigma-Aldrich, Germany) and starved in EBSS supplemented with MG-132 and Cycloheximide for 0 and 6 h. Cells were fixed in 4% PFA in PBS at the respective time points

and stored at 4°C for a maximum of 2 days until measurement. Prior to analysis, cell debris and aggregates were excluded by pre-gating on FSC/SSC. Median fluorescence intensities were calculated using the FlowLogic 700.2A software (Inivai Technologies Pty. Ltd).

Spectral analysis

Images of Purkinje cells of sagittal brain sections were captured with a laser scanning microscope (TCS SP8 Leica Microsystems, Germany). The fluorescent signals of deposits and the Cy5 secondary antibodies were recorded and further analyzed by linear unmixing as described previously (Khundadze et al., 2013).

Ultrastructural analysis and morphometry

For the ultrastructural analysis of the Golgi apparatus, cells were fixed at room temperature by adding fixative (2.5% glutaraldehyde and 2% formaldehyde, Electron Microscopy Sciences) in 0.1M phosphate buffer, (pH7.4) 1:1 to culture medium for 10 min. This was replaced by fresh fixative for 2 hours at room temperature. Cells were then postfixed with 1% OsO_4/1.5% $K_3Fe(III)(CN)_6$ in 0.065 M phosphate buffer, for 2 h at 4°C and finally 1 h with 0.5% uranyl acetate in demineralized water. After fixation cells were dehydrated and embedded in Epon epoxy resin (Polysciences, USA). Ultrathin sections of 60 nm were contrasted with uranyl acetate and lead citrate using the AC20 (Leica) and examined with a T12 electron microscope (ThermoFisher, Eindhoven, the Netherlands). Images were collected from three different grids per condition. Random pictures of 40 cells per set were collected for quantification. All morphometric measurements were done using the ImageJ software. To measure the compactness of the area containing the Golgi complex, cells were randomly screened for the presence of one or more Golgi stacks. When a Golgi area was encountered the smallest possible ellipse enclosing all visible Golgi stacks was drawn in ImageJ and the surface area of that ellipse was measured. This was done for 40 cells per condition, after which the average surface area was calculated. Similarly, the area of 40 individual Golgi stacks per condition was measured with the ellipse selection tool.

Video S1. Lysosomal tubulation in WT MEFs (attached in CD-ROM).

Video S2. Lysosomal tubulation in AP5 zeta KO MEFs (attached in CD-ROM).
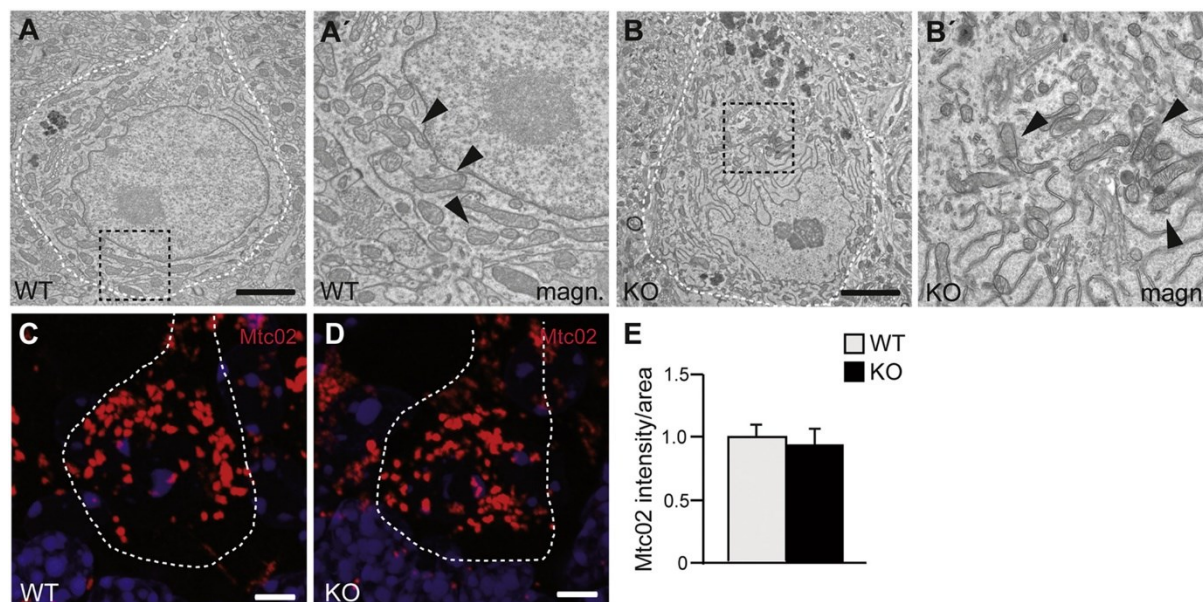
Fig. S1. AP5 zeta knockout mice do not show major alterations of mitochondria. (A-B´) Electron microscopic images of Purkinje cells. The cell bodies are indicated by a dashed line. The magnifications of the highlighted regions in (A) and (B) are shown in (A´) and (B´), respectively. Individual mitochondria are indicated by arrowheads. Scale bars: 2.5 µm for (A, B). The distribution and the overall intensity of the mitochondrial protein marker Mtc02 (red) was not changed in Purkinje cell bodies from brain sections of 20-month-old mice. Scale bars: 5 µm. Student's t-test (>30 cells from three mice per genotype; $*p < 0.05$).
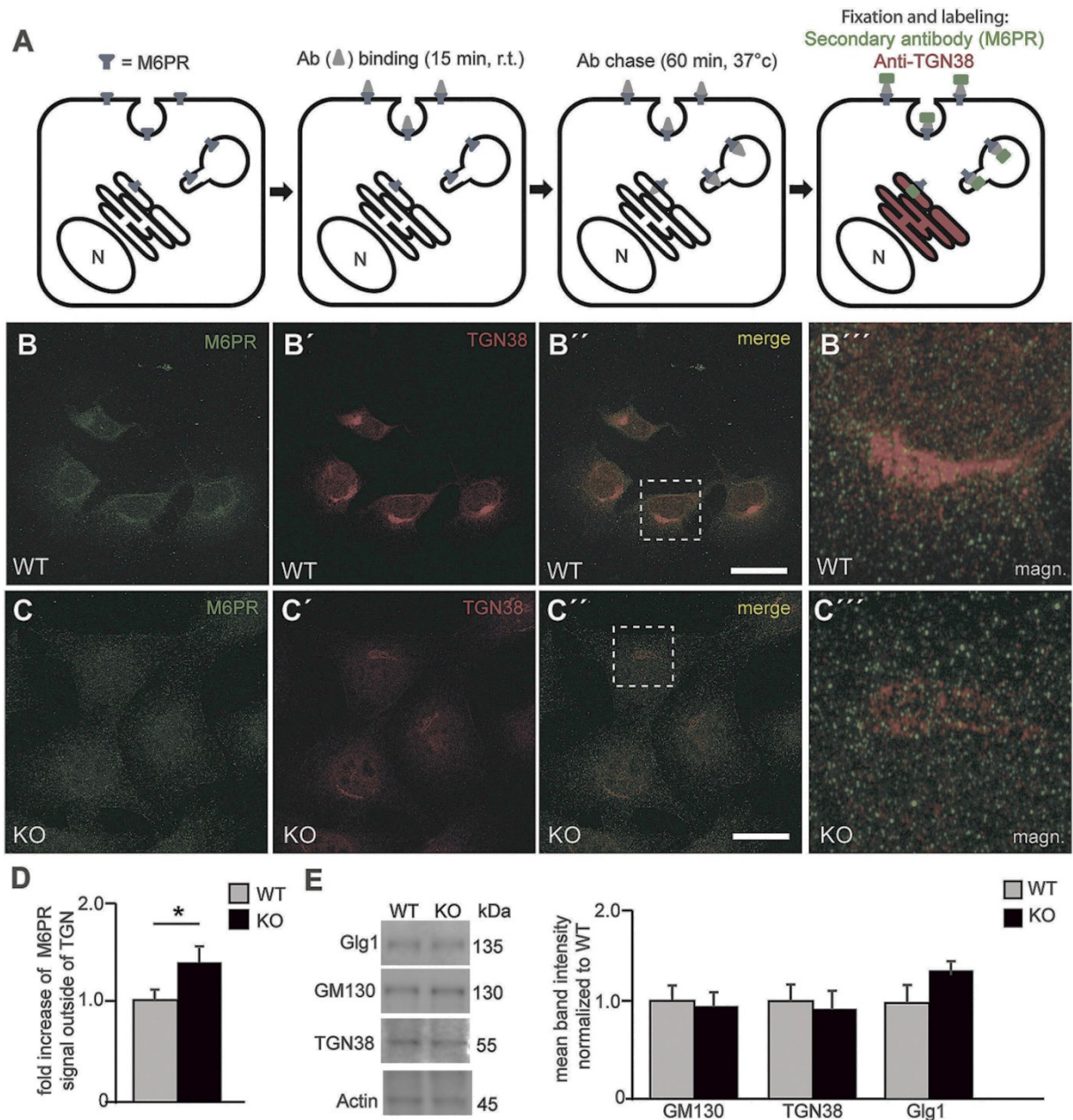
Fig. S2. Impaired late endosome-to-Golgi retrieval in AP5 zeta deficient MEFs. (A) Schematic illustration of the M6PR retrieval assay. Ab: antibody; M6PR: mannose-6-phosphate receptor; N: nucleus; KO: knockout; TGN: *trans*Golgi network. (B-C″) Indirect immunofluorescence microscopy of wild-type and AP5 zeta knockout MEFs, which were pulse chased with an antibody against M6PR. In knockout cells, more M6PRs are found outside of the *trans*Golgi network, which is labeled by TGN38. Scale bar: 20 µm. (D) Analysis of TGN38 and M6PR co-localization using the ZEN Blue co-localization plugin. Student's *t*-test (>100 cells were analyzed per genotype; three independent experiments; * $p < 0.05$). (E) Protein abundance of Glg1 and TGN38 was not significantly changed in total brain lysates of six-month-old mice. Actin served as a loading control. Student's *t*-test (three mice per genotype; $p > 0.05$). Error bars in (D, E) represent mean ± SEM.

Supplementary table 1. List of upregulated proteins identified in lysosomal fractions from WT and KO by SILAC-based mass spectrometric analysis (black: Golgi associated proteins; lilac: endosome-lysosome associated proteins)

Uniprot ID	Description	Gene name	Abundance ratio: KO / WT	Log 2 fold change	Abundance ratio adj. P-value: KO / WT	Neg log10 p values
Q02013	Aquaporin-1 OS=Mus musculus GN=Aqp1 PE=1 SV=3	Aqp1	21,02	4,393690764	2,8E-16	15,55284197
Q6IME9	Keratin, type II cytoskeletal 72 OS=Mus musculus GN=Krt72 PE=3 SV=1	Krt72; Krt72-ps	31,813	4,991544521	2,8E-16	15,55284197
Q8VHY0	Chondroitin sulfate proteoglycan 4 OS=Mus musculus GN=Cspg4 PE=1 SV=3	Cspg4	11,216	3,487486349	6,13149E-15	14,21243371
Q9Z2K1	Keratin, type I cytoskeletal 16 OS=Mus musculus GN=Krt16 PE=1 SV=3	Krt16	11,632	3,540027269	1,2179E-14	13,91438857
Q07235	Glia-derived nexin OS=Mus musculus GN=Serpine2 PE=1 SV=2	Serpine2	10,448	3,385154897	3,0036E-14	13,52235742
Q8K479	Complement C1q tumor necrosis factor-related protein 5 OS=Mus musculus GN=C1qtnf5 PE=1 SV=1	Mfrp; C1qtnf5	17,456	4,125651102	3,0036E-14	13,52235742
P97447	Four and a half LIM domains protein 1 OS=Mus musculus GN=Fhl1 PE=1 SV=3	Fhl1	13,83	3,789729251	3,07664E-12	11,51192355
P14602	Heat shock protein beta-1 OS=Mus musculus GN=Hspb1 PE=1 SV=3	Hspb1	12,752	3,672651629	6,58955E-12	11,18114408
Q99JY8	Phospholipid phosphatase 3 OS=Mus musculus GN=Plpp3 PE=1 SV=1	Ppap2b; Plpp3	8,127	3,022722894	2,06102E-11	10,68591821
Q9CS42	Ribose-phosphate pyrophosphokinase 2 OS=Mus musculus GN=Prps2 PE=1 SV=4	Prps2	12,032	3,588804567	7,6682E-11	10,1153066
Q8CI59	Metalloreductase STEAP3 OS=Mus musculus GN=Steap3 PE=1 SV=1	Steap3	8,318	3,056236685	8,42688E-11	10,07433324
Q62009	Periostin OS=Mus musculus GN=Postn PE=1 SV=2	Postn	7,469	2,900915098	1,52025E-10	9,818085569
Q8R0Y6	Cytosolic 10-formyltetrahydrofolate dehydrogenase OS=Mus musculus GN=Aldh1l1 PE=1 SV=1	Aldh1l1	7,841	2,97103766	3,3764E-10	9,471546481
P97299	Secreted frizzled-related protein 2 OS=Mus musculus GN=Sfrp2 PE=2 SV=2	Sfrp2	6,461	2,691757475	3,46437E-09	8,460375583
Q922P8	Transmembrane protein 132A OS=Mus musculus GN=Tmem132a PE=1 SV=2	Tmem132a	8,382	3,067294521	5,51646E-08	7,258339483
E9Q557	Desmoplakin OS=Mus musculus GN=Dsp PE=1 SV=1	Dsp	6,354	2,66766509	1,17468E-07	6,930081494
Q61391	Neprilysin OS=Mus musculus GN=Mme PE=1 SV=3	Mme	5,417	2,437494091	1,54713E-07	6,81047413
Q06335	Amyloid-like protein 2 OS=Mus musculus GN=Aplp2 PE=1 SV=4	Aplp2	5,988	2,582074221	1,72741E-07	6,762603387
Q62219	Transforming growth factor beta-1-induced transcript 1 protein OS=Mus musculus GN=Tgfb1i1 PE=1	Tgfb1i1	9,563	3,257463276	5,31945E-07	6,274133331
Q9JLM8	Serine/threonine-protein kinase DCLK1 OS=Mus musculus GN=Dclk1 PE=1 SV=1	Dclk1	6,51	2,702657543	6,29172E-07	6,201230529
Q9QWL7	Keratin, type I cytoskeletal 17 OS=Mus musculus GN=Krt17 PE=1 SV=3	Krt17	6,241	2,641777212	1,12964E-06	5,947059029
Q922U2	Keratin, type II cytoskeletal 5 OS=Mus musculus GN=Krt5 PE=1 SV=1	Krt5	5,266	2,396707521	3,01339E-06	5,520944261
Q9R257	Heme-binding protein 1 OS=Mus musculus GN=Hebp1 PE=1 SV=2	Hebp1	5,378	2,427069755	6,86863E-06	5,16312994
Q9CZT5	Vasorin OS=Mus musculus GN=Vasn PE=2 SV=2	Vasn	4,259	2,09051473	1,03947E-05	4,983186506
Q61781	Keratin, type I cytoskeletal 14 OS=Mus musculus GN=Krt14 PE=1 SV=2	Krt14	5,248	2,39176772	1,04634E-05	4,980327327
Q78S06	Protein SYS1 homolog OS=Mus musculus GN=Sys1 PE=2	Sys1	5,801	2,536301619	2,17979E-05	4,661585907
O70258	SV=1 Epsilon-sarcoglycan OS=Mus musculus GN=Sgce PE=1 SV=2	Sgce	5,939	2,570220033	3,11187E-05	4,5069786
Q9R0Y5	Adenylate kinase isoenzyme 1 OS=Mus musculus GN=Ak1 PE=1 SV=1	Ak1	4,869	2,283625501	4,24108E-05	4,372523578
P21460	Cystatin-C OS=Mus musculus GN=Cst3 PE=1 SV=2	Cst3	3,961	1,985864701	7,26797E-05	4,138586784
P28653	Biglycan OS=Mus musculus GN=Bgn PE=1 SV=1	Bgn	3,756	1,909197063	9,42249E-05	4,025834513
P11862	Growth arrest-specific protein 2 OS=Mus musculus GN=Gas2 PE=1 SV=1	Gas2	4,8	2,263034406	0,000115126	3,938826937
P21956	Lactadherin OS=Mus musculus GN=Mfge8 PE=1 SV=3	Mfge8	3,691	1,884011738	0,000123484	3,908390477
Q64442	Sorbitol dehydrogenase OS=Mus musculus GN=Sord PE=1 SV=3	Sord	5,747	2,522809049	0,000143494	3,84316706
P14094	Sodium/potassium-transporting ATPase subunit beta-1 OS=Mus musculus GN=Atp1b1 PE=1 SV=1	Atp1b1	3,707	1,890252115	0,000168503	3,773392271
O35459	Delta(3,5)-Delta(2,4)-dienoyl-CoA isomerase, mitochondrial OS=Mus musculus GN=Ech1 PE=1 SV=1	Ech1	4,388	2,133563526	0,000179754	3,745322282
P16110	Galectin-3 OS=Mus musculus GN=Lgals3 PE=1 SV=3	Lgals3	3,498	1,806530289	0,000269102	3,570082522
P09602	Non-histone chromosomal protein HMG-17 OS=Mus musculus GN=Hmgn2 PE=1 SV=2	Hmgn2; Gm7931	5,058	2,338567037	0,000269102	3,570082522
Q9EQJ0	Two pore calcium channel protein 1 OS=Mus musculus GN=Tpcn1 PE=1 SV=1	Tpcn1	4,881	2,287176752	0,000368239	3,433869845

P97350	Plakophilin-1 OS=Mus musculus GN=Pkp1 PE=1 SV=1	Pkp1	4,129	2,045792419	0,000398538	3,399530041
P35441	Thrombospondin-1 OS=Mus musculus GN=Thbs1 PE=1 SV=1	Thbs1	3,361	1,748890543	0,000473132	3,325017655
Q64133	Amine oxidase [flavin-containing] A OS=Mus musculus GN=Maoa PE=1 SV=3	Maoa	3,36	1,748461233	0,000473654	3,324539055
O08532	Voltage-dependent calcium channel subunit alpha-2/delta-1 OS=Mus musculus GN=Cacna2d1 PE=1	Cacna2d1	3,37	1,752748591	0,000504325	3,297289575
P07091	Protein S100-A4 OS=Mus musculus GN=S100a4 PE=1 SV=1	S100a4	3,996	1,998556583	0,000515848	3,287477954
Q91VK4	Integral membrane protein 2C OS=Mus musculus GN=Itm2c PE=1 SV=2	Itm2c	3,581	1,840362519	0,000529314	3,276286706
P97857	A disintegrin and metalloproteinase with thrombospondin motifs 1 OS=Mus musculus GN=Adamts1	Adamts1	3,449	1,786178129	0,000678024	3,168755224
Q62087	Serum paraoxonase/lactonase 3 OS=Mus musculus GN=Pon3 PE=1 SV=2	Pon3	3,732	1,899948986	0,000801663	3,096008421
Q9JKZ2	Sodium/myo-inositol cotransporter OS=Mus musculus GN=Slc5a3 PE=1 SV=2	Slc5a3	3,618	1,855192408	0,00084581	3,072727436
Q9CZ52	Anthrax toxin receptor 1 OS=Mus musculus GN=Antxr1 PE=1 SV=2	Antxr1	4,396	2,136191386	0,000981958	3,007907267
Q9CQW9	Interferon-induced transmembrane protein 3 OS=Mus musculus GN=Ifitm3 PE=1 SV=1	Ifitm3	3,154	1,65718266	0,001125237	2,948755988
Q9R112	Sulfide:quinone oxidoreductase, mitochondrial OS=Mus musculus GN=Sqor PE=1 SV=3	Sqrdl; Sqor	3,325	1,733354341	0,001176533	2,929395945
P25785	Metalloproteinase inhibitor 2 OS=Mus musculus GN=Timp2 PE=1 SV=2	Timp2	4,026	2,009347172	0,001303744	2,884807685
Q61838	Pregnancy zone protein OS=Mus musculus GN=Pzp PE=1 SV=3	Pzp	3,313	1,728138203	0,001311109	2,882361077
Q9D6X6	Serine protease 23 OS=Mus musculus GN=Prss23 PE=2 SV=2	Prss23	3,707	1,890252115	0,001311867	2,882110208
Q8R2Q8	Bone marrow stromal antigen 2 OS=Mus musculus GN=Bst2 PE=1 SV=1	Bst2	3,073	1,619647767	0,001574135	2,802958049
P97333	Neuropilin-1 OS=Mus musculus GN=Nrp1 PE=1 SV=2	Nrp1	3,565	1,833902077	0,00201608	2,69549223
Q6NSU3	Glycosyltransferase 8 domain-containing protein 1 OS=Mus musculus GN=Glt8d1 PE=1 SV=1	Glt8d1	3,689	1,883229789	0,00235694	2,62765144
P06151	L-lactate dehydrogenase A chain OS=Mus musculus GN=Ldha PE=1 SV=3	Ldha	2,97	1,570462931	0,002460382	2,608997493
Q61543	Golgi apparatus protein 1 OS=Mus musculus GN=Glg1 PE=1 SV=1	Glg1	2,963	1,567058626	0,00252347	2,598001797
Q9D7S7	60S ribosomal protein L22-like 1 OS=Mus musculus GN=Rpl22l1 PE=1 SV=1	Rpl22l1	3,166	1,662661255	0,002847922	2,545471918
P00342	L-lactate dehydrogenase C chain OS=Mus musculus GN=Ldhc PE=1 SV=2	Ldhc	2,971	1,570948605	0,003220276	2,492106919
P35492	Histidine ammonia-lyase OS=Mus musculus GN=Hal PE=1 SV=1	Hal	3,363	1,749748779	0,003565009	2,447939367
Q61469	Phospholipid phosphatase 1 OS=Mus musculus GN=Plpp1 PE=1 SV=1	Ppap2a; Plpp1	2,955	1,56315813	0,003582945	2,445759831
Q8CGU1	Calcium-binding and coiled-coil domain-containing protein 1 OS=Mus musculus GN=Calcoco1 PE=1	Calcoco1	3,73	1,89917563	0,003753731	2,425536869
Q9CQ91	NADH dehydrogenase [ubiquinone] 1 alpha subcomplex subunit 3 OS=Mus musculus GN=Ndufa3 PE	Ndufa3	3,832	1,938097561	0,004014885	2,396326937
Q3TW96	UDP-N-acetylhexosamine pyrophosphorylase-like protein 1 OS=Mus musculus GN=Uap1l1 PE=1 SV=	Uap1l1	2,864	1,518031493	0,004092777	2,387981954
Q8VCR7	Protein ABHD14B OS=Mus musculus GN=Abhd14b PE=1 SV=1	Abhd14b	3,308	1,725959235	0,004143421	2,38264092
P08074	Carbonyl reductase [NADPH] 2 OS=Mus musculus GN=Cbr2 PE=1 SV=1	Cbr2	2,823	1,497229129	0,004445661	2,352063699
Q61292	Laminin subunit beta-2 OS=Mus musculus GN=Lamb2 PE=1 SV=2	Lamb2	3,039	1,603596675	0,004489824	2,347770725
P12023	Amyloid-beta A4 protein OS=Mus musculus GN=App PE=1 SV=3	App	2,799	1,484911487	0,004862315	2,313156904
Q3V4B5	COMM domain-containing protein 6 OS=Mus musculus GN=Commd6 PE=1 SV=1	Commd6	3,354	1,745882689	0,004862315	2,313156904
P56818	Beta-secretase 1 OS=Mus musculus GN=Bace1 PE=1 SV=2	Bace1	3,253	1,701770822	0,004862315	2,313156904
Q9CQH7	Transcription factor BTF3 homolog 4 OS=Mus musculus GN=Btf3l4 PE=1 SV=1	Btf3l4	3,499	1,806942665	0,004862315	2,313156904
Q80Z71	Tenascin-N OS=Mus musculus GN=Tnn PE=1 SV=2	Tnn	3,268	1,708407983	0,005081762	2,293985694
Q9R1Q6	Transmembrane protein 176B OS=Mus musculus GN=Tmem176b PE=1 SV=1	Tmem176b	3,183	1,670387157	0,005081762	2,293985694
Q4FZC9	Nesprin-3 OS=Mus musculus GN=Syne3 PE=1 SV=1	4831426I19Rik; Syn	3,68	1,879705766	0,005370696	2,269969449
Q8K007	Extracellular sulfatase Sulf-1 OS=Mus musculus GN=Sulf1 PE=2 SV=1	Sulf1	3,494	1,804879608	0,005526973	2,257512655
Q00560	Interleukin-6 receptor subunit beta OS=Mus musculus GN=Il6st PE=1 SV=2	Il6st	2,85	1,510961919	0,008215772	2,085351645
P08121	Collagen alpha-1(III) chain OS=Mus musculus GN=Col3a1 PE=1 SV=4	Col3a1	2,658	1,410341105	0,008734084	2,05878266
P54071	Isocitrate dehydrogenase [NADP], mitochondrial OS=Mus musculus GN=Idh2 PE=1 SV=3	Idh2	2,651	1,40653667	0,008987871	2,046343178
O89051	Integral membrane protein 2B OS=Mus musculus GN=Itm2b PE=1 SV=1	Itm2b	2,612	1,385154897	0,010588891	1,975149513
Q9CY18	Sorting nexin-7 OS=Mus musculus GN=Snx7 PE=1 SV=1	Snx7	2,95	1,560714954	0,010769564	1,967801873

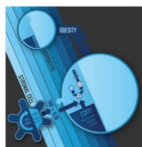|						
Q3UKC1	Tax1-binding protein 1 homolog OS=Mus musculus GN=Tax1bp1 PE=1 SV=2	Tax1bp1	2,987	1,578697238	0,011174681	1,95176488
Q9QZ85	Interferon-inducible GTPase 1 OS=Mus musculus GN=Iigp1 PE=1 SV=2	Iigp1; Iigp1b	2,948	1,559736524	0,011581481	1,936235907
Q91ZJ5	UTP--glucose-1-phosphate uridylyltransferase OS=Mus musculus GN=Ugp2 PE=1 SV=3	Ugp2	2,695	1,430285273	0,011581481	1,936235907
Q60961	Lysosomal-associated transmembrane protein 4A OS=Mus musculus GN=Laptm4a PE=1 SV=1	Laptm4a	2,654	1,408168371	0,01426252	1,845803732
P47934	Carnitine O-acetyltransferase OS=Mus musculus GN=Crat PE=1 SV=3	Crat	2,822	1,496717988	0,014725654	1,831925415
Q99KR8	Plasma alpha-L-fucosidase OS=Mus musculus GN=Fuca2 PE=1 SV=1	Fuca2	2,897	1,534559685	0,015053746	1,822355407
Q9D379	Epoxide hydrolase 1 OS=Mus musculus GN=Ephx1 PE=1 SV=2	Ephx1	2,514	1,32998465	0,015962259	1,796905635
P15626	Glutathione S-transferase Mu 2 OS=Mus musculus GN=Gstm2 PE=1 SV=2	Gstm2	3,515	1,813524689	0,0182355	1,739082313
P97449	Aminopeptidase N OS=Mus musculus GN=Anpep PE=1 SV=4	Anpep	2,621	1,390117354	0,019624248	1,707206972
Q8BS03	Peptidase inhibitor 15 OS=Mus musculus GN=Pi15 PE=2 SV=2	Pi15	3,149	1,654893757	0,020360767	1,691205872
P97821	Dipeptidyl peptidase 1 OS=Mus musculus GN=Ctsc PE=1 SV=1	Ctsc	2,475	1,307428525	0,021948652	1,658592152
P53690	Matrix metalloproteinase-14 OS=Mus musculus GN=Mmp14 PE=2 SV=3	Mmp14	2,407	1,267236142	0,024878193	1,604181175
O70433	Four and a half LIM domains protein 2 OS=Mus musculus GN=Fhl2 PE=1 SV=1	Fhl2	2,773	1,471447616	0,026422993	1,578017997
Q7TT15	Polypeptide N-acetylgalactosaminyltransferase 17 OS=Mus musculus GN=Galnt17 PE=1 SV=1	Wbscr17	2,88	1,526068812	0,028166956	1,55026008
Q9Z2M6	Ubiquitin-like protein 3 OS=Mus musculus GN=Ubl3 PE=1 SV=1	Ubl3	2,618	1,388465097	0,028905318	1,539022243
Q61001	Laminin subunit alpha-5 OS=Mus musculus GN=Lama5 PE=1 SV=4	Lama5	2,977	1,573859222	0,029282521	1,533391534
P07214	SPARC OS=Mus musculus GN=Sparc PE=1 SV=1	Sparc	2,362	1,240008965	0,02970107	1,527227907
Q01721	Growth arrest-specific protein 1 OS=Mus musculus GN=Gas1 PE=2 SV=2	Gas1	2,72	1,443606651	0,030222612	1,519668009
Q9D4V7	Rab-like protein 3 OS=Mus musculus GN=Rabl3 PE=1 SV=1	Rabl3	2,997	1,583519084	0,031555752	1,500921468
P26618	Platelet-derived growth factor receptor alpha OS=Mus musculus GN=Pdgfra PE=1 SV=3	Pdgfra	2,684	1,424384672	0,032425111	1,489118525
P55264	Adenosine kinase OS=Mus musculus GN=Adk PE=1 SV=2	Adk	2,608	1,38294387	0,035728272	1,446987993
P51655	Glypican-4 OS=Mus musculus GN=Gpc4 PE=1 SV=2	Gpc4	2,345	1,229587923	0,036696383	1,43537674
Q9D0A3	Arpin OS=Mus musculus GN=Arpin PE=1 SV=1	2610034B18Rik; Arp	2,775	1,472487771	0,037435372	1,426717848
Q8BH95	Enoyl-CoA hydratase, mitochondrial OS=Mus musculus GN=Echs1 PE=1 SV=1	Echs1	2,302	1,202887833	0,037653967	1,424189265
Q9DC11	Plexin domain-containing protein 2 OS=Mus musculus GN=Plxdc2 PE=1 SV=1	Plxdc2	2,394	1,259423152	0,039666139	1,401580071
Q99L13	3-hydroxyisobutyrate dehydrogenase, mitochondrial OS=Mus musculus GN=Hibadh PE=1 SV=1	Hibadh	2,386	1,254594043	0,042424363	1,372384675
O35375	Neuropilin-2 OS=Mus musculus GN=Nrp2 PE=1 SV=2	Nrp2	2,335	1,22342255	0,044104836	1,355513793
Q640N1	Adipocyte enhancer-binding protein 1 OS=Mus musculus GN=Aebp1 PE=1 SV=1	Aebp1	2,416	1,272620455	0,044236968	1,354214643
Q60648	Ganglioside GM2 activator OS=Mus musculus GN=Gm2a PE=1 SV=2	Gm2a	2,261	1,176960992	0,044855574	1,34818358
P14430	H-2 class I histocompatibility antigen, Q8 alpha chain OS=Mus musculus GN=H2-Q8 PE=3 SV=1	H2-Q8	2,536	1,342554745	0,045524814	1,34175182
Q8R2G6	Coiled-coil domain-containing protein 80 OS=Mus musculus GN=Ccdc80 PE=1 SV=2	Ccdc80	2,662	1,412510571	0,045760574	1,339508536
P97432	Next to BRCA1 gene 1 protein OS=Mus musculus GN=Nbr1 PE=1 SV=1	Nbr1	2,706	1,436161839	0,04634995	1,333950731
O08807	Peroxiredoxin-4 OS=Mus musculus GN=Prdx4 PE=1 SV=1	Prdx4	2,235	1,160274831	0,04967365	1,303873927

Supplementary table 2. List of downregulated proteins identified in lysosomal fractions from WT and KO by SILAC-based mass spectrometric analysis (Red: AP5 beta).

Uniprot ID	Description	Gene name	Abundance ratio: KO / WT	Log 2 fold change	Abundance ratio adj. P-value: KO / WT	Neg log10 p values
P62965	Cellular retinoic acid-binding protein 1 OS=Mus musculus GN=Crabp1 PE=1 SV=2	Crabp1	0,034	-4,878321443	2,8E-16	15,55284197
Q9WUF3	CASP8-associated protein 2 OS=Mus musculus GN=Casp8ap2 PE=1 SV=2	Casp8ap2	0,048	-4,380821784	6,13149E-15	14,21243371
O70326	Gremlin-1 OS=Mus musculus GN=Grem1 PE=2 SV=1	Grem1	0,069	-3,857259828	1,7304E-13	12,76185398
P15306	Thrombomodulin OS=Mus musculus GN=Thbd PE=1 SV=1	Thbd	0,077	-3,698997744	9,30556E-13	12,03125731
Q09163	Protein delta homolog 1 OS=Mus musculus GN=Dlk1 PE=1 SV=1	Dlk1	0,09	-3,473931188	2,25077E-11	10,64766841
O35474	EGF-like repeat and discoidin I-like domain-containing protein 3 OS=Mus musculus GN=Edil3 PE=1 SV=2	Edil3	0,124	-3,011587974	1,43854E-10	9,842076996
O70126	Aurora kinase B OS=Mus musculus GN=Aurkb PE=1 SV=2	Aurkb	0,043	-4,53951953	3,77991E-10	9,422518129
O08842	GDNF family receptor alpha-2 OS=Mus musculus GN=Gfra2 PE=1 SV=2	Gfra2	0,108	-3,210896782	1,63237E-09	8,78718149
Q8R5M8	Cell adhesion molecule 1 OS=Mus musculus GN=Cadm1 PE=1 SV=2	Cadm1	0,112	-3,158429363	4,78461E-09	8,320153421
Q9CPY1	39S ribosomal protein L51, mitochondrial OS=Mus musculus GN=Mrpl51 PE=1 SV=1	Mrpl51	0,06	-4,058893689	1,04571E-08	7,980587168
Q6P5H2	Nestin OS=Mus musculus GN=Nes PE=1 SV=1	Nes	0,133	-2,910501849	1,77539E-07	6,750705188
P48193	Protein 4.1 OS=Mus musculus GN=Epb41 PE=1 SV=2	Epb4.1; Epb41	0,124	-3,011587974	3,09867E-06	5,508824111
Q9D8W7	OCIA domain-containing protein 2 OS=Mus musculus GN=Ociad2 PE=1 SV=1	Ociad2	0,131	-2,932361283	4,27259E-06	5,369308507
P15331	Peripherin OS=Mus musculus GN=Prph PE=1 SV=2	Prph	0,155	-2,689659879	5,53959E-06	5,256522212
P21995	Embigin OS=Mus musculus GN=Emb PE=1 SV=2	Emb	0,195	-2,358453971	8,1285E-06	5,089989405
Q8R1S9	Sodium-coupled neutral amino acid transporter 4 OS=Mus musculus GN=Slc38a4 PE=1 SV=1	Slc38a4	0,126	-2,988504361	9,62094E-06	5,016782459
Q61555	Fibrillin-2 OS=Mus musculus GN=Fbn2 PE=1 SV=2	Fbn2	0,176	-2,506352666	1,03947E-05	4,983186506
P11609	Antigen-presenting glycoprotein CD1d1 OS=Mus musculus GN=Cd1d1 PE=1 SV=3	Cd1d1	0,172	-2,53951953	1,10116E-05	4,958147842
P13595	Neural cell adhesion molecule 1 OS=Mus musculus GN=Ncam1 PE=1 SV=3	Ncam1	0,231	-2,114035243	3,26231E-05	4,486474487
Q9CSN1	SNW domain-containing protein 1 OS=Mus musculus GN=Snw1 PE=1 SV=3	Snw1	0,191	-2,388355457	4,40081E-05	4,356467376
B1AXP6	Mitochondrial import receptor subunit TOM5 homolog OS=Mus musculus GN=Tomm5 PE=3 SV=1	Tomm5	0,114	-3,13289427	9,16624E-05	4,037808774
Q9Z1M8	Protein Red OS=Mus musculus GN=Ik PE=1 SV=2	Ik	0,164	-2,60823228	0,000129405	3,888050293
P11610	Antigen-presenting glycoprotein CD1d2 OS=Mus musculus GN=Cd1d2 PE=2 SV=2	Cd1d2	0,213	-2,231074664	0,000134245	3,872103059
Q8K298	Anillin OS=Mus musculus GN=Anln PE=1 SV=2	Anln	0,186	-2,426625474	0,000139397	3,855745328
Q8JZS0	Protein lin-7 homolog A OS=Mus musculus GN=Lin7a PE=1 SV=2	Lin7a	0,129	-2,954557029	0,000172583	3,763001714
Q9D8M4	60S ribosomal protein L7-like 1 OS=Mus musculus GN=Rpl7l1 PE=1 SV=1	Rpl7l1	0,175	-2,514573173	0,00022339	3,650936548
Q8BHX3	Borealin OS=Mus musculus GN=Cdca8 PE=1 SV=2	Cdca8	0,175	-2,514573173	0,000227492	3,643033045
Q6YGZ1	Heparanase OS=Mus musculus GN=Hpse PE=1 SV=3	Hpse	0,191	-2,388355457	0,000232353	3,633851187
Q9JJ80	Ribosome production factor 2 homolog OS=Mus musculus GN=Rpf2 PE=2 SV=2	Rpf2	0,162	-2,625934282	0,000320551	3,494102256
P28481	Collagen alpha-1(II) chain OS=Mus musculus GN=Col2a1 PE=1 SV=2	Col2a1	0,233	-2,10159814	0,001013131	2,994334434

P09803	Cadherin-1 OS=Mus musculus GN=Cdh1 PE=1 SV=1	Cdh1	0,221	-2,177881725	0,002707232	2,567474601
Q8BMJ3	Eukaryotic translation initiation factor 1A, X-chromosomal OS=Mus musculus GN=Eif1ax PE=2 SV=3	Eif1ax	0,242	-2,046921047	0,002898008	2,537900412
Q61033	Lamina-associated polypeptide 2, isoforms alpha/zeta OS=Mus musculus GN=Tmpo PE=1 SV=4	Tmpo	0,231	-2,114035243	0,005434566	2,264835108
Q3TAP4	AP-5 complex subunit beta-1 OS=Mus musculus GN=Ap5b1 PE=1 SV=1	Ap5b1	0,264	-1,921390165	0,005770395	2,238794464
P70297	Signal transducing adapter molecule 1 OS=Mus musculus GN=Stam PE=1 SV=3	Stam	0,256	-1,965784285	0,005770395	2,238794464
Q9CWY8	Ribonuclease H2 subunit A OS=Mus musculus GN=Rnaseh2a PE=1 SV=2	Rnaseh2a	0,226	-2,145605322	0,00669864	2,174013387
Q3UW53	Protein Niban OS=Mus musculus GN=Fam129a PE=1 SV=2	Fam129a	0,292	-1,775959726	0,007066432	2,150799843
Q9D0I8	mRNA turnover protein 4 homolog OS=Mus musculus GN=Mrto4 PE=1 SV=1	Mrto4	0,306	-1,708396442	0,007518502	2,123868691
Q8R0F6	Integrin-linked kinase-associated serine/threonine phosphatase 2C OS=Mus musculus GN=Ilkap PE=1 SV=1	Ilkap	0,223	-2,164884385	0,007753009	2,110529686
Q9WVP1	AP-1 complex subunit mu-2 OS=Mus musculus GN=Ap1m2 PE=1 SV=3	Ap1m2	0,303	-1,722610301	0,008347709	2,078432684
Q9EQG7	Ectonucleotide pyrophosphatase/phosphodiesterase family member 5 OS=Mus musculus GN=Enpp5 PE=1 SV=3	Enpp5	0,351	-1,510457064	0,009408154	2,026495568
P14873	Microtubule-associated protein 1B OS=Mus musculus GN=Map1b PE=1 SV=2	Map1b; Mtap1b	0,303	-1,722610301	0,009726153	2,012058917
Q9JM62	Receptor expression-enhancing protein 6 OS=Mus musculus GN=Reep6 PE=1 SV=1	Reep6	0,304	-1,717856771	0,010588891	1,975149513
Q61009	Scavenger receptor class B member 1 OS=Mus musculus GN=Scarb1 PE=1 SV=1	Scarb1	0,357	-1,486004021	0,011266211	1,948222104
A6X935	Inter alpha-trypsin inhibitor, heavy chain 4 OS=Mus musculus GN=Itih4 PE=1 SV=2	Itih4	0,211	-2,244685096	0,012982567	1,886639428
Q8VCH6	Delta(24)-sterol reductase OS=Mus musculus GN=Dhcr24 PE=1 SV=1	Dhcr24	0,321	-1,639354798	0,015978553	1,796462564
P15379	CD44 antigen OS=Mus musculus GN=Cd44 PE=1 SV=3	Cd44	0,373	-1,422752464	0,018059265	1,743299927
P02469	Laminin subunit beta-1 OS=Mus musculus GN=Lamb1 PE=1 SV=3	Lamb1	0,374	-1,418889825	0,018470682	1,733517065
Q9DAR7	m7GpppX diphosphatase OS=Mus musculus GN=Dcps PE=1 SV=1	Dcps	0,22	-2,184424571	0,018674521	1,728750519
O55125	Protein NipSnap homolog 1 OS=Mus musculus GN=Nipsnap1 PE=1 SV=1	Nipsnap1	0,329	-1,603840511	0,018863113	1,72438664
Q641P0	Actin-related protein 3B OS=Mus musculus GN=Actr3b PE=1 SV=1	Actr3b	0,316	-1,662003536	0,020229111	1,694023201
P63089	Pleiotrophin OS=Mus musculus GN=Ptn PE=1 SV=1	Ptn	0,279	-1,841662973	0,022464068	1,648511599
Q8CFI5	Probable proline--tRNA ligase, mitochondrial OS=Mus musculus GN=Pars2 PE=1 SV=2	Pars2	0,31	-1,689659879	0,024150378	1,617076063
Q9WVJ3	Carboxypeptidase Q OS=Mus musculus GN=Cpq PE=1 SV=1	Cpq; Pgcp	0,339	-1,560642822	0,024382507	1,612921644
Q61490	CD166 antigen OS=Mus musculus GN=Alcam PE=1 SV=3	Alcam	0,38	-1,395928676	0,025246618	1,597796788
P22777	Plasminogen activator inhibitor 1 OS=Mus musculus GN=Serpine1 PE=1 SV=1	Serpine1	0,378	-1,40354186	0,025799192	1,588393902
Q5FWI3	Cell surface hyaluronidase OS=Mus musculus GN=Tmem2 PE=1 SV=1	Tmem2	0,289	-1,790858602	0,027357849	1,562918057
Q9DB10	Essential MCU regulator, mitochondrial OS=Mus musculus GN=Smdt1 PE=1 SV=1	1500032L24 Rik; Smdt1	0,277	-1,852042119	0,029282521	1,533391534
Q9R118	Serine protease HTRA1 OS=Mus musculus GN=Htra1 PE=1 SV=2	Htra1	0,39	-1,358453971	0,031919156	1,495948596
Q9JHU9	Inositol-3-phosphate synthase 1 OS=Mus musculus GN=Isyna1 PE=1 SV=1	Isyna1	0,296	-1,756330919	0,037435372	1,426717848
Q9D8T2	Gasdermin-D OS=Mus musculus GN=Gsdmdc1 PE=1 SV=1	Gsdmd	0,32	-1,64385619	0,037435372	1,426717848

3.2 Manuscript II

Mouse models for hereditary spastic paraplegia uncover a role of PI4K2A in autophagic lysosome reformation

Mukhran Khundadze, Federico Ribaudo, Adeela Hussain, Henry Stahlberg, Nahal Brocke-Ahmadinejad, Patricia Franzka, Rita-Eva Varga, Milena Zarkovic, Thanakorn Pungsrinont, Miriam Kokal, Ian G. Ganley, Christian Beetz, Marc Sylvester & Christian A. Hübner

View supplementary material

Published online: 09 Mar 2021.

Submit your article to this journal

Article views: 208

View related articles

View Crossmark data

Taylor & Francis
Taylor & Francis Group

RESEARCH PAPER

Check for updates

Mouse models for hereditary spastic paraplegia uncover a role of PI4K2A in autophagic lysosome reformation

Mukhran Khundadze[a,‡], Federico Ribaudo[a,‡], Adeela Hussain[a], Henry Stahlberg[a], Nahal Brocke-Ahmadinejad[b], Patricia Franzka[a], Rita-Eva Varga[a], Milena Zarkovic[a], Thanakorn Pungsrinont[a], Miriam Kokal[a], Ian G. Ganley[c], Christian Beetz[d], Marc Sylvester[b], and Christian A. Hübner[a]

[a]Institute of Human Genetics, University Hospital Jena, Friedrich-Schiller-University Jena, Jena, Germany; [b]Core Facility Mass Spectrometry, Institute of Biochemistry and Molecular Biology, Medical Faculty, University of Bonn, Bonn, Germany; [c]MRC Protein Phosphorylation and Ubiquitylation Unit, School of Life Sciences, University of Dundee, Dundee, Scotland; [d]Institute of Clinical Chemistry, University Hospital Jena, Friedrich-Schiller-University Jena, Germany; Current Affiliation: Centogene GmbH, Rostock, Germany

ABSTRACT

Hereditary spastic paraplegia (HSP) denotes genetically heterogeneous disorders characterized by leg spasticity due to degeneration of corticospinal axons. SPG11 and SPG15 have a similar clinical course and together are the most prevalent autosomal recessive HSP entity. The respective proteins play a role for macroautophagy/autophagy and autophagic lysosome reformation (ALR). Here, we report that *spg11* and *zfyve26* KO mice developed motor impairments within the same course of time. This correlated with enhanced accumulation of autofluorescent material in neurons and progressive neuron loss. In agreement with defective ALR, tubulation events were diminished in starved KO mouse embryonic fibroblasts (MEFs) and lysosomes decreased in neurons of KO brain sections. Confirming that both proteins act in the same molecular pathway, the pathologies were not aggravated upon simultaneous disruption of both. We further show that PI4K2A (phosphatidylinositol 4-kinase type 2 alpha), which phosphorylates phosphatidylinositol to phosphatidylinositol-4-phosphate (PtdIns4P), accumulated in autofluorescent deposits isolated from KO but not WT brains. Elevated PI4K2A abundance was already found at autolysosomes of neurons of presymptomatic KO mice. Immunolabelings further suggested higher levels of PtdIns4P at LAMP1-positive structures in starved KO MEFs. An increased association with LAMP1-positive structures was also observed for clathrin and DNM2/dynamin 2, which are important effectors of ALR recruited by phospholipids. Because PI4K2A overexpression impaired ALR, while its knockdown increased tubulation, we conclude that PI4K2A modulates phosphoinositide levels at autolysosomes and thus the recruitment of downstream effectors of ALR. Therefore, PI4K2A may play an important role in the pathogenesis of SPG11 and SPG15.

Abbreviations: ALR: autophagic lysosome reformation; AP-5: adaptor protein complex 5; BFP: blue fluorescent protein; dKO: double knockout; EBSS: Earle's balanced salt solution; FBA: foot base angle; GFP: green fluorescent protein; HSP: hereditary spastic paraplegia; KO: knockout; LAMP1: lysosomal-associated membrane protein 1; MAP1LC3B/LC3: microtubule-associated protein 1 light chain 3 beta; MEF: mouse embryonic fibroblast; SQSTM1/p62: sequestosome 1; PI4K2A: phosphatidylinositol 4-kinase type 2 alpha; PtdIns3P: phosphatidylinositol-3-phosphate; PtdIns4P: phosphatidylinositol-4-phosphate; RFP: red fluorescent protein; SPG: spastic paraplegia gene; TGN: trans-Golgi network; WT: wild type

Introduction

Hereditary spastic paraplegia (HSP) refers to a group of neurodegenerative disorders, which are characterized by the degeneration of upper motoneuron axons thus resulting in lower limb spasticity and weakness [1]. Additional symptoms such as cognitive deficits, a thinning of the corpus callosum, optic atrophy, cerebellar atrophy, amyotrophy, peripheral nerve involvement, and seizures can occur and characterize complicated HSPs. Up to date more than 80 different genetic loci have been identified, which are termed as SPGs with a running number reflecting the order of its

identification. Mutations in SPG11 (SPG11 vesicle trafficking associated, spatacsin) are the most common cause of autosomal recessively inherited HSP [2]. Affected patients often suffer from mental retardation, ataxia, Parkinsonism, retinopathy or polyneuropathy and show a thinning of the corpus callosum and cortical atrophy. Clinically SPG11 patients cannot be distinguished from SPG15 patients, another autosomal recessive form of HSP [3], which is caused by mutations in ZFYVE26/Spastizin (zinc finger FYVE-type containing 26). Therefore, it was concluded

CONTACT Mukhran Khundadze ✉ Mukhran.Khundadze@med.uni-jena.de; Christian A. Hübner ✉ Christian.Huebner@med.uni-jena.de ▣ Institute of Human Genetics, University Hospital Jena, Friedrich-Schiller-University Jena, Am Klinikum 1, 07747 Jena, Germany.
‡These authors share first authorship on this work.
🅑 Supplemental data for this article can be accessed here.

that SPG11 and ZFYVE26 may act in the same cellular pathway. Indeed, both SPG11 and ZFYVE26 co-precipitate with other proteins [4], which were later identified as members of the newly identified adaptor protein (AP) complex AP-5 [5].

AP complexes mediate intracellular membrane trafficking along endocytic and secretory transport pathways. It is assumed that AP-5 serves as a backup system for the retrieval of proteins from late endosomes to the *trans* Golgi, because knockdown [6] or disruption [7] of its AP5Z1/ζ-subunit impair the retrieval of some Golgi-related proteins from endosomes back to the Golgi. Notably, mutations in AP5Z1 cause SPG48 [4], which shows many similarities with SPG11 and SPG15 [8]. Because SPG11 and ZFYVE26 have predicted secondary structures containing alpha-solenoids related to those of clathrin heavy chain and COPI (coatomer protein complex I) subunits and because SPG11 also has an N-terminal, beta-propeller-like domain, which interacts with AP-5, both may contribute to the scaffold of AP-5 [9]. Thus, AP-5 might be involved in protein sorting, while ZFYVE26 facilitates the docking of the coat onto membranes by interacting with PtdIns3P via its FYVE domain and SPG11 forms the scaffold.

Because AP-5 subunits have been coordinately lost in many organisms, in which the SPG11 and ZFYVE26 orthologs are still present, it was proposed that ZFYVE26 and SPG11 may also serve functions independent of AP-5 [5]. A role in cell division [10], DNA repair [4], endosomal trafficking [9], autophagy [11] and autophagic lysosome reformation (ALR) [12–14] has been reported. The latter mechanism is regulated by MTOR (mechanistic target of rapamycin kinase), which allows the recycling of lysosomes from autolysosomes after prolonged starvation [15]. It was proposed that defective ALR may alter the subcellular distribution of cholesterol and thus affect intracellular calcium homeostasis, which may impair lysosome tubulation via TFEB (transcription factor EB), the master regulator of lysosomes [16].

We and others characterized knockout (KO) mouse models for either SPG11 [14,17] or ZFYVE26 [7] and AP5Z1 [18]. Both *spg11* KO and *zfyve26* KO mice developed a gait disorder compatible with HSP. As a correlate we found a progressive intracellular accumulation of LAMP1- and SQSTM1-positive autofluorescent material in cortical motoneurons and in Purkinje neurons of *spg11* KO and *zfyve26* KO mice, which are finally lost. Supporting a defect of autophagy, levels of lipidated LC3 were increased in *spg11* KO mouse embryonic fibroblasts (MEFs). In agreement with a possible defect of ALR, lysosome numbers were reduced in *spg11* KO Purkinje neurons *in vivo*.

Here, we report the generation of *spg11 zfyve26* double KO (dKO) mice. We observed a similar time dependent massive accumulation of lysosome-related autofluorescent material in neurons, progressive neuron loss and motor impairments in KO and dKO mice adding support to the notion that SPG11 and ZFYVE26 act together. Our unbiased mass spectrometry approach identified PI4K2A (phosphatidylinositol 4-kinase type 2 alpha) in autofluorescent material isolated from brains of *spg11* KO and *zfyve26* KO but not WT mice. Immunostainings of brain sections further revealed that PI4K2A abundance is already increased at autolysosomes of KO mice before onset of overt neurodegeneration. PI4K2A overexpression in U2-OS cells inhibited autolysosomal tubulation and increased the association of clathrin and DNM2/dynamin 2 with LAMP1-positive structures similar to our findings in KO MEFs. Here, we propose that increased PI4K2A abundance contributes to the pathophysiology of SPG11 and SPG15, because PI4K2A modulates phosphoinositide levels at autolysosomes and thus down-stream effectors involved in ALR.

Results

The simultaneous disruption of Spg11 in zfyve26 KO mice does not aggravate the phenotype of spg11 KO or zfyve26 KO mice

We previously generated *zfyve26* KO [7] and *spg11* KO [14] mouse models. Since the initial description both lines had been backcrossed with C57BL/6 J for more than 10 generations resulting in an almost pure C57BL/6 J background. To get more insights into the molecular function of SPG11 or ZFYVE26 we crossed both lines and obtained mice heterozygous for both the *spg11* KO and the *zfyve26* KO allele. Notably, double heterozygous KO mice did not develop any gait abnormalities (data not shown), even beyond 18 months of age. Mating of double heterozygous KO mice finally resulted in homozygous *spg11 zfyve26* double knockout (dKO) mice, which were born in the expected Mendelian ratio. To compare the severity of the motor phenotypes of the different genotypes we measured the foot-base-angle (FBA) at toe-off position of the hind-paw over time. While there was no difference between genotypes at 6 months of age, the FBA was similarly flatter in *spg11* KO, *zfyve26* KO and dKO mice at 12 months of age as compared to WT (wild-type) littermates (Figure 1A). At the same age, we noted a comparable body weight loss, in *spg11* KO, *zfyve26* KO and dKO littermates (Figure 1B). We also measured the brain weight at 16 months of age, which was reduced in *spg11* KO, *zfyve26* KO, and dKO mice compared to WT. Again, there was no difference between single KO and dKO mice (Figure 1C). We further quantified cortical neurons in brain sections stained for the neuronal marker RBFOX3/NeuN (Figure 1D-G). Neuron numbers in layer V to VI were reduced in 16-months-old *spg11* KO and *zfyve26* KO compared to WT mice, but the loss was not worsened by simultaneous disruption of *Spg11* and *Zfyve26* (Figure 1H). Similar results were obtained for the loss of Purkinje cells, which were identified by the expression of CALB1/calbindin 1 (Figure 1I-M).

Taken together, these data suggest that the phenotype is not aggravated by simultaneous disruption of both *Spg11* and *Zfyve26*.
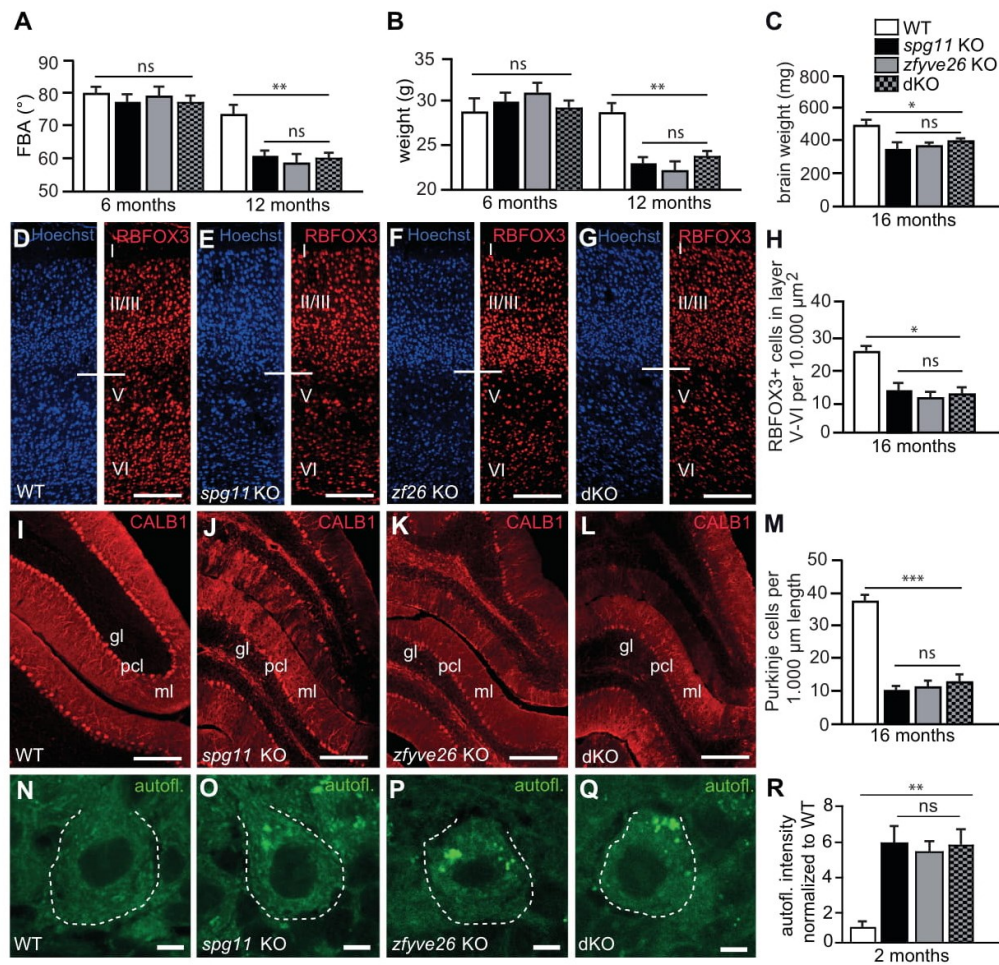
Figure 1. Spg11 KO and zfyve26 KO mice share the same phenotype which is not aggravated by simultaneous disruption of both. (A) At 6 months of age the mean foot base angle (FBA) at toe-off position is not altered in spg11 KO, zfyve26 KO, and spg11 zfyve26 double KO (dKO) compared to WT mice. Six months later, the FBA is likewise decreased in spg11 KO, zfyve26 KO and dKO mice compared to WT (n = 6 mice per genotype; two-way ANOVA followed by Bonferroni test; ** p < 0.01; ns: not significant). (B) The mean body weight of spg11 KO, zfyve26 KO and dKO compared to control mice is decreased at 12 months of age (n = 6 mice per genotype for body weight; two-way ANOVA followed by Bonferroni test; * p < 0.05; ns: not significant). (C) The mean brain weight is significantly reduced in 16-months-old KO and dKO mice (n = 4 mice per genotype for brain weight; one-way ANOVA followed by Tukey's Multiple Comparison Test; * p < 0.05; ns: not significant). (D-H) Compared to WT (D) RBFOX3 stained neurons (red) in motor cortex layers V–VI of 16-months-old spg11 KO (E), zfyve26 KO (F) and dKO (G) mice are likewise reduced (H; n = 3 mice per genotype with n = 1 section; one-way ANOVA followed by Tukey's Multiple Comparison Test; * indicates p < 0.05; ns: not significant). Individual cortical layers are labeled (I–VI). Scale bars: 100 μm. (I-M) Compared to WT (I) mice, CALB1 labeled Purkinje cells (red) are decreased as well in 16-months-old spg11 KO (J), zfyve26 KO (K) and dKO (L) mice (n = 3 mice per genotype with n = 1 section; one-way ANOVA followed by Tukey's Multiple Comparison Test; *** indicates p < 0.001; ns: not significant). ml: molecular layer; pcl: Purkinje cell layer; gl: granular layer. Scale bars: 100 μm. (N-R) Compared to WT (N) autofluorescence (green, excitation at 488 nm) is similarly increased in Purkinje cells of 2-months-old spg11 KO (O), zfyve26 KO (P) and dKO (Q) mice (at least 10 cells per mouse; n = 3 mice per genotype; one-way ANOVA followed by Tukey's Multiple Comparison Test; ** indicates p < 0.01; ns: not significant). Scale bars: 5 μm. Error bars represent SEM.

Autophagy related autofluorescent material is similarly increased in neurons of spg11 KO, zfyve26 KO, and dKO mice

We previously reported that the accumulation of lipofuscin-like autofluorescent intracellular material (emission wavelength between 460 and 630 nm) is drastically increased in Purkinje cells and cortical motoneurons of both spg11 KO and zfyve26 KO mice starting from 2 months of age onwards [7,14]. Notably, the autofluorescent material detected in Purkinje cells of mice heterozygous for one spg11 KO and

one zfyve26 KO allele did not differ from control mice (**Fig. S1A-C**). Autofluorescence quantification for Purkinje cells did not suggest that the intracellular pathology was more severe in dKO mice at 2 (Figure 1N-R) or 16 (**Fig. S1D-H**) months of age compared to spg11 KO and zfyve26 KO mice.

To better characterize the material, we stained brain sections with different markers such as LAMP1, SQSTM1 and LC3. We applied a spectral analysis to distinguish the labeled compartment from autofluorescence using a linear unmixing algorithm as described previously [7]. As already observed in spg11 KO mice [14], the autofluorescent material in zfyve26 KO and dKO
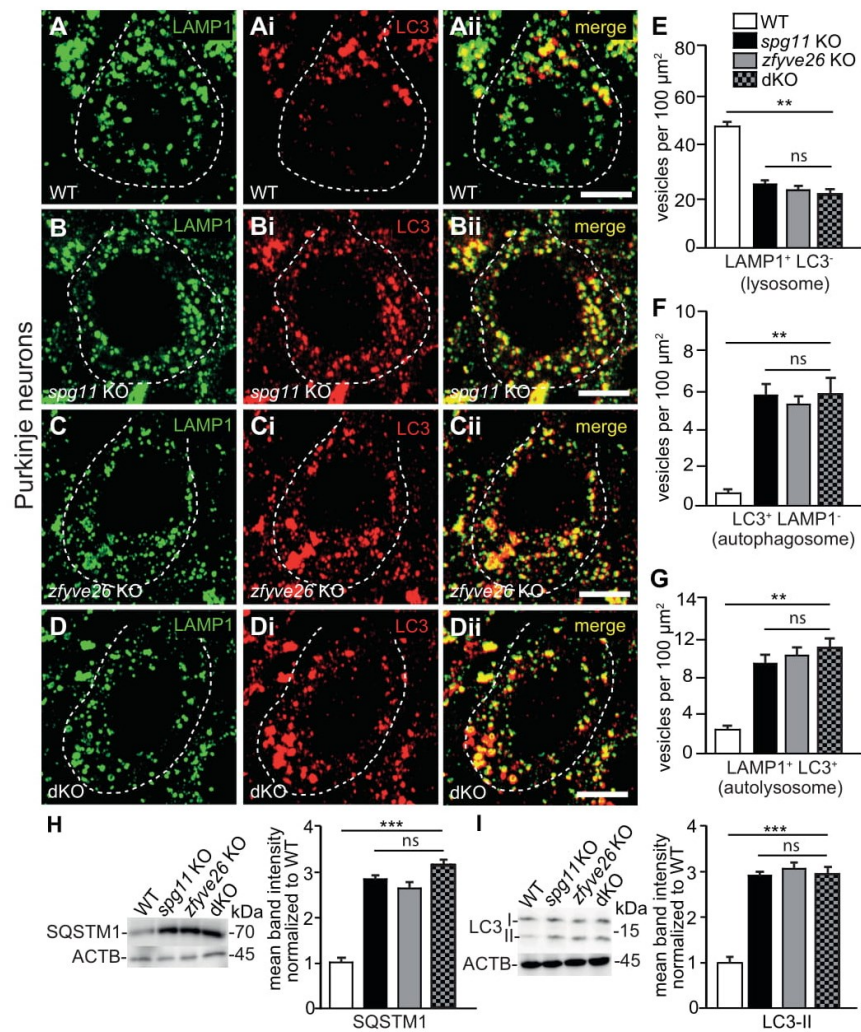
Figure 2. Less lysosomes in Purkinje cells of *spg11* KO, *zfyve26* KO and *spg11 zfyve26* double KO (dKO) mice. (A-E) Lysosomes numbers are likewise reduced in Purkinje cells of 2-months-old *spg11* KO, *zfyve26* KO and dKO mice. Representative Purkinje cells in brain sections of WT (A-Aii), *spg11* KO (B-Bii), *zfyve26* KO (C-Cii) and dKO mice (D-Dii) stained for LAMP1 (green) and LC3 (red). Purkinje cell somata are marked by a dashed line. Quantification of lysosomes defined as LAMP1-positive and LC3-negative puncta (E), autophagosomes defined as LAMP1-negative but LC3-psotive puncta (F) and autolysosomes defined as LAMP1- and LC3-positive puncta (G). More than 30 cells from 3 mice per genotype were analyzed (one-way ANOVA followed by Tukey's Multiple Comparison Test; ** $p < 0.01$; ns: not significant). Scale bars: 5 µm. (H and I) SQSTM1 (H) and LC3-II (I) protein abundances were likewise increased in brain lysates of 16-months-old *spg11* KO, *zfyve26* KO and dKO mice. ACTB/β-actin served as loading control (4 mice per genotype; one-way ANOVA followed by Tukey's Multiple Comparison Test; *** $p < 0.001$; ns: not significant). Error bars represent SEM.

mice labeled for SQSTM1 (**Fig. S1Di,Ei** and **Fi**) and signal intensities did not differ between genotypes at 16 months of age (**Fig. S1I**). We also co-stained brain sections from 2-months-old WT, KO, and dKO mice for the lysosomal marker LAMP1 and LC3 (Figure 2A-**Dii**), which labels autophagic vesicles. Lysosomes defined as LAMP1-positive but LC3-negative puncta were decreased in KO and dKO mice (Figure 2E), while autophagosomes (LAMP1-negative but LC3-positive puncta, Figure 2F) and autolysosomes (puncta labeled for LAMP1 and LC3, Figure 2G) were increased. Similar results

were obtained, when we co-stained brain sections with LAMP1 and SQSTM1 (**Fig. S2**). Again, we did not observe that these alterations were more pronounced in dKO mice.

In accordance with our immunostainings, overall abundances for SQSTM1 and LC3 were increased in brain lysates of 16-months-old *spg11* KO, *zfyve26* KO and dKO mice (Figure 2H and **I**).

Together these findings suggest that the clearance of autophagic material is impaired upon disruption of either *Spg11* or *Zfyve26* and thus accumulates over time.

Autophagic lysosome reformation is compromised in spg11 *KO*, zfyve26 *KO and dKO mice*

To scrutinize the autophagic capacity during starvation, we isolated MEFs from *spg11* KO, *zfyve26* KO and dKO mice. Consistent with a defect of the degradative system, LC3-II abundance was increased in *spg11* KO, *zfyve26* KO, and dKO MEFs at baseline and further increased after starvation with EBSS (Figure 3A). Addition of the mTOR inhibitor Torin 1 during starvation did not increase LC3-II abundance any further. Starvation of cells in the presence of bafilomycin A₁, which inhibits lysosomal acidification as well as the fusion of lysosomes with autophagosomes [19], abolished the difference in LC3-II abundances between *spg11* KO, *zfyve26* KO, dKO and WT MEFs (Figure 3B). This suggests that the formation of autophagosomes is not impaired upon disruption of *Spg11* or *Zfyve26*.

We co-stained MEFs for LC3 and LAMP1 to distinguish autophagosomes (LC3-positive puncta), lysosomes (LAMP1-positive puncta), and autolysosomes (LC3- and LAMP1-positive puncta) (Figure 3C-**J**) at steady state and after 2 h of EBSS starvation. Consistent with our *in vivo* findings, the number of lysosomes was reduced in *spg11* KO, *zfyve26* KO and dKO MEFs already at nutrient conditions and further decreased after EBSS starvation (Figure 3K). Although the number of autophagosomes was increased in *spg11* KO, *zfyve26* KO and dKO MEFs at steady state, this difference was gone during EBSS starvation (Figure 3L). The number of autolysosomes was significantly increased in *spg11, zfyve26* KO and dKO MEFs under challenged conditions (Figure 3M) suggesting that the fusion of lysosomes with autophagosomes still occurs in the absence of ZFYV26, SPG11 or both. This assumption was corroborated by flux analysis with an mRFP-eGFP-LC3 reporter (ptfLC3), which labels autophagosomes in red and green and autolysosomes in red, because the GFP signal is quenched by the acidic pH in autolysosomes (**Fig. S3**).

Our findings are consistent with previous reports that the recycling of lysosomes from autolysosomes might be affected in SPG11 and SPG15 [13]. To visualize ALR we transiently expressed LAMP1-GFP in WT (**Movie S1**), *spg11* KO (**Movie S2**), *zfyve26* KO (**Movie S3**), and dKO (**Movie S4**) MEFs and quantified LAMP1-positive tubules longer than 2 μm between 8 and 9 h of starvation. In agreement with a similar defect in ALR, the ratio of cells with more than 5 tubules longer than 2 μm was decreased likewise in *spg11* KO and *zfyve26* KO MEFs (Figure 3N-**R**). Tubules longer than 5 μm were very rare events in both WT and in KO MEFs.

Altogether our *in vivo* and *in vitro* data support a similar defect of ALR upon disruption of either *Spg11* or *Zfyve26* or both.

PI4K2A (phosphatidylinositol 4-kinase type 2 alpha) accumulates in autofluorescent deposits of spg11 *KO and* zfyve26 *KO mice*

The drastic increase of autofluorescent material in *spg11* KO and *zfyve26* KO compared to WT neurons, prompted us to analyze the protein composition of these deposits. The

material was isolated by density centrifugation from brains of 6-months-old WT, *spg11* KO and *zfyve26* KO mice as described previously [20]. Quantitative mass spectrometry identified more than 2,000 proteins in each sample (**Table S1**, raw data). There was a large overlap between proteins previously detected in rat and human lipofuscin [20] with proteins identified in deposits isolated from WT,*spg11* KO and *zfyve26* KO mice (**Table S2**). To get further insights into the pathophysiology of SPG11 and SPG15 we filtered for proteins that were significantly changed in the same direction in both *spg11* KO and *zfyve26* KO mice compared to WT (fold change log2 FC>1, q value -Log10 q > 1,3). This resulted in a list of 64 significantly down- or upregulated proteins (Figure 4A and **B; Table S3**). Notably, twenty-seven of these candidates were classified as endomembrane associated proteins with the cellular compartment tool of the Genome Ontology Consortium (GO) website [21]. The majority of these proteins were found to be enriched in KO samples (red dots, Figure 4A and **B; Table S3**, red lines). We also filtered for proteins that were only found in deposits from both *spg11* KO and *zfyve26* KO mice (**Table S4**). Out of the 15 proteins identified, PI4K2A was the most abundant in KO deposits.

To validate the accumulation of PI4K2A *in vivo* we stained brain sections from 6-months-old WT, *spg11* KO, and *zfyve26* KO mice. While there was only partial overlap with lipofuscin in aged WT mice (Figure 4C-**Cii**), PI4K2A colocalized with autofluorescent deposits in *spg11* KO (Figure 4D-**Dii**) and *zfyve26* KO (Figure 4E-**Eii**) Purkinje cells.

Immunoblot analysis showed a roughly 2-fold increase of PI4K2A abundance in the Triton X insoluble fraction of total brain lysates from 16-months-old *spg11* KO, *zfyve26* KO and dKO mice (Figure 4F and **G**). Significantly increased levels of PI4K2A were also observed in *spg11* KO and *zfyve26* KO MEFs (Figure 4F and **G**).

To further address why PI4K2A is increased upon disruption of *Spg11* or *Zfyve26*, we assessed *Pi4k2a* transcript abundance by quantitative PCR in MEFs, which was not increased in KO samples (**Fig. S4A**). We also transfected MEFs with a PI4K2A-GFP construct and quantified fluorescence intensity over time after inhibition of protein translation with Cycloheximide. While the decrease of fluorescence intensity in MEFs transfected with a GFP-construct alone did not differ between genotypes (**Fig. S4B**), the turnover of PI4K2A-GFP was impaired in *spg11* KO and *zfyve26* KO MEFs (**Fig. S4C**).

Taken together, we show that PI4K2A abundance is increased in brain lysates and in MEFs isolated from *spg11* KO or *zfyve26* KO mice, which may result from a delayed turnover of PI4K2A upon disruption of either *Spg11* or *Zfyve26*.

PI4K2A abundance is increased in autolysosomes of pre-symptomatic spg11 *KO and* zfyve26 *KO mice*

PI4K2A is a membrane-bound phosphatidylinositol 4-kinase, which mainly localizes to endosomes, the TGN [22], and lysosomes [23] and is recruited to autophagosomes during starvation [23]. To study whether the subcellular distribution of PI4K2A is altered upon disruption of *Spg11* or *Zfyve26*, we co-stained brain sections of 2-months-
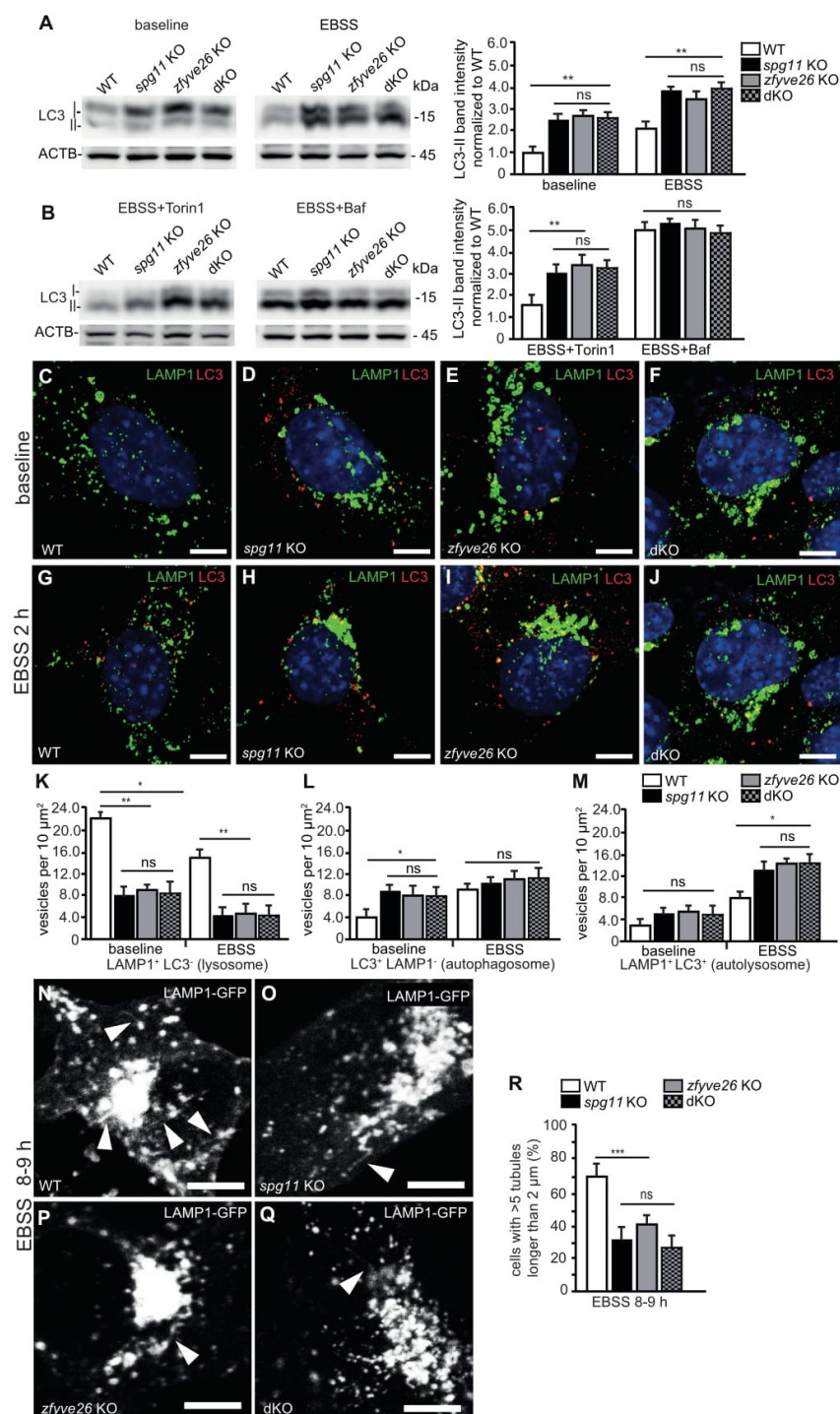
Figure 3. Autophagic lysosome reformation is compromised in *spg11* KO, *zfyve26* KO and *spg11 zfyve26* double KO (dKO) mouse embryonic fibroblasts. (A and B) Defective autophagy in *spg11* KO, *zfyve26* KO and dKO mouse embryonic fibroblasts (MEFs). Semi-quantitative western blotting analysis of LC3 abundance in WT, *spg11* KO, *zfyve26* KO and dKO MEFs at steady state and upon 6 h EBSS starvation with or without Torin1 or bafilomycin A$_1$ (Baf). ACTB served as loading control. Normalization is relative to baseline WT (n = 3 experiments; one-way ANOVA followed by Tukey's Multiple Comparison Test; * p < 0.05; ** p < 0.01; ns: not significant). (C-M) Autophagic flux is similarly compromised in *spg11* KO, *zfyve26* KO and dKO MEFs. LAMP1 (green) and LC3 (red) stainings of WT (C and G), *spg11* KO (D and H), *zfyve26* KO (E and I) and dKO (F and J) MEFs at baseline and after 2 h of EBSS starvation. Scale bars: 10 μm. (K-M) Quantification of lysosomes (K) defined as LAMP1-positive but LC3-negative puncta, autophagosomes (L) defined as LC3-positive but LAMP1-negative puncta, and autolysosomes (M) defined as LAMP1- and

LC3-positive puncta (at least 30 cells per genotype from n = 3 experiments; one-way ANOVA followed by Tukey's Multiple Comparison Test; ** p < 0.01; * p < 0.05; ns: not significant). (N-R) ALR is similarly compromised in *spg11* KO, *zfyve26* KO and dKO MEFs. Representative live cell imaging time frames of WT (N), *spg11* KO (O), *zfyve26* KO (P) and dKO (Q) MEFs between 8 and 9 h of EBSS starvation. LAMP1-positive tubules are marked by white arrowheads. Scale bars: 10 μm. (R) Quantification of cells with more than 5 LAMP1-positive tubules longer than 2 μm (at least 30 cells per genotype from n = 3 independent experiments; one-way ANOVA followed by Newman-Keuls Multiple Comparison Test; *** p < 0.001; ns: not significant). Error bars represent SEM.

old pre-symptomatic KO mice for PI4K2A, LAMP1 and SQSTM1 (Figure 5A-Ciii). The number of PI4K2A-positive puncta negative for LAMP1 and SQSTM1 was decreased in Purkinje cells of *spg11* KO and *zfyve26* KO mice (Figure 5D). Nearly all autolysosomes defined as LAMP1- and SQSTM1-positive puncta also labeled for PI4K2A irrespective of the genotype and the number of PI4K2A-positive autolysosomes was elevated in KO mice (Figure 5E). Notably, mean signal intensities for PI4K2A on autolysosomes were more than doubled in KO mice (Figure 5F).

In summary, PI4K2A abundance is already increased in autolysosomes of pre-symptomatic *spg11* KO and *zfyve26* KO mice.

PI4K2A modulates ALR

We considered that the increased abundance of PI4K2A may be causally linked with the defect of ALR upon disruption of either *Spg11* or *Zfyve26*. To validate our hypothesis, we transfected U2-OS cells stably expressing LAMP1-GFP and mCherry-LC3 [24] with a construct encoding PI4K2A-BFP. Using live cell microscopy, we observed that PI4K2A-BFP was targeted to lysosomes and autolysosomes (Figure 6A-Aii). Recapitulating our findings in starved *spg11* or *zfyver26* KO MEFs, the ratio of cells with more than 5 tubules longer than 2 μm emerging from LAMP1 and LC3-labeled autolysosomes was drastically decreased in PI4K2A-BFP-positive cells between 8 and 9 h after initiation of EBSS starvation (Figure 6A-C). The ratio of cells with more than 5 tubules longer than 5 μm was low and did not change upon overexpression of PI4K2A-BFP (Figure 6D).

Next, we assessed whether the siRNA-mediated knockdown of PI4K2A in U2-OS cells affects ALR (Figure 6E-I). The knockdown of PI4K2A slightly increased the ratio of cells with more than 5 tubules longer than 2 μm (Figure 6H), while we observed a strong increase in the ratio of cells with more than 5 tubules longer than 5 μm emerging from autolysosomes (Figure 6I), suggesting that the scission of tubules might be affected. Along this line, inhibition of the GTPase DNM2, which is required for the scission of reformation tubules, with Dynasore also increased the ratio of cells with more than 5 tubules longer than 5 μm in starved U2-OS cells, while Dynasore did not increase this fraction any further upon knockdown of PI4K2A (Figure 6J-N).

Because PI4K2A catalyzes the phosphorylation of phosphatidylinositol to PtdIns4P we immunostained WT and KO MEFs for PtdIns4P. Suggesting that higher levels of PI4K2A also entail increased levels of its product, PtdIns4P signals per cell were increased in *spg11* KO and *zfyve26* KO MEFs both at nutrient (Fig. S5A-D) and even more pronounced at starved conditions (Fig. S5E-H). We also quantified PtdIns4P signals at LAMP1-positive puncta after prolonged starvation.

Notably, the PtdIns4P signals at LAMP1-positive puncta was increased in *spg11* KO and *zfyve26* KO MEFs (Figure 7A-D).

When we transfected U2-OS cells stably expressing LAMP1-mCherry with a PtdIns4P-specific fluorescent probe [25], the probe was clearly recruited to emerging LAMP1-positive tubules during ALR (Figure 7E-Eiii, Movie S5). Thus, our data support the assumption that PtdIns4P localizes to reformation tubules in accordance with a previous report [26]. Here, PtdIns4P may interact with a yet unidentified effector or may be further phosphorylated to phosphatidylinositol-4,5-bisphosphate (PtdIns $[4,5]P_2$), which recruits clathrin and AP-2 (adaptor protein complex 2) [26] as well as KIF5B (kinesin family member 5B) [27] to budding and elongating reformation tubules.

To obtain further mechanistic insights we also assessed the association of clathrin with LAMP1-positive puncta during ALR, which was increased in KO MEFs (Figure 8A-D). We also quantified the association of the GTPase DNM2, which can bind to PtdIns(4,5)P_2 [28] and is required for the scission of proto-lysosomal vesicles from reformation tubules during the final step of ALR [29], with LAMP1-positive structures. Remarkably, the DNM2 signals associated with LAMP1-positive puncta were increased as well (Figure 8E-H). Overexpression of PI4K2A in WT MEFs enhanced the colocalization of clathrin (Fig. S6A-C) and DNM2 (Fig. S6D-F) with LAMP1-positive structures.

Taken together, our data suggest that the increased abundance of PI4K2A disturbs the tightly regulated balance between different PIP species and may thus disturb proper ALR.

Discussion

Because SPG11 and SPG15 cannot be distinguished on clinical terms [3] and because the respective proteins were reported to partially colocalize [30], it has been speculated that SPG11 and SPG15 may be pathophysiologically related. The observation that SPG11 and ZFYVE26 co-precipitate in a complex with AP-5, was the first molecular correlate that both proteins act in the same pathway [4,5]. To further address this issue, we compared the phenotypes of *spg11* KO and *zfyve26* KO mice and crossed both lines to obtain dKO mice. Consistent with the assumption that SPG11 and ZFYVE26 act in the same molecular pathway, we did not observe any differences between the phenotypes of *spg11* KO and *zfyve26* KO mice. Moreover, the onset and the severity of symptoms were not aggravated upon simultaneous disruption of both. Notably, mice heterozygous for both KO alleles did not develop any gait abnormalities and did not show an accelerated accumulation of autofluorescent material in neurons as observed in KO mice. This is in contrast to data reported for zebrafish, in which the simultaneous partial knockdown of the *Spg11* and *Zfyve26* orthologues compromised motoneuron axon
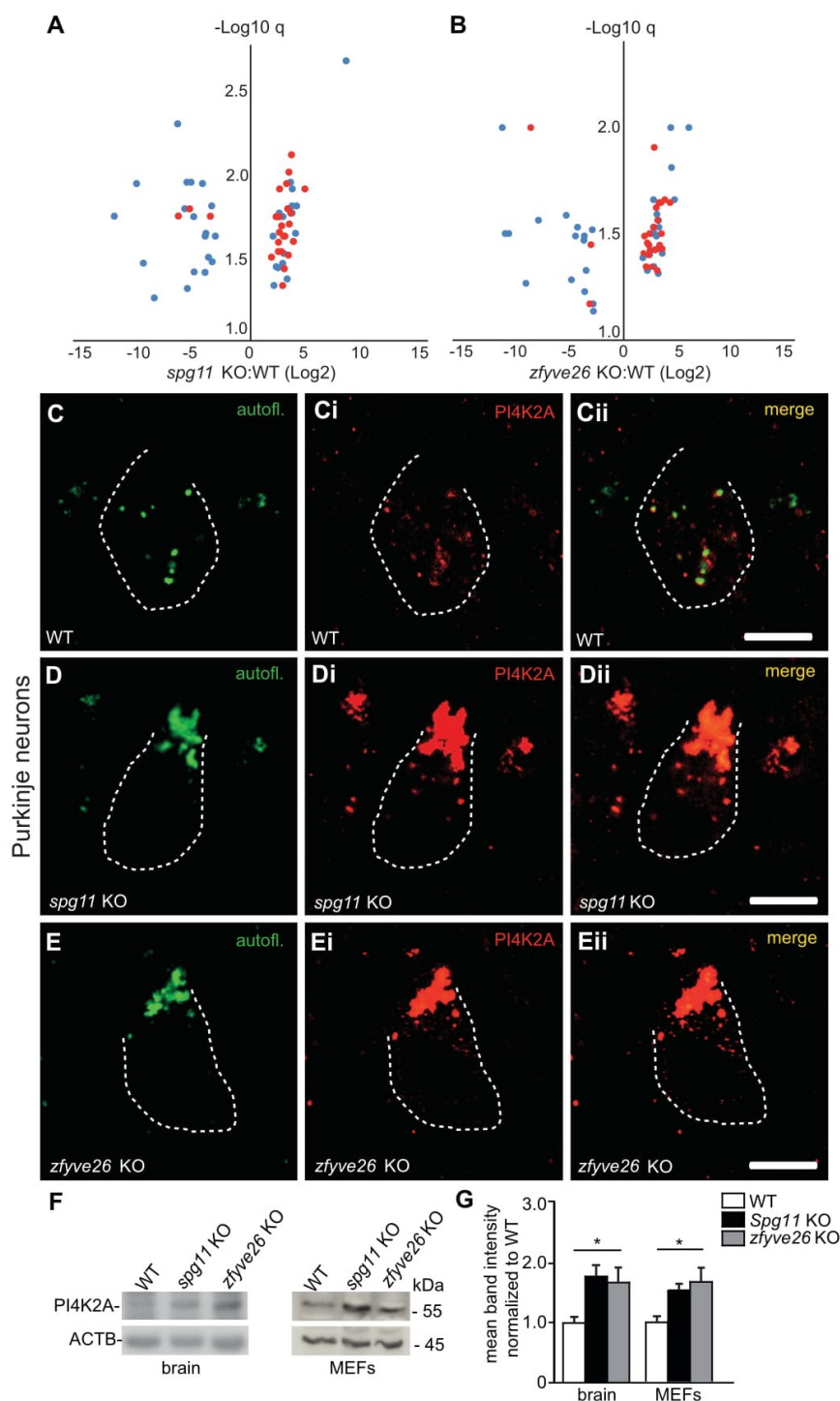
Figure 4. Increased abundance of PI4K2A in autofluorescent deposits of *spg11* KO and *zfyve26* KO mouse brains. (A and B) Autofluorescent material from brains of 6-months-old WT, *spg11* KO and *zfyve26* KO mice was isolated and analyzed by mass spectrometry. Volcano plot displaying log2 fold change of proteins vs. minimal limma q-value changed in the same direction in both *spg11* KO and *zfyve26* KO samples compared to WT. Endomembrane proteins are shown in red. (**C-Eii**) Immunostainings of cerebellar sections confirm the accumulation of PI4K2A (red) in autofluorescent deposits (green) in Purkinje cells of 6-months-old *spg11* KO (D-Dii) and *zfyve26* KO (E-Eii) mice. Purkinje cell somata are marked by a dashed line. Scale bars: 5 μm. (F and G) Western blot analysis confirms the increased abundance of PI4K2A in brain lysates of 16-months-old *spg11* KO and *zfyve26* KO mice and in MEFs of respective genotypes. ACTB served as loading control (n = 5 experiments for MEFs and n = 4 mice per genotype for brain lysates; one-way ANOVA followed by Tukey's Multiple Comparison Test; * p < 0.05). Error bars represent SEM.
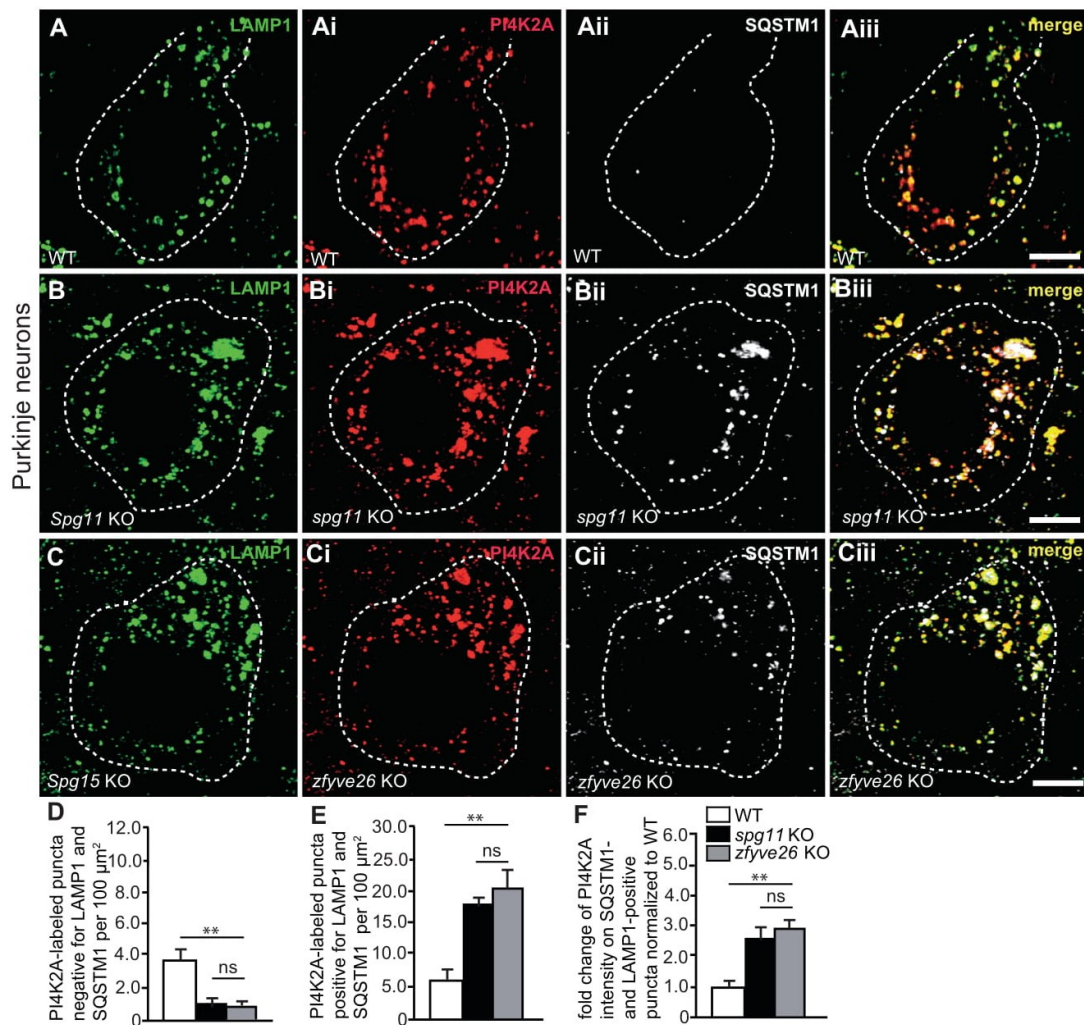
Figure 5. PI4K2A abundance is increased in autolysosomes of pre-symptomatic *spg11* or *zfyve26* KO mice. (**A-Ciii**) Stainings of brain sections of 2-months-old mice. Representative Purkinje cells in brain sections of WT (A-Aiii), *spg11* KO (B-Biii) and *zfyve26* KO mice (C-Ciii) are shown stained for LAMP1 (green), PI4K2A (red) and SQSTM1 (white). Purkinje cell somata are marked by a dashed line. Scale bars: 5 μm. (D) PI4K2A-positive puncta negative for LAMP1 and SQSTM1 are decreased in *spg11* KO and *zfyve26* KO mice. (E) Puncta positive for PI4K2A, LAMP1 and SQSTM1 are increased in *spg11* KO and *zfyve26* KO mice. (F) Mean PI4K2A signal intensities are increased in SQSTM1- and LAMP1-positive puncta in Purkinje cells of *spg11* KO and *zfyve26* KO mice. More than 30 cells from n = 3 mice per genotype were analyzed (one-way ANOVA followed by Tukey's Multiple Comparison Test; ** p < 0.01; ns: not significant). Error bars represent SEM.

outgrowth, while the partial knockdown of either one alone was ineffective [31]. The conflicting data may either point to species differences, off-target effects or unspecific toxic effects of the Morpholino based knockdown, which is frequently observed [32]. Thus, our data argue against the assumption that HSP may be caused by the combination of a heterozygous mutation in one *SPG11* and one *ZFYVE26* allele [31]. To our knowledge such patients have not been reported to date.

Because of its predicted structure it is assumed that SPG11 may be a component of the outer part of the AP-5-containing coat, possibly acting as a membrane-deforming scaffold, while ZFYVE26 may target the complex to membranes enriched in

the endosomal phosphoinositide PtdIns3P via its FYVE-domain [9]. M6PR (mannose-6-phosphate receptor, cation dependent) and SORT1/sortilin 1 both interact with ZFYVE26 and may thus represent cargo receptors of AP-5 [6]. Impaired retrieval of proteins from late endosomes to the Golgi possibly involving SORT1 may thus explain the redistribution of Golgi-related proteins to late endosomes/lysosomes upon disruption of AP-5 [6,18].

Apart from its interaction with AP-5, ZFYVE26 was also shown to interact with BECN1/Beclin 1 [11], a central regulator of autophagosome maturation. Notably, this interaction was disturbed in disease causing ZFYVE26 variants [33] and
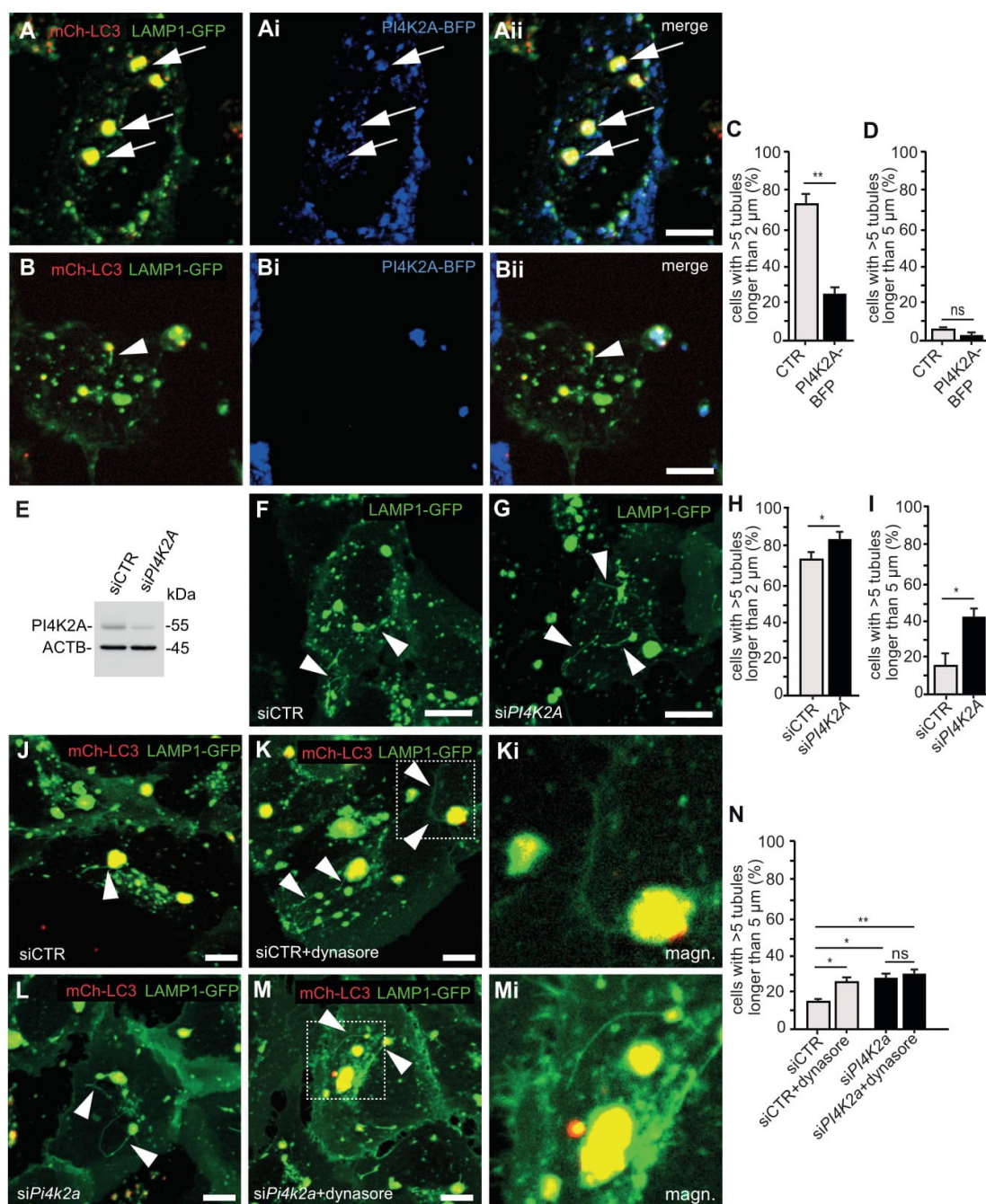
Figure 6. PI4K2A modulates autophagic lysosome reformation. (A-D) Overexpression of PI4K2A-BFP in U2-OS cells stably expressing LAMP1-GFP and mCherry-LC3 impairs ALR. Less tubulation of LAMP1-GFP (green) and mCherry-LC3 (red) labeled autolysosomes in a cell expressing PI4K2A-BFP (blue, marked with white arrows) (A-Aii) compared with a cell not expressing PI4K2A-BFP (B-Bii). Cells were starved with EBSS for 8–9 h. (C and D) Quantification of the ratio of cells with > 5 tubules longer than 2 μm or 5 μm in PI4K2A-BFP positive and negative (CTR) cells (at least 30 cells per group from n = 3 experiments; Student's t-test: ** p < 0.01; ns: not significant). Scale bars: 10 μm. (E-I) SiRNA mediated knockdown of *PI4K2A* in U2-OS cells stably expressing LAMP1-GFP. (E) Immunoblot analysis of cells transfected with either scrambled siRNA (siCTR) or siRNA targeting *PI4K2A* (si*PI4K2A*) with ACTB as loading control. (F and G) Tubulation events (white arrowheads) in control (F) and knockdown (G) cells. Scale bars: 10 μm. (H and I) The ratio of cells with more than 5 LAMP1-positive tubules longer than 2 (H) or 5 μm (I) is increased upon knockdown of *PI4K2A* between 8 and 9 h of EBSS starvation (at least 30 cells per group from n = 3 experiments; Student's t-test: * p < 0.05). (J-N) Inhibition of tubule scission with Dynasore resembles the tubulation defect observed upon knockdown of *PI4K2A* and does not aggravate the effect of *PI4K2A* knockdown on ALR (quantification of at least 30 cells per genotype from n = 3 independent experiments; one-way ANOVA followed by Newman-Keuls Multiple Comparison Test; *** p < 0.001; ns: not significant). Scale bars: 10 μm. Error bars represent SEM.
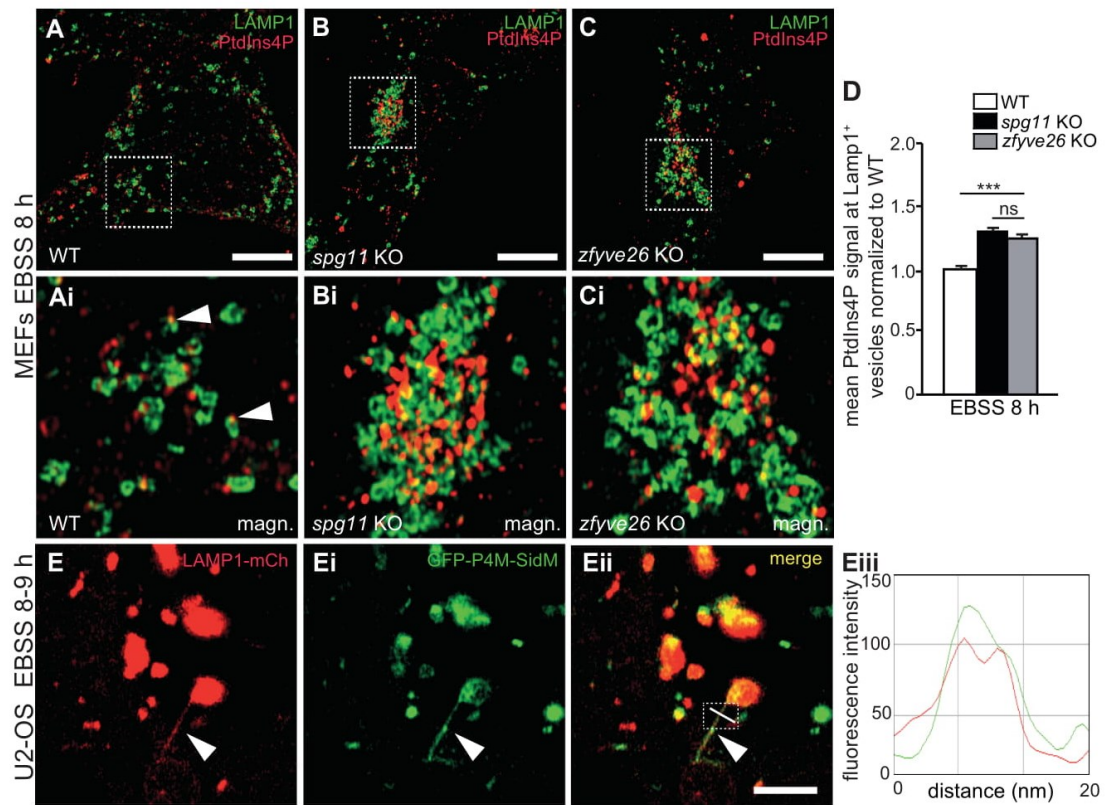
Figure 7. The abundance of PtdIns4P at LAMP1-positive structures is increased in *spg11* KO and *zfyve26* KO MEFs. (A-D) Compared to WT (A and Ai), PtdIns4P signals at LAMP1-positive puncta are increased in starved *spg11* KO (B and Bi) and *zfyve26* KO (C and Ci) MEFs. More than 30 cells from n = 3 independent experiments were analyzed (one-way ANOVA followed by Tukey's Multiple Comparison Test; *** p < 0.001; ns: not significant). Scale bar: 10 μm. Error bars represent SEM. (**E-Eiii**) LAMP1-positive reformation tubules of starved U2-OS cells stably expressing LAMP1-mCherry are labeled by a PtdIns4P-specific fluorescent sensor. Scale bar: 5 μm. (Eiii) Line scan as indicated in (Eii).

caused an accumulation of immature autophagosomes upon starvation in patient derived fibroblasts [11,34]. Both SPG11 and ZFYVE26 interact with RAB5A (RAB5A, member RAS oncogene family) and RAB11 [35], two proteins involved in endosome maturation and trafficking. Only disease associated ZFYVE26, but not SPG11 variants affected RAB protein interactions and impaired the fusion of endosomes and autophagosomes, thus causing a more severe autophagy defect compared to *SPG11* [35]. This is in contrast to our data, which do not support a fusion defect of autophagosomes with lysosomes in *zfyve26* KO MEFs. Possibly, the disease-associated variants studied may not represent full KOs and differences may thus reflect variant-specific effects. Although autophagosome numbers were elevated in *spg11* KO, *zfyve26* KO and dKO MEFs at base line, the numbers did not differ from WT at starved conditions. Instead, we found an accumulation of autolysosomes in starved KO MEFs, which resembles previous reports for the knockdown of *SPG11* or *ZFYVE26* in HeLa cells [12]. A fusion of autophagosomes and lysosomes in *spg11* KO and *zfyve26* KO MEFs was also evident in our flux analysis with a LC3 tandem reporter. As suggested by our LAMP1 and LC3 staining of brain sections,

a depletion of lysosomes and an accumulation of autolysosomes also apply *in vivo* upon disruption of *Spg11* or *Zfyve26*.

To get further clues about the pathophysiology of SPG11 and SPG15, we performed an unbiased mass spectrometry analysis of autofluorescent material isolated from WT, *spg11* KO and *zfyve26* KO brains. We identified high levels of PI4K2A in material isolated from both KO mice, while PI4K2A was not detected in autofluorescent material isolated from control mice. Immunoblot analysis of brain lysates and MEFs suggested a significant increase of PI4K2A abundance upon disruption of *Spg11* or *Zfyve26*. PI4K2A is a membrane-bound phosphatidylinositol 4-kinase, which mainly localizes to LAMP1-positive endosomes and lysosomes [36] and the TGN [22,37] and is recruited to autophagosomes during starvation [23,38]. Here, we show that PI4K2A is also present in autolysosomes and our analyses suggest that the abundance of PI4K2A in autolysosomes is increased upon disruption of either *Spg11* or *Zfyve26*. As suggested by our immunostainings in MEFs this likely changes local levels of its product PtdIns4P. PtdIns4P plays important roles in exocytosis, Golgi function, protein sorting and membrane trafficking [39,40] and may also affect ALR as the terminal step of autophagy.
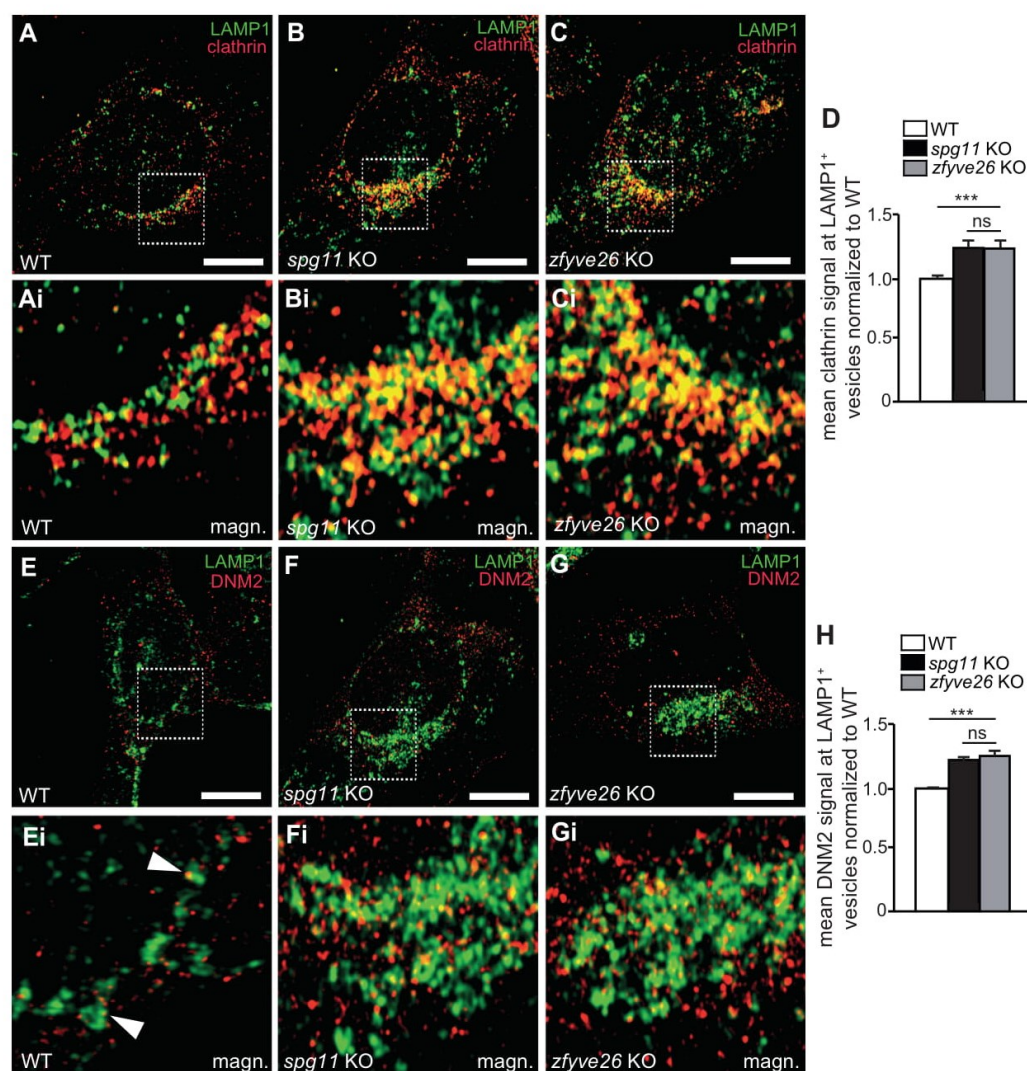
Figure 8. PI4K2A is involved in the recruitment of clathrin and DNM2 during ALR. (A-D) The association of clathrin with LAMP1-positive puncta is increased in starved *spg11* KO and *zfyve26* KO MEFs. Quantification of at least 30 cells per genotype from n = 3 independent experiments (one-way ANOVA followed by Newman-Keuls Multiple Comparison Test; *** p < 0.001; ns: not significant). Scale bars: 10 μm. (E-H) The association of DNM2 with LAMP1-positive puncta is increased in starved *spg11* KO and *zfyve26* KO MEFs. Quantification of at least 30 cells per genotype from n = 3 independent experiments (one-way ANOVA followed by Newman-Keuls Multiple Comparison Test; *** p < 0.001; ns: not significant). Scale bars: 10 μm. Error bars represent SEM.

To mimic our observation that PI4K2A abundance is increased upon disruption of either *Spg11* or *Zfyve26* we over-expressed PI4K2A in control U2-OS cells. Of note, this caused a reduction of LAMP1-positive tubules upon prolonged starvation. Overexpression of PI4K3B (phosphatidylinositol 4-kinase 3 beta), another lipid kinase contributing to the production of PtdIns4P, also decreased the number of lysosomal tubules, while tubules were increased upon PI4K3B knockdown [41]. Likely, the role of these kinases for ALR is complex, because PtdIns4P can be phosphorylated to PtdIns(4,5)P₂, which recruits clathrin to lysosomal budding sites in an AP-2 dependent process [26] and can also bind DNM2, which is required for tubule scission [29]. Indeed, we found that the association of PtdIns4P

and clathrin and DNM2 with LAMP1-postivie structures was increased in *spg11* KO and *zfyve26* KO MEFs. Notably, we observed the same effect upon overexpression of PI4K2A in WT MEFs.

Of note, a gene trap-based mouse model, which lacks the catalytic domain of PI4K2A, also accumulated autofluorescent deposits in neurons, which subsequently degenerated [42]. It thus appears that local PtdIns4P concentrations on autolysosomes have to be tightly controlled in both directions to allow autophagy and ALR. This is further highlighted by recent findings for the lipid phosphatase INPP5K (inositol polyphosphate-5-phosphatase K), which hydrolyzes PtdIns(4,5)P₂ to PtdIns4P. Its disruption caused the accumulation of

PtdIns(4,5)P$_2$ on autolysosomes and prevented the disengagement of clathrin from reformation tubules [43], thus suppressing ALR. A similar mechanism may also apply to DNM2 and tubule scission further contributing to defective ALR. Thus, the bidirectional interconversion of PtdIns4P/PtdIns(4,5)P$_2$ on autolysosomes appears to be a critical event for lysosomal homeostasis.

So far, we do not know why PI4K2A accumulates in LAMP1-positive compartments in the absence of SPG11 or ZFYVE26. This cannot be explained at the transcriptional level, because *Pi4k2a* transcript abundance was not changed upon disruption of either *Spg11* or *Zfyve26*. Analysis of PI4K2A protein abundance after inhibition of translation rather suggests that the turnover of PI4K2A is delayed. Notably, PI4K2A is a target of the E3 ubiquitin ligase Itch, which localizes to the TGN and endosomal compartments [44]. Since SPG11 and ZFYVE26 interact with AP-5, it is tempting to speculate that the retrieval of PI4K2A from autolysosomes is impaired upon disruption of AP-5. Notably, mutations in AP5Z1 are associated with SPG48 [4]. *ap5z1* KO mice also accumulate autolysosome-related autofluorescent material in neurons and show a defect of autophagic flux [18].

Material and methods

Animals

All animal experiments were approved by the "Thüringer Landesamt für Lebensmittelsicherheit und Verbraucherschutz" (TLLV) in Germany (Approval number: 02–039-14). *spg11 zfyve26* double knockout dKO mice were obtained by mating *spg11* KO [14] and *zfyve26* KO [7] mice. Studies were performed with mice on a C57BL/6 background. Mice were housed with a 12 h light/dark cycle and fed on a regular diet *ad libitum*.

Behavioral analysis

For gait analysis mice were trained to walk on a horizontal 20-cm elevated plastic beam (1,000-mm long, either 38-mm broad for cohorts between 8 and 12 months of age or 48-mm broad for mice with an age between 2 and 12 months of age) leading to their home cage as described [7]. After the initial learning phase, the foot-base-angle at toe-off positions of the hind-paws was measured with ImageJ using single video frames from recordings of beam walking mice.

Histological analysis

Immunohistochemistry was done on formalin fixed free floating sections as described previously [45]. Cortical motoneuron and Purkinje cell numbers were quantified on 40-μm sagittal brain sections after staining of brain sections with an antibody directed against RBFOX3 and CALB1. For statistical analysis the number of RBFOX3-positive neurons per 10,000 μm^2 area per layer from motocortex and/or Purkinje cells per 1,000 μm distance along the Purkinje cell layer was counted from 3 different brain sections from 3 mice per

genotype. Images of the sagittal sections of wild-type and knockout brains were taken with a confocal scanning fluorescence microscope (Zeiss LSM 880) with Airyscan using a Plan-Apochromat 63x/1.4 oil DIC M27 objective. Neurons and intracellular vesicles were quantified manually with the cell counter plugin and the area measurement tool of the ImageJ online software. For spectral analysis the fluorescent signals of deposits and the Cy5 secondary antibodies were recorded and further analyzed by linear unmixing as described previously [7].

Western blotting

For immunoblot analysis, brain samples were homogenized in a buffer containing 25 mM sucrose (Sigma-Aldrich, S7903), 50 mM Tris-HCl, pH 7.4, 1 mM EDTA, completed with protease inhibitor mix (Roche, 04693124001). The homogenates were centrifuged at 500 g at 4°C for 10 min. The supernatants were collected and mixed with a buffer containing 25 mM sucrose, 50 mM Tris-HCl, pH 7.4, 1 mM EDTA, 1% Triton X-100 (Sigma-Aldrich, T9284) completed with proteinase inhibitors and gently rotated for 1 h at 4°C (i.e., Triton X-100 soluble fraction). After centrifugation at 13,000 g and 4°C for 15 min the pellets were dissolved in 1% (w:v) SDS-PBS (137 mM NaCl, 2.7 mM KCl, 10 mM Na$_2$HPO$_4$, 1.8 mM KH$_2$PO$_4$) buffer (i.e., Triton X-100 insoluble fraction). The samples were denatured at 95°C in Laemmli buffer and separated in 4–20% pre-cast gradient gels (Bio-Rad). After transfer on a PVDF membrane (GE Healthcare Amersham, GE10600023), 2.5% (w:v) milk powder (Santa Cruz Biotechnology, sc-2325) with 2.5% (w:v) BSA (Serva, 11930.03) in TBS-T buffer (Tris-buffered saline (137 mM NaCl, 25 mM Tris-Base, 2.7 mM KCl, pH 7.4) with Tween 20 (Sigma-Aldrich, P9416) was used in order to block the membrane. Primary and secondary antibodies were incubated in blocking solution. For detection of proteins the ECL Western Blotting Detection System (Bio Rad, 170–5061) was used. For autophagy studies mouse embryonic fibroblasts (MEFs obtained from *spg11* KO, *zfyve26* KO and dKO mice, as described above) were either incubated for 6 h with 1 μM Torin 1 (Merck Millipore, 475991) to initiate or 100 nM bafilomycin A$_1$ (Merck Millipore, 19–148) to block autophagy and subsequently lysed in a buffer containing 50 mM Tris-HCl pH 8.0, 120 mM NaCl, 0.5% NP-40 (VWR, A1694.0250), 2 mM EDTA completed with protease inhibitor mix (Roche, 4693159001). The lysates were rotated for 30 min and centrifuged at 10,000 g at 4°C. The resulting supernatant was denatured in sample buffer for 5 min at 95°C and separated in 8–15% polyacrylamide pre-cast gradient gels. 3% BSA in TBS-T (MEFs) or 10% skimmed milk served as blocking solution.

Mass spectrometric analysis of deposits

The deposits for mass spectrometry were isolated from total brain lysates of 6-months-old mice (n = 6 per genotype) as described [20] and used for the quantitative proteomics modified from [46,47]. In brief, protein solutions were reduced with 20 mM DTT at 55°C for 20 min and loaded onto

centrifugal filter units with a 10 kDa cutoff modified Polyethersulfone (PES) membrane (Pall, OD010C34). The buffer was exchanged by centrifugation and addition of 20 mM triethylammonium bicarbonate (TEAB) (Sigma-Aldrich, T7408), 0.5% sodium deoxycholate (SDC) (Sigma-Aldrich, 30968). Alkylation of thiol groups was done with 40 mM acrylamide (Sigma-Aldrich, A9099) for 20 min at room temperature. After another buffer exchange 1 μg trypsin (Promega, V5111) was added in 20 mM TEAB, 0.5% SDC in a total volume of 50 μl. Digestion proceeded overnight at 37° C. Peptides were collected and SDC was precipitated with TFA (VWR, 85049.001P) (2.5% final). Remaining SDC was removed by phase transfer with equal volume of ethyl acetate. Peptides were vacuum concentrated and labeled with amine-reactive, 6-plex tandem mass tag reagents (Thermo Fisher Scientific, 90061) according to manufacturer's instructions. The labeling reaction was quenched by addition of 5% hydroxylamine (Sigma-Aldrich, 467804). Labeled peptides were pooled and desalted on Oasis HLB cartridges (Waters GmbH, WAT094225). Eluates containing 70% acetonitrile (AppliChem, 7218811612), 0.1% formic acid (FA) (VWR, 85048.001P) were dried and fractionated into 12 fractions by isoelectric point with an Offgel fractionator (Agilent Technologies). Peptide fractions were dried and stored at −20°C.

Peptides were dissolved in 10 μl 0.1% FA (solvent A). 1.5 μl were injected onto a C18 trap column (20 mm length, 100 μm inner diameter, ReproSil-Pur 120 C18-AQ, 5 μm, Dr. Maisch GmbH) made in-house. Bound peptides were eluted onto a C18 analytical column (200 mm length, 75 μm inner diameter, ReproSil-Pur 120 C18-AQ, 1.9 μm). Peptides were separated during a linear gradient from 2% to 35% solvent B (90% acetonitrile, 0.1% formic acid) within 120 min at 300 nl/min. The nanoHPLC was coupled online to an LTQ Orbitrap Velos mass spectrometer (Thermo Fisher Scientific). Peptide ions between 330 and 1600 m/z were scanned in the Orbitrap detector with a resolution of 30,000 (maximum fill time 400 ms, AGC target 10^6). The 20 most intense precursor ions (threshold intensity 5,000, isolation width 1.1 Da) were subjected to higher collision dissociation (HCD, stepped collision energy 32, 42, 52%) and analyzed in the Orbitrap detector (R = 7500). Fragmented peptide ions were excluded from repeat analysis for 17 s. Raw data processing and analysis of database searches were performed with Proteome Discoverer software 2.1.1.21 (Thermo Fisher Scientific). Peptide identification was done with an in house Mascot server version 2.5 (Matrix Science Ltd). MS2 data were searched against the Uniprot mouse reference proteome (release 2016_11). Precursor ion m/z tolerance was 9 ppm, fragment ion 20 mmu. a-, b- and y-ion series were included. Tryptic peptides with up to two missed cleavages were searched. Propionamide modification of cysteines and TMT-modification of peptide N-termini were set as static modifications. Oxidation of methionine, protein N-terminal acetylation, and TMT-modification of lysines were allowed as dynamic modifications. Mascot results were assigned q-values by the percolator algorithm [47] version 2.05 as implemented in Proteome Discoverer. Spectra of peptide spectrum matches (PSMs) with q > 0.01 were sent to a second round of database search with semitryptic enzyme specificity (one missed cleavage allowed). Dynamic modifications were the same as above plus propionamide (cysteine), di-Gly on lysine, and TMT on N-termini. Proteins were included if at least two peptides were identified with q ≤ 0.01. False positive rates were estimated to be 1.0%, 1.2%, and 4.5% on PSM, peptide, and protein level respectively. In order to reduce the reporter ion compression bias PSMs with >30% co-isolation were excluded from quantification. Only unique peptides were included in protein quantification. 2,088 proteins with intensities in ≥ 2 biological replicates were used for median normalization. KO:WT ratios of proteins with ≥ 3 replicates were sent to limma and rank product tests with correction for multiple testing [48]. A threshold of corrected p-value ≤ 0.05 defined significant regulation.

Antibodies and DNA constructs

The following commercially obtained antibodies were used: rat anti-LAMP1, 1:250 for immunofluorescence (IF) and 1:500 for western blotting (WB) (BD Pharmigen, 553792); mouse anti-RBFOX3/NeuN, 1:500 (Millipore, MAB377); mouse anti-SQSTM1/p62, 1:500 for IF and 1:1,000 for WB (Abcam, ab56416); mouse anti-PI4K2A, 1:50 for IF and 1:500 for WB (Santa Cruz Biotechnology, sc-390026); and rabbit anti-PtdIns4P, 1:200 (Echelon biosc., Z-P004) mouse anti-ACTB/β-actin (Abcam, ab6276), 1:5,000 and mouse ant-GFP, 1:2,000 (Millipore, MAB3580); rabbit anti-LC3B, 1:1,000 for WB and 1:200 for ICC (Cell Signaling Technology, 2775S); mouse anti LC3B, 1:50 for IHC (Nanotools, 0231–100/LC3-5 F10); rabbit anti-GAPDH, 1:1,000 for WB (Santa Cruz Biotechnology, sc-25778); mouse anti-clathrin (Abcam, ab2731) 1:1,000 for IF; rabbit anti-DNM2/Dynamin-2 1:15,000 (R2641, a generous gift of IGBMC). Horseradish peroxidase-labeled secondary antibodies for western blotting: goat anti-rabbit (NA9340) and goat anti-mouse (NA9310), both 1:2,000 (Amersham Bioscience) and goat anti-rat, 1:1,000 (Santa Cruz Biotechnology, sc-2032).

The following fluorescently labeled secondary antibodies were used from Thermo Fisher Scientific: goat anti-mouse-Alexa Fluor 488 (A11029) and 546 (A11030), goat anti-rabbit Alexa Fluor 488 (A11008) and 546 (A11035), 1:1,000; goat anti-rabbit (A10523), goat anti-mouse (A10524) and goat anti-rat Cy5 (A10525), 1:1,000; goat anti-mouse IgM chain specific Cy5 conjugated (Merk, AP500S), goat anti-mouse IgG1 Alexa Fluor 546 (Thermo Fisher Scientific, A-21123) and goat anti-mouse IgG2a, Alexa Fluor 647 (Thermo Fisher Scientific, A-21241). Nuclei were stained with Hoechst-33258, 1:10,000 (H3569).

The LAMP1-GFP plasmid was a gift from Esteban Dell'Angelica (Addgene, 34831) [49]. PI4K2A-GFP, and EGFP-x2P4M-SidM plasmids were provided by Dr. Tamas Balla (National Institutes of Health, Bethesda, USA) [25]. For cloning of the PI4K2A-BFP DNA construct, the C-terminal GFP of PI4K2A-GFP was exchanged by BFP sequence using the EcoRI and NotI restriction sites. RFP-

LC3 was a kind gift of Dr. Christoph Kaether (Fritz-Lipmann-Institute Jena, Germany). The ptfLC3 plasmid [50] was a gift from Tamotsu Yoshimori (Addgene, 21074).

Knockdown studies

siRNAs directed against human *PI4K2A* transcripts was purchased from Santa Cruz Biotechnology (sc-90773) and used according to the manufacturer. The knockdown was verified by immunoblotting.

Cell culture and Time-lapse imaging

U2-OS LAMP1-GFP or LAMP1-mCherry single *knockin* and U2-OS mCherry-LC3/LAMP1-GFP double *knockin* cell lines were provided by Dr. Ian G. Ganley from the University of Dundee, which were previously characterized in [24]. Mouse embryonic fibroblasts (MEFs) were prepared from E13.5 mouse pups as described [45]. The cells were cultured in the following growth medium: Dulbecco's Modified Eagle medium (DMEM, Gibco, 31-966–021) supplemented with 10% fetal bovine serum (bio-west, S1810-500) and 1% penicillin streptomycin (Gibco, 15070–063) and maintained in a humidified atmosphere with 5% CO_2 and 37°C. For autophagic flux analysis by western blotting MEFs were cultured onto 6-well dishes at a density of 300,000 per well in growth medium overnight. At day 2 cells were washed 3 times with ice-cold PBS and then treated with EBSS, EBSS supplemented with 1 μmol Torin (Calbbiochem, 475991) and/or additionally with 100 nM bafilomycin A_1 (Sigma-Aldrich, 19–148) for 6 h. After treatment, cells were washed twice on ice in ice-cold PBS and lysed directly by addition of RIPA lysis buffer. Samples were sonicated, boiled and subjected to SDS-PAGE and western blotting as described previously [7].

For detection of lysosomal tubules, MEFs and/or U2-OS cells were plated on 42 mm coverslips (PeCon, 000380) in 6 cm plates and transfected after 24 h with 3 μg of each plasmid DNA: LAMP1-GFP, PI4K2A- BFP, or PI4K2A siRNA using Lipofectamine 3000 (Thermo Fischer, L3000008) for 48 h. To induce autophagy, cells were incubated with EBSS medium (Thermo Fischer, 24010043) for 8–9 h. For inhibition of DNM2, 40 μM Dynasore solution (Millipore, 324410) was added 2 h before the acquisition. Tubulation events were visualized with a fluorescence microscope (CellObserver Z1, Zeiss) equipped with an incubation chamber (37°C, 5% CO_2). Time-lapse images were acquired every 2 s for 3 min using the ApoTome mode and the 40x/1.2 W objective. Number and length of tubules were evaluated for at least 30 cells of each genotype in 3 independent experiments using ImageJ (National institutes of health).

To detect PtdIns4P in live cell microscopy experiments, U2-OS LAMP1-mCherry cells were plated in a μ-Slide 8 well chamber slide (IBIDI, 80,826) and after 24 h transfected with 0.5 μg pEGFP-x2P4M-SidM [25]. After 8 h treatment with EBSS, tubulation events were visualized with a confocal scanning fluorescence microscope (Zeiss LSM 880) with Airyscan equipped with an incubation chamber (37°C, 5% CO_2, Tokai hit WSBX incubator) using a Plan-Apochromat 63x/1.4 oil DIC M27 objective.

Immunocytochemistry

Cells were seeded on 14 mm coverslips and fixed in 4% PFA or 100% ice-cold methanol (LC3 staining) for 10 min. Cells were washed three times, permeabilized with 0.25% Triton X-100 for 10 min. and blocked using 5% normal goat serum (BIOZOL, S-1000) for 1 h at room temperature. Coverslips were incubated overnight with primary antibodies diluted in blocking solution at 4°C. The next day the coverslips were washed three times and incubated with secondary antibodies conjugated with a fluorophore for 1 h at room temperature. After washing three times with 1xPBS cells were stained with Hoechst (1:10,000, Invitrogen, H3569) and mounted with fluoromount mounting medium (BIOZOL, SBA-0100-01) Stainings with for PtdIns4P were perfomed as described previously [51]. Images were acquired with a confocal scanning fluorescence microscope (Zeiss LSM 880) with Airyscan using the Plan-Apochromat 63x/1.4 oil DIC M27 objective, and further analyzed in ImageJ. For the particle colocalization analyses the ComDet plugin of ImageJ was used.

Flow Cytometry

To investigate the degradation of PI4K2A in MEFs cells were transfected with PI4K2A-GFP or empty vector (pEGFP-N1). After 48 h cells were harvested or treated with 10 μg/ml Cycloheximide (Sigma-Aldrich, C4859) for 4 h. Cells were fixed in 4% PFA and stored at 4°C until measurement. Flow cytometry was performed and analyzed with the BD Accuri C6 Plus Flow cytometer and software (BD biosciences) according to manufacturer's protocol. Prior the analysis of GFP fluorescence, cell debris and aggregates were excluded with pre-gating on FSC/SSC.

Quantitative reverse transcription PCR

RNA was isolated from MEFs using preGOLD TriFast (VWR, 30–2010) according to the manufacturer's protocol. Two-step quantitative reverse transcription PCR (qRT-PCR) was performed with the following specific primers: *Pi4k2a*-F: CTC CCTGAGAACACGAACCG *Pi4k2a*-R: ATCACCC AATCTGTGTCCCG; *Actb*-F: AGAGGGAAATCGT GCGTGAC *Actb*-R: CAATAGTGATGACCTGGCCGT.

Statistical analysis

The results were blinded to experimenter and were analyzed in Graphpad Prism 6 (Graphpad Software Inc). Data in graphs are presented as mean ± SEM. In some of the results, values are normalized on the mean of control samples, which is represented as 1. The differences between many groups were determined by using of one-way ANOVAs followed by Tukey's Multiple Comparison test or by Newman-Keuls Multiple Comparison test. The differences between many groups and repeated measurements were estimated by two-way ANOVAs with Bonferroni posthoc test. For differences

between 2 groups statistical significance was determined by using of unpaired two-tailed Student's t-tests. The significance values are represented as; p* < 0.05, p** < 0.01 and p*** < 0.001. Non-significant p values are represented as: ns.

Acknowledgments

Disclosure statement

Funding

References

[1] Fink JK. Hereditary spastic paraplegia: clinical principles and genetic advances. Semin Neurol. 2014;34(3):293–305.

[2] Shribman S, Reid E, Crosby AH, et al. Hereditary spastic paraplegia: from diagnosis to emerging therapeutic approaches. Lancet Neurol. 2019;18(12):1136–1146.

[3] Schule R, Schols L. Genetics of hereditary spastic paraplegias. Semin Neurol. 2011;31(5):484–493.

[4] Slabicki M, Theis M, Krastev DB, et al. A genome-scale DNA repair RNAi screen identifies SPG48 as a novel gene associated with hereditary spastic paraplegia. PLoS Biol. 2010;8(6):e1000408.

[5] Hirst J, Barlow LD, Francisco GC, et al. The fifth adaptor protein complex. PLoS Biol. 2011;9(10):e1001170.

[6] Hirst J, Itzhak DN, Antrobus R, et al. Role of the AP-5 adaptor protein complex in late endosome-to-Golgi retrieval. PLoS Biol. 2018;16(1):e2004411.

[7] Khundadze M, Kollmann K, Koch N, et al. A hereditary spastic paraplegia mouse model supports a role of ZFYVE26/SPASTIZIN for the endolysosomal system. PLoS Genet. 2013;9(12):e1003988.

[8] Pensato V, Castellotti B, Gellera C, et al. Overlapping phenotypes in complex spastic paraplegias SPG11, SPG15, SPG35 and SPG48. Brain. 2014;137(7):1907–1920.

[9] Hirst J, Borner GH, Edgar J, et al. Interaction between AP-5 and the hereditary spastic paraplegia proteins SPG11 and SPG15. Mol Biol Cell. 2013;24(16):2558–2569.

[10] Sagona AP, Nezis IP, Pedersen NM, et al. PtdIns(3)P controls cytokinesis through KIF13A-mediated recruitment of FYVE-CENT to the midbody. Nat Cell Biol. 2010;12(4):362–371.

[11] Vantaggiato C, Crimella C, Airoldi G, et al. Defective autophagy in spastizin mutated patients with hereditary spastic paraparesis type 15. Brain. 2013;136(10):3119–3139.

[12] Boutry M, Branchu J, Lustremant C, et al. Inhibition of lysosome membrane recycling causes accumulation of gangliosides that contribute to neurodegeneration. Cell Rep. 2018;23(13):3813–3826.

[13] Chang J, Lee S, Blackstone C. Spastic paraplegia proteins spastizin and spatacsin mediate autophagic lysosome reformation. J Clin Invest. 2014;124(12):5249–5262.

[14] Varga RE, Khundadze M, Damme M, et al. In Vivo Evidence for Lysosome Depletion and Impaired Autophagic Clearance in Hereditary Spastic Paraplegia Type SPG11. PLoS Genet. 2015;11 (8):e1005454.

[15] Yu L, McPhee CK, Zheng L, et al. Termination of autophagy and reformation of lysosomes regulated by mTOR. Nature. 2010;465 (7300):942–946.

[16] Boutry M, Pierga A, Matusiak R, et al. Loss of spatacsin impairs cholesterol trafficking and calcium homeostasis. Commun Biol. 2019;2(1):380.

[17] Branchu J, Boutry M, Sourd L, et al. Loss of spatacsin function alters lysosomal lipid clearance leading to upper and lower motor neuron degeneration. Neurobiol Dis. 2017;102:21–37.

[18] Khundadze M, Ribaudo F, Hussain A, et al. A mouse model for SPG48 reveals a block of autophagic flux upon disruption of adaptor protein complex five. Neurobiol Dis. 2019;127:419–431.

[19] Mauvezin C, Neufeld TP. Bafilomycin A1 disrupts autophagic flux by inhibiting both V-ATPase-dependent acidification and Ca-P60A/SERCA-dependent autophagosome-lysosome fusion. Autophagy. 2015;11(8):1437–1438.

[20] Ottis P, Koppe K, Onisko B, et al. Human and rat brain lipofuscin proteome. Proteomics. 2012;12(15–16):2445–2454.

[21] Ashburner M, Ball CA, Blake JA, et al. Gene ontology: tool for the unification of biology. the gene ontology consortium. Nat Genet. 2000;25(1):25–29.

[22] Wang YJ, Wang J, Sun HQ, et al. Phosphatidylinositol 4 phosphate regulates targeting of clathrin adaptor AP-1 complexes to the Golgi. Cell. 2003;114(3):299–310.

[23] Baba T, Toth DJ, Sengupta N, et al. Phosphatidylinositol 4,5-bisphosphate controls Rab7 and PLEKMH1 membrane cycling during autophagosome-lysosome fusion. Embo J. 2019;38(8): e10031238.

[24] Munson MJ, Allen GF, Toth R, et al. mTOR activates the VPS34-UVRAG complex to regulate autolysosomal tubulation and cell survival. Embo J. 2015;34(17):2272–2290.

[25] Hammond GR, Machner MP, Balla T. A novel probe for phosphatidylinositol 4-phosphate reveals multiple pools beyond the Golgi. J Cell Biol. 2014;205(1):113–126.

[26] Rong Y, Liu M, Ma L, et al. Clathrin and phosphatidylinositol-4,5-bisphosphate regulate autophagic lysosome reformation. Nat Cell Biol. 2012;14(9):924–934.

[27] Du W, Su QP, Chen Y, et al. Kinesin 1 Drives Autolysosome Tubulation. Dev Cell. 2016;37(4):326–336.

[28] Achiriloaie M, Barylko B, Albanesi JP. Essential role of the dynamin pleckstrin homology domain in receptor-mediated endocytosis. Mol Cell Biol. 1999;19(2):1410–1415.

[29] Schulze RJ, Weller SG, Schroeder B, et al. Lipid droplet breakdown requires dynamin 2 for vesiculation of autolysosomal tubules in hepatocytes. J Cell Biol. 2013;203(2):315–326.

[30] Murmu RP, Martin E, Rastetter A, et al. Cellular distribution and subcellular localization of spatacsin and spastizin, two proteins involved in hereditary spastic paraplegia. Mol Cell Neurosci. 2011;47(3):191–202.

[31] Martin E, Yanicostas C, Rastetter A, et al. Spatacsin and spastizin act in the same pathway required for proper spinal motor neuron axon outgrowth in zebrafish. Neurobiol Dis. 2012;48(3):299–308.

[32] Ekker SC, Larson JD. Morphant technology in model developmental systems. Genesis. 2001;30(3):89–93.

[33] Vantaggiato C, Clementi E, Bassi MT. ZFYVE26/SPASTIZIN: a close link between complicated hereditary spastic paraparesis and autophagy. Autophagy. 2014;10(2):374–375.

[34] Renvoise B, Chang J, Singh R, et al. Lysosomal abnormalities in hereditary spastic paraplegia types SPG15 and SPG11. Ann Clin Transl Neurol. 2014;1(6):379–389.

[35] Vantaggiato C, Panzeri E, Castelli M, et al. ZFYVE26/SPASTIZIN and SPG11/SPATACSIN mutations in hereditary spastic paraplegia types AR-SPG15 and AR-SPG11 have different effects on autophagy and endocytosis. Autophagy. 2019;15(1):34–57.

[36] Balla A, Tuymetova G, Barshishat M, et al. Characterization of type II phosphatidylinositol 4-kinase isoforms reveals association of the enzymes with endosomal vesicular compartments. J Biol Chem. 2002;277:20041–20050.

[37] Wei YJ, Sun HQ, Yamamoto M, et al. Type II phosphatidylinositol 4-kinase beta is a cytosolic and peripheral membrane protein that is recruited to the plasma membrane and activated by Rac-GTP. J Biol Chem. 2002;277(48):46586–46593.

[38] Wang H, Sun HQ, Zhu X, et al. GABARAPs regulate PI4P-dependent autophagosome:lysosome fusion. Proc Natl Acad Sci U S A. 2015;112(22):7015–7020.

[39] Ebner M, Koch PA, Haucke V. Phosphoinositides in the control of lysosome function and homeostasis. Biochem Soc Trans. 2019;47(4):1173–1185.

[40] Minogue S. The Many Roles of Type II Phosphatidylinositol 4-Kinases in Membrane Trafficking: New Tricks for Old Dogs. BioEssays 2018;40:1700145.

[41] Sridhar S, Patel B, Aphkhazava D, et al. The lipid kinase PI4KIIIbeta preserves lysosomal identity. Embo J. 2013;32 (3):324–339.

[42] Simons JP, Al-Shawi R, Minogue S, et al. Loss of phosphatidylinositol 4-kinase 2alpha activity causes late onset degeneration of spinal cord axons. Proc Natl Acad Sci U S A. 2009;106 (28):11535–11539.

[43] McGrath MJ, Eramo MJ, Gurung R, et al. Defective lysosome reformation during autophagy causes skeletal muscle disease. J Clin Invest. 2021;131(1):e135124.

[44] Mossinger J, Wieffer M, Krause E, et al. Phosphatidylinositol 4-kinase IIalpha function at endosomes is regulated by the ubiquitin ligase Itch. EMBO Rep. 2012;13(12):1087–1094.

[45] Sinning A, Liebmann L, Kougioumtzes A, et al. Synaptic glutamate release is modulated by the Na$^+$-driven Cl$^-$/HCO$_3^-$ exchanger Slc4a8. J Neurosci. 2011;31(20):7300–7311.

[46] Manza LL, Stamer SL, Ham AJ, et al. Sample preparation and digestion for proteomic analyses using spin filters. Proteomics. 2005;5(7):1742–1745.

[47] Kall L, Storey JD, Noble WS. Non-parametric estimation of posterior error probabilities associated with peptides identified by tandem mass spectrometry. Bioinformatics. 2008;24(16):i42–8.

[48] Schwammle V, Vaudel M. Computational and Statistical Methods for High-Throughput Mass Spectrometry-Based PTM Analysis. Methods Mol Biol. 2017;1558:437–458.

[49] Falcon-Perez JM, Nazarian R, Sabatti C, et al. Distribution and dynamics of Lamp1-containing endocytic organelles in fibroblasts deficient in BLOC-3. J Cell Sci. 2005Nov15; 118(Pt 22):5243–5255.

[50] Kimura S, Noda T, Yoshimori T. Dissection of the autophagosome maturation process by a novel reporter protein, tandem fluorescent-tagged LC3. Autophagy. 2007;3(5):452–460.

[51] Judith D, Jefferies HBJ, Boeing S, et al. ATG9A shapes the forming autophagosome through Arfaptin 2 and phosphatidylinositol 4-kinase IIIbeta. J Cell Biol. 2019;218(5):1634–1652.
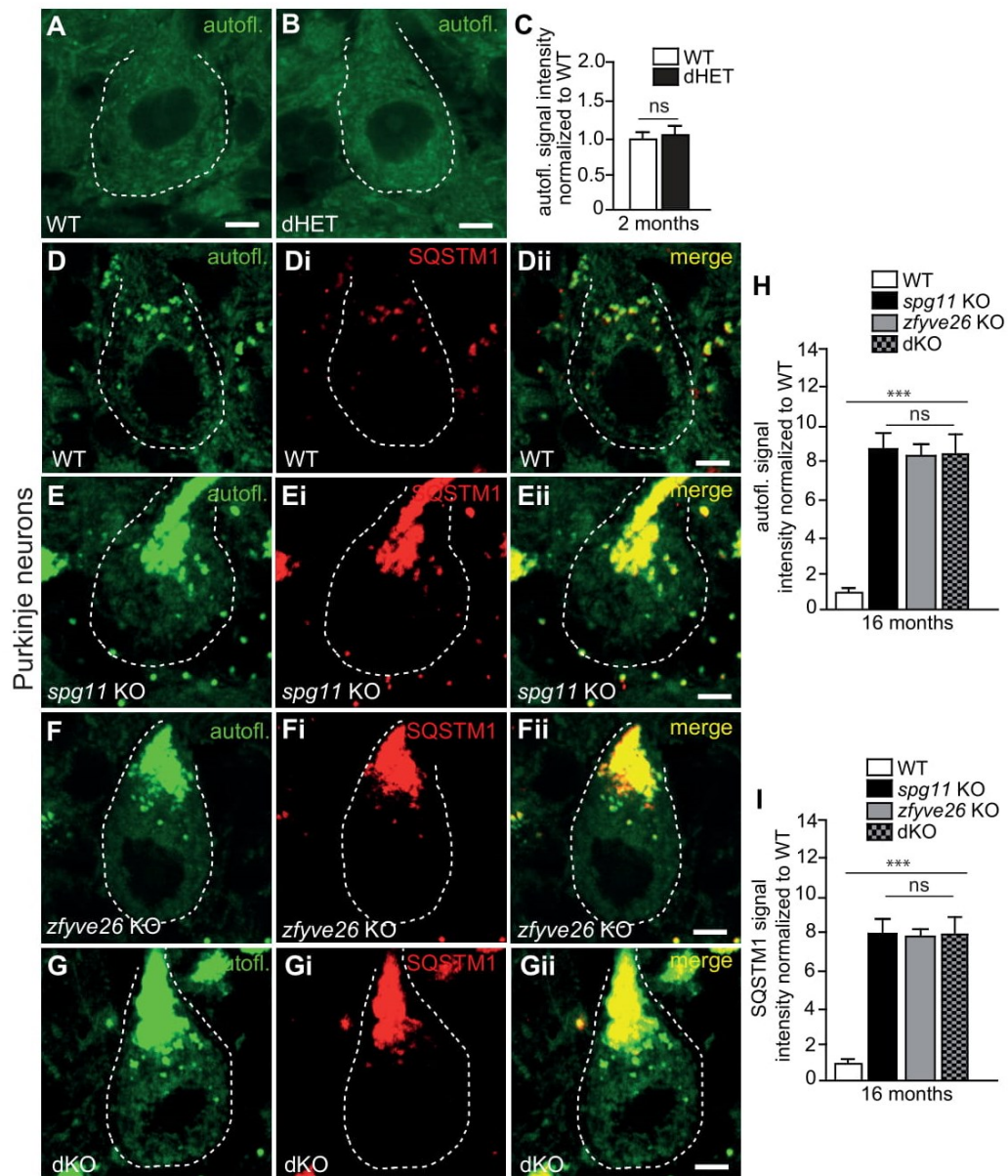
3.2.1 Supplementary Material

Figure S1

Figure S1. Autofluorescence and SQSTM1 abundance is likewise increased in Purkinje cells of 16-months-old *Spg11* KO, *Zfyve26* KO and *Spg11 Zfyve26* double-KO mice (dKO). (**A-C**) Compared to WT (A) Purkinje cell autofluorescence (green, excitation at 488 nm) is not increased in 2-months-old mice heterozygous for the *Spg11* and *Zfyve26* (dHET) allele (B) (more than 30 cells per genotype; n=3 mice per genotype; one-way ANOVA followed by Tukey's Multiple Comparison Test; ns: not significant). Scale bars: 5 μm. (**D-Gii**) Autofluorescent material in Purkinje cells of 16-months-old WT mice (D-Dii) rarely co-localizes with SQSTM1, while the large autofluorescent deposits in S*pg11* KO (E-Eii), *Zfyve26* KO (F-Fii) and double (G-Gii) KO mice regularly stain for SQSTM1. Purkinje cell somata are marked by a dashed line. Scale bars: 5 μm. (**H** and **I**) Quantification of autofluorescence and of SQSTM1 signal intensities. More than 30 cells from 3 mice per genotype were analyzed (one-way ANOVA followed by Tukey's Multiple Comparison Test; *** p<0.001; ns: not significant). Error bars represent SEM.
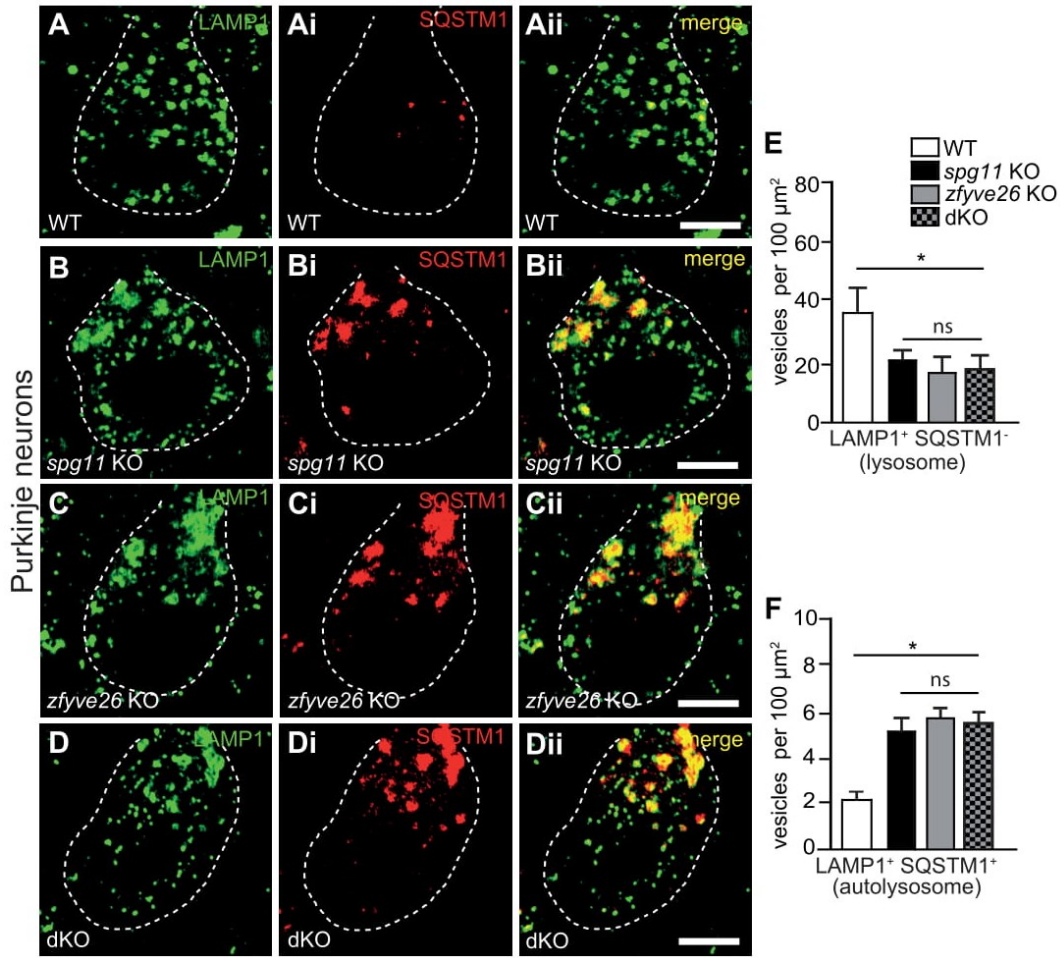
Figure S2. Less lysosomes in Purkinje cells of *spg11* KO, *zfyve26* KO and *spg11 zfyve26* double KO mice. (**A-F**) Lysosome numbers are likewise reduced in Purkinje cells of 2-months-old *spg11* KO, *zfyve26* KO and double KO mice. Representative Purkinje cells in brain sections of WT (A-Aii), *spg11* KO (B-Bii), *zfyve26* KO (C-Cii) and double KO (D-Dii) mice stained for LAMP1 (green) and SQSTM1 (red). Purkinje cell somata are marked by a dashed line. (E and F) Quantification of lysosomes (E) defined as LAMP1-positive and-negative puncta and autolysosomes (F) defined as LAMP1-positive and SQSTM1-positive puncta. More than 30cells from 3 mice per genotype were analyzed (one-way ANOVA followed by Tukey's Multiple Comparison Test; * $p<0.05$; ns: not significant). Scale bars: 5 µm. Error bars represent SEM.
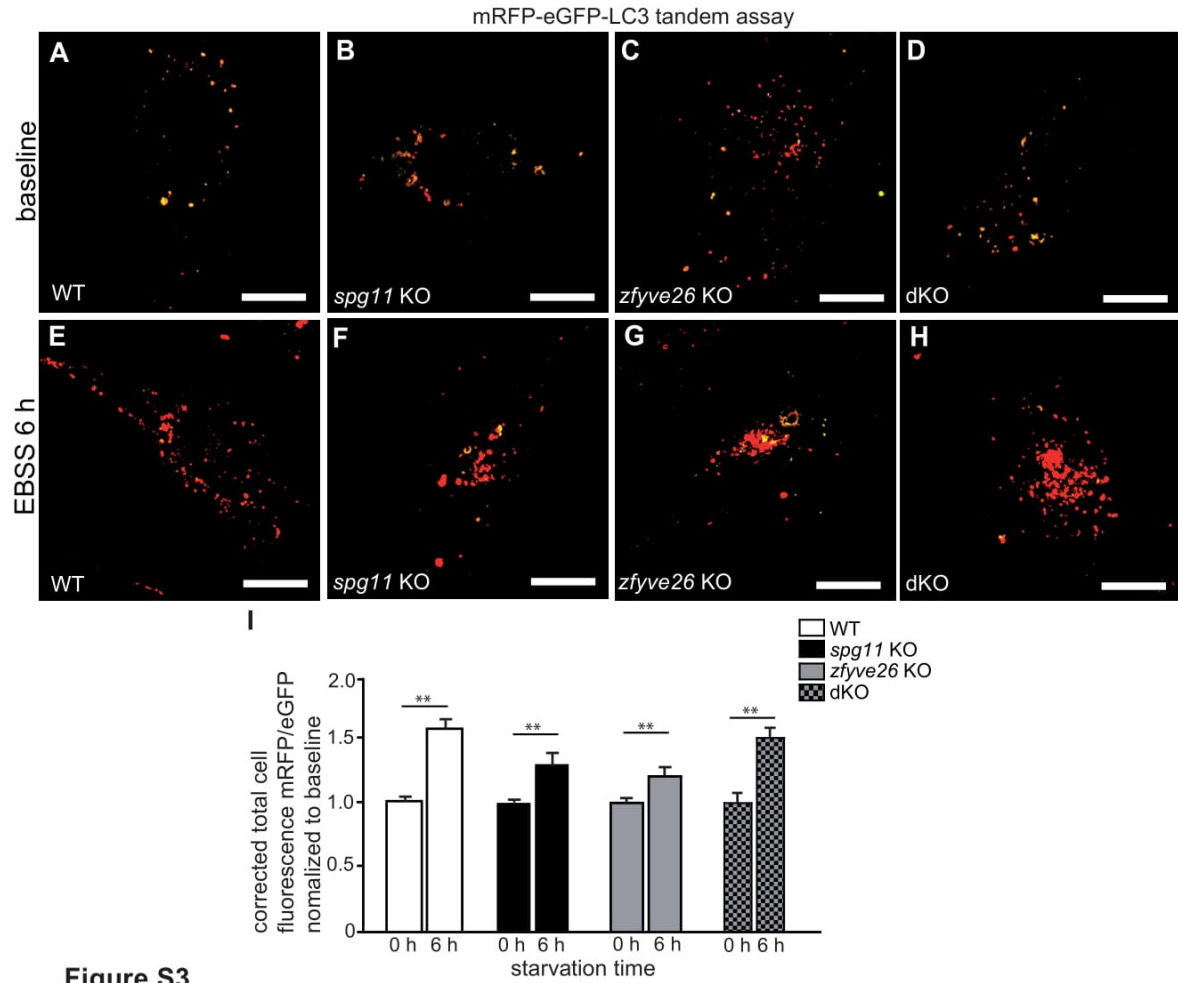
Figure S3. The fusion of lysosomes with autophagosomes occurs in *spg11* KO, *zfyve26* KO and *spg11 zfyve26* double KO (dKO) MEFs. (**A-I**) Cells were transfected with the mRFP-eGFP-LC3 reporter and the ratio between total mRFP and eGFP fluorescence calculated per cell at steady-state (A-D) and 6 h after induction of EBSS starvation (E-H). Scale bars: 10 μm. (I) Because eGFP signals are quenched in acidic compartments, an increased mRFP:eGFP ratio upon starvation indicates fusion of autophagosomes with lysosomes (quantification of at least 30 cells per group from n=3 experiments; one-way ANOVA; ** $p<0.01$). Error bars represent SEM.
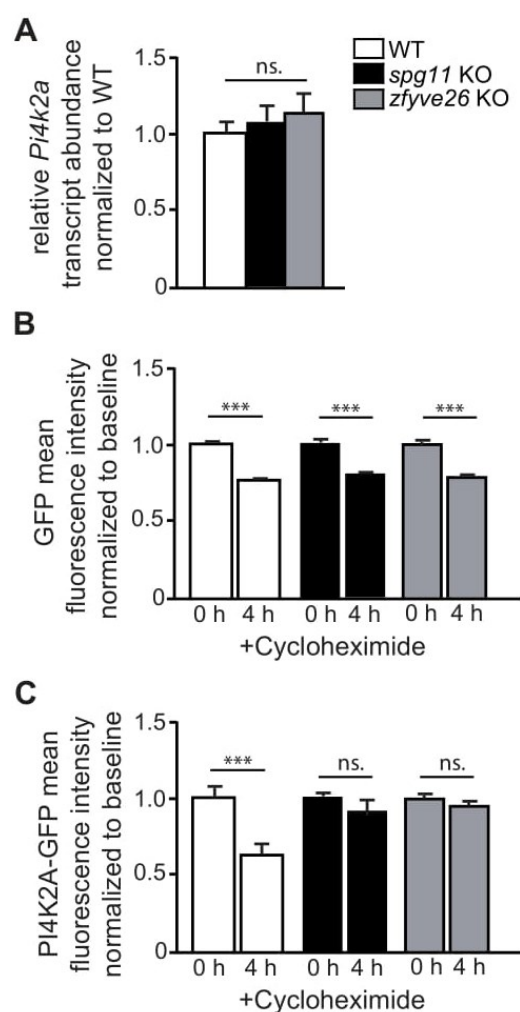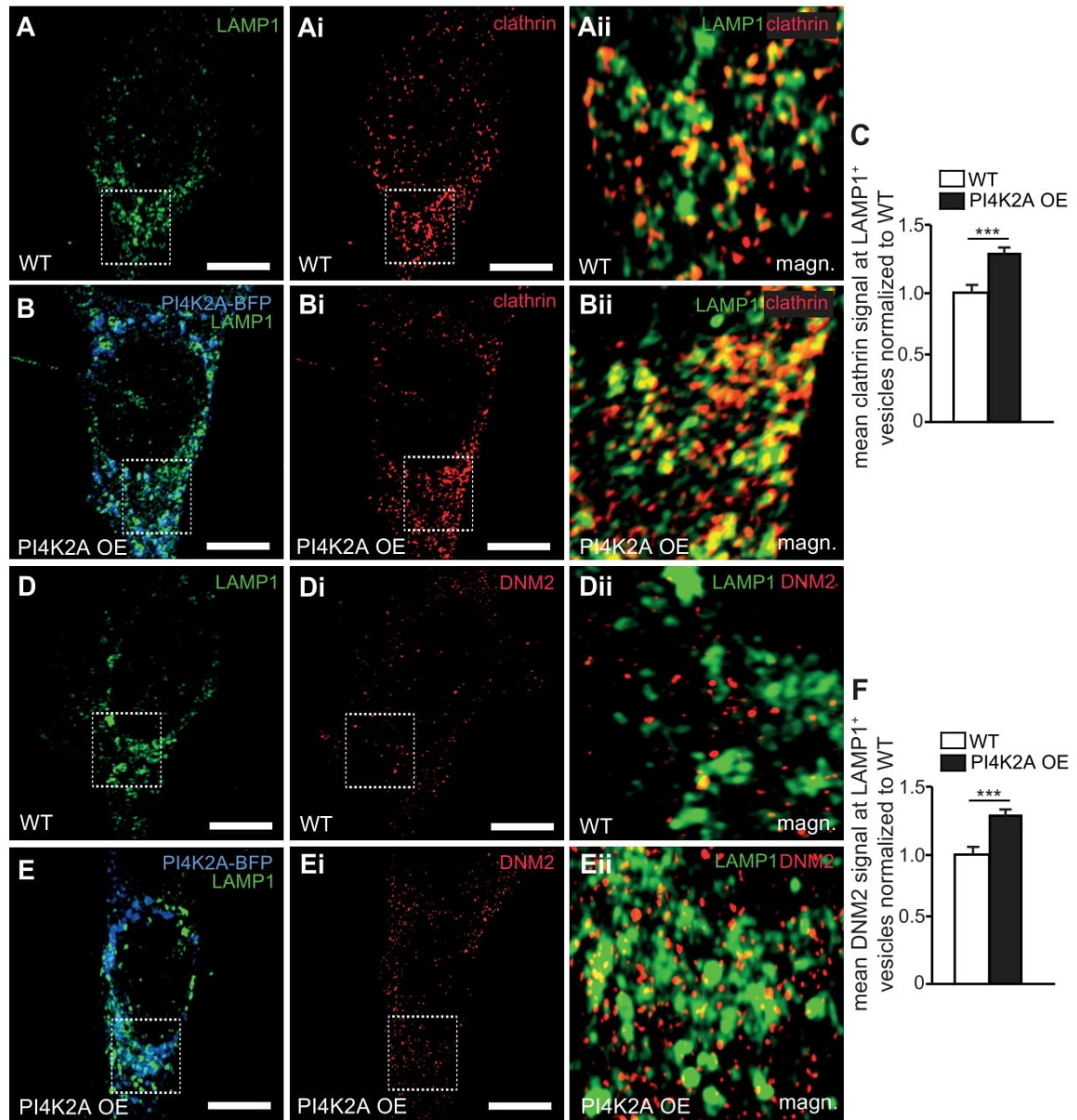
Figure S4

Figure S4. Delayed turnover of PI4K2A-GFP upon disruption of either *Spg11* or *Zfyve26*. (**A**) Quantitative real-time PCR suggests that *Pi4k2a* transcript abundance normalized to *Actb* is not changed in *spg11* KO and *zfyve26* KO MEFs (quantification from 3 replicates each and n=3 independent experiments; one-way ANOVA; ns: not significant). (**B**) FACS analysis of mean GFP fluorescence intensity in MEFs transfected with a GFP construct before and 4 h after addition of Cycloheximide normalized to baseline (n=3 independent experiments; one-way ANOVA; *** p<0.001). (**C**) FACS analysis of mean GFP fluorescence intensity in MEFs transfected with a PI4K2A-GFP construct before and 4 h after addition of Cycloheximide (n=3 independent experiments; one-way ANOVA; *** p<0.001; ns: not significant). Error bars represent SEM.
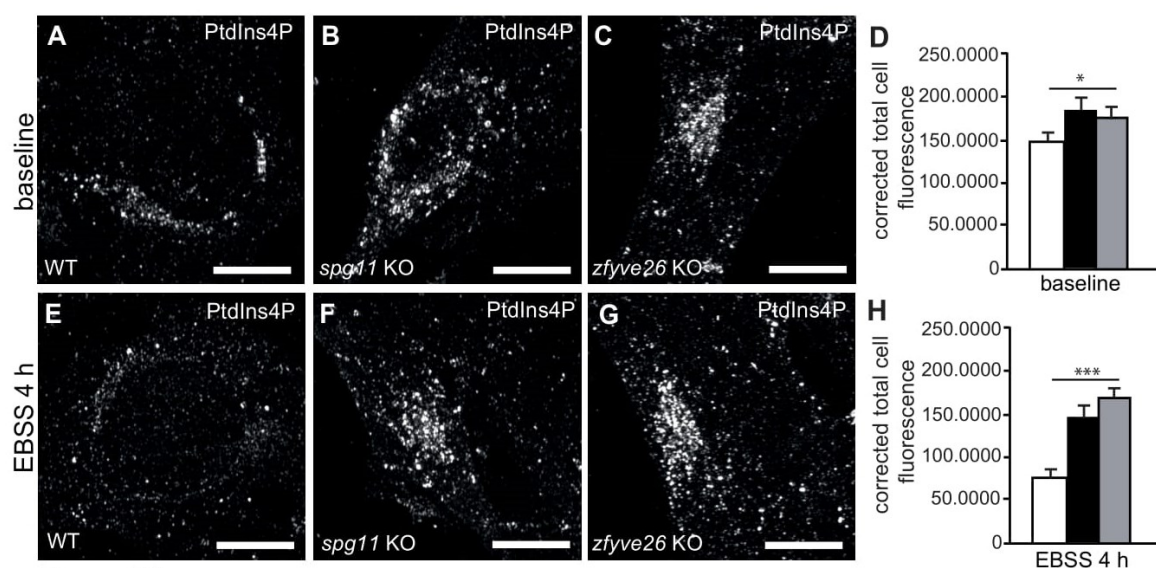
Figure S5

Figure S5. PtdIns4P signals are increased in *spg11* KO and *zfyve26* KO mouse embryonic fibroblasts. (**A-D**) Compared to WT (A) PtdIns4P signals are significantly increased in *spg11* KO (B) and *zfyve26* KO (C) MEFs at steady state (more than 30 cells per genotype; n=3 experiments; one-way ANOVA followed by Tukey's Multiple Comparison Test; * $p < 0.05$). (**E-H**) Upon induction of autophagy by 4 h of EBSS starvation, PtdIns4P signals decrease in WT (E) but remain elevated in *spg11* KO (F) and *zfyve26* KO (G) MEFs (more than 30 cells per genotype; n=3 experiments; one-way ANOVA followed by Tukey's Multiple Comparison Test; *** $p < 0.001$). Scale bars: 5 µm. Error bars represent SEM.

Figure S6

Figure S6. PI4K2A-BFP overexpression in WT MEFs increases the recruitment of clathrin and DNM2 to LAMP1-positive structures. (**A-C**) Co-stainings for LAMP1 and clathrin in control MEFs (A-Aii) and after overexpression of PI4K2A (B-Bii). (C) Quantification of at least 30 cells per genotype from n=3 independent experiments (Student's t-test; *** p<0.001). (**D-F**) Co-stainings for LAMP1 and DNM2 in control MEFs (D-Dii) and after overexpression of PI4K2A (E-Eii). (F) Quantification of at least 30 cells per genotype from n=3 independent experiments (Student's t-test; *** p<0.001). Scale bars: 10 μm. Error bars represent SEM.

Movie S1. LAMP1-GFP-positive tubules in WT MEF (attached in CD-ROM).

Movie S2. LAMP1-GFP-positive tubules in *spg11* KO MEF (attached in CD-ROM).

Movie S3. LAMP1-GFP-positive tubules in *zfyve26* KO MEF (attached in CD-ROM).

Movie S4. LAMP1-GFP-positive tubules in dKO MEF (attached in CD-ROM).

Movie S5. LAMP1-mCherry- and PtdIns4P-positive tubules in U2-OS cells (attached in CD-ROM).

Table S1. Full list of proteins identified in autofluorescent material isolated from 6-months-old WT, *spg11* KO and *zfyve26* KO mice (attached in CD-ROM).

Table S2. List of proteins from *spg11* KO and *zfyve26* KO deposits, which have also been reported for human and rat lipofuscin (attached in CD-ROM).

Table S3. List of significantly regulated proteins identified in autofluorescent deposits isolated from *spg11* KO and *zfyve26* KO brains (attached in CD-ROM).

Table S4. List of proteins identified only in autofluorescent deposits isolated from 6-months-old *spg11* KO and *zfyve26* KO brains.

Nr	Accession	Protein name	Sum of counts	Subcellular location	# Unique Peptides	Sum of *spg11*KO abundances Counts	Sum of *zfyve26*KO abundances counts
1	Q2TBE6	Phosphatidylinositol 4-kinase type 2 alpha	12	plasma membrane, mitochondrion, cytoplasm, lysosome, endosome, Golgi	2	6	6
2	Q3TDD9	Protein phosphatase 1, regulatory subunit 21	9	membrane	2	6	3
3	Q3UGY8	ARFGEF family member 3	8	nucleus	2	3	5
4	A2A5R2	ADP-ribosylation factor guanine nucleotide-exchange factor 2 (brefeldin A-inhibited)	8	cytoskeleton, cytoplasm, Golgi, endosome	2	4	4
5	Q60673	Protein tyrosine phosphatase, receptor type, N	6	nucleus, plasma membrane	2	3	3
6	O70404	Vesicle-associated membrane protein 8	4	plasma membrane, extracellular, cytoplasm, lysosome, endosome	2	2	2
7	Q3UHU5	Microtubule crosslinking factor 1	4	cytoskeleton, cytoplasm, nucleus	1	2	2
8	P42209	Septin 1	4	cytoskeleton	1	2	2
9	Q80XI4	Phosphatidylinositol-5-phosphate 4-kinase, type II, beta	4	nucleus, cytoplasm	1	2	2
10	Q6NXH9	Keratin 73	3	cytoskeleton	1	1	2
11	Q9QYR7	Acyl-CoA thioesterase 3	3	peroxisome	1	2	1
12	Q32Q92	Acyl-CoA thioesterase 6	3	peroxisome, cytoplasm	1	2	1
13	Q6Q2Z6	Acyl-CoA thioesterase 5	3	peroxisome	1	2	1
14	Q8BWN8	Acyl-CoA thioesterase 4	3	peroxisome	1	2	1
15	Q9ERI2	RAB27A, member RAS oncogene family	2	extracellular, cytoplasm, lysosome, endosome	1	1	1

5. Discussion

In our study we focused on SPG11, SPG15 and SPG48, three HSP forms which are highly related. In order to analyze the pathogenesis and get insights into the functions of the related proteins, we used *Spg11, Zfyve26* dKO mice and *Ap5z1* KO mice. Previous reports showed that mouse models for SPG11 and SPG15 develop identical phenotypes, which are in agreement with reports on patients suffering from SPG11 or SPG15 (Khundadze et al. 2013; Varga et al. 2015). Comparable with SPG48 patients, SPG48 mice showed a milder phenotype, which was only detected at the age of 20 months. We also found a degeneration of lumbar corticospinal tract fibers and a reduction of large diameter axons. Consistent with neurodegeneration, we found an activation of astrocytes in *Ap5z1* KO mice. In contrast, *Spg11* KO and *Zfyve26* KO as well as dKO mice displayed motor impairment already at the age of 12 months. In contrast to previous findings in *Spg11* KO and *Zfyve26* KO mice (Khundadze et al. 2013; Varga et al. 2015) and the dKO mice, we found no loss of Purkinje cells in *Ap5z1* KO mice. This might contribute to the milder motor phenotype in SPG48. In all analyses performed in this study, we did not observe differences between single and dKO mice. Previous findings in zebrafish reported that the partial depletion of both *SPG11* and *ZFYVE26* orthologues resulted in severe locomotor impairment, abnormal branching of the spinal cord and developmental defects, while a partial knockdown (KD) of each alone was ineffective (Martin et al. 2012). Our results, however, are in contrast with this observation since the single KO for either *SPG11* or *ZFYVE26* resulted in a motor phenotype while the simultaneous loss of *SPG11* and *ZFYVE26* did not worsen the phenotype. This suggests a common role of these proteins in the pathogenesis of HSP.

Adaptor protein complexes are heterotetrametric protein complexes that facilitate the transport of cargos from one membrane compartment to another within cells (Sanger et al. 2019). Based on this definition, we decided to investigate the role of AP-5 in protein sorting. Since a role in the endolysosomal system has been suggested previously (Hirst et al. 2012), we focused on the delivery of lysosomal proteins to lysosomes. Mass spectrometry of isolated lysosomes did not reveal any significant difference in the number of lysosomal proteins upon disruption of AP-5. Surprisingly, we observed a redistribution of some Golgi proteins in lysosomes, i.e. GLG1. This is supported by previous findings which showed a role of AP-5 as a backup system for the retrieval of proteins from late endosomes to the TGN (Hirst et al. 2018). The authors found an increased amount of the Mannose 6-Phosphate Receptor (M6PR) and other Golgi proteins outside the TGN upon disruption of AP-5. A similar approach was carried out on our *Ap5z1*

KO mouse embryonic fibroblasts (MEFs) where we confirmed an increase of M6PR outside of the TGN region. However, we noticed that the absence of AP-5 resulted in structural alterations of the *trans*Golgi. In detail, our immunofluorescence and EM studies revealed that the TGN was reduced in size and more vesiculated, while the *cis*Golgi was unaffected. We found similar Golgi alterations in 20-month-old KO mice. At earlier time points, we could not detect any structural change suggesting that these alterations might not be a primary event in the pathogenesis of the disease, but probably a secondary effect. *trans*Golgi alterations have been already observed in Parkinson´s disease, amyotrophic lateral sclerosis (ALS) and Alzheimer disease (Nakagomi et al. 2008; Mizuno et al. 2001; Gonatas et al. 1992; Stieber et al. 1996). Thus, the alterations observed in our KO mice might contribute to the pathogenesis.

SPG11 and ZFYVE26 have been previously described to interact and colocalize with endosomes and lysosomes (Murmu et al. 2011; Khundadze et al. 2013; Hirst et al. 2013). Also different roles in autophagy have been suggested (Vantaggiato et al. 2019). An accumulation of undigested material was already found in cortical neurons and Purkinje cells of 2-month-old *Spg11* KO and *Zfyve26* KO mice (Khundadze et al. 2013; Varga et al. 2015). Similar findings were observed in dKO mice starting from the age of 2 months and in older *Ap5z1* KO mice (8-month-old). Immunofluorescence analyses of this undigested material revealed a colocalization with autophagic markers (LAMP1, LC3 and p62). In accordance to our observations, also SPG11, SPG15 and SPG48 patient fibroblasts displayed enlarged LAMP1 positive structures with accumulation of undigested material (Renvoisé et al. 2014; Hirst et al. 2015). Furthermore, corticospinal tracts of our *Ap5z1* KO mice showed an accumulation of densely packed organelles like mitochondria, lysosomes and autolysosomes leading to axonal swelling. This accumulation might result in an impairment of the intracellular transport leading to axonal degeneration, which has already been observed for other types of HSP (Ferreirinha et al. 2004; Edgar et al. 2004; Pace et al. 2018).

Similarly to SPG11 and ZFYVE26, also AP-5 has been suggested to localize to the endolysosomal system and to play a role in autophagy (Hirst et al. 2013). Additionally, we found *in vitro* that in the absence of AP-5 zeta the numbers of autophagosomes were increased under challenged conditions, i.e. starvation, while autolysosomes were decreased. In agreement, levels of LC3-II were increased after induction of autophagy in western blot. This difference was abolished after induction of autophagy while blocking the autophagosome-lysosome fusion by Bafilomycin A1 treatment. No difference in LAMP1 levels as well as in the number of lysosomes were observed in KO MEFs. These observations might suggest an

impairment of the autophagosome-lysosome fusion. Instead, we observed a reduction in lysosomes and an increased number of autophagosomes and autolysosomes in single KOs and dKO samples for *SPG11* and *ZFYVE26*. The results were corroborated by western blots of brain lysates which showed increased levels of SQSTM1 and LC3-II in KO mice. Again, no difference was observed between single KOs and dKO. These results suggest a block in autophagy. Our results, however, are in contrast with Vantaggiato *et* al. who showed that SPG11 and ZFYVE26 play different roles in autophagy. The authors describe that both proteins interact with RAB5 and RAB11, proteins which are important for endosome maturation and trafficking (Vantaggiato et al. 2019). Moreover, the authors suggest that only the absence of ZFYVE26 affects the fusion of endosomes and autophagosomes with a more severe effect on autophagy compared to SPG11 (Vantaggiato et al. 2019). The different results observed by Vantaggiato *et al*. and our study may be explained by the use of disease-associated variants, which may not represent complete loss-of-function mutations. Our *in vitro* autophagy flux analysis in *Spg11* KO and *Spg15* KO MEFs using a mRFP-eGFP-LC3 reporter also does not support the hypothesis of a defect of autophagosome-lysosome fusion. With the use of this reporter, we were able to evaluate the fusion between autophagosomes and lysosomes. The data showed that the fusion of autophagosomes and lysosomes still occurs in the absence of Spatacsin and Spastizin. This was corroborated by counting vesicles after autophagy induction, where an accumulation of autolysosomes was observed in KOs. Interestingly, the number of lysosomes was diminished already under basal conditions and was even more reduced under challenged conditions, which is in accordance with the *in vivo* analysis. Also in *Ap5z1* KO mice the number of autolysosomes was increased in Purkinje neurons already before onset of the disease (2-month-old). Thus, these results suggest an impairment at later stage of autophagy.

Reduction of lysosomes and an increased amount of autolysosomes are typical signs of ALR impairment, as already observed in other diseases (Magalhaes et al. 2016; McGrath et al. 2021). ALR is the final step of autophagy, which occurs after prolonged starvation and is essential for the homeostasis of lysosomes. It has been shown that the absence of Spatacsin and Spastizin impairs this process under prolonged starvation (Chang et al. 2014; Varga et al. 2015). Since these proteins were shown to interact with AP-5, we evaluated whether this impairment could be also detected in our KO MEFs. Here, we showed for the first time that the absence of AP-5 drastically reduces the reformation of lysosomes from autolysosomes. Moreover, we confirmed by live cell imaging that the process of ALR is impaired upon disruption of either Spatacsin or Spastizin.

ALR is a process tightly regulated by mTORC1. Indeed, ALR can take place only after reactivation of mTORC1 due to the release of nutrients from autolysosomes (Chen and Yu 2018). The evaluation of the abundance of phosphorylated p70S6 Kinase (p-S6K) was used to evaluate mTORC1 activity. Decreased amount of p-S6K was observed in *Ap5z1* KO MEFs under prolonged starvation, suggesting a defect in mTORC1 reactivation. This can be due to a defect of lysosome function. Indeed, both MEFs and primary neurons lacking AP-5 showed a defect in the degradative capacity for protein aggregates, i.e. Huntingtin. These data suggest that the absence of AP-5 impairs the capacity of neurons to degrade material via autophagy. Unfortunately, we were unable to determine whether this autophagy block is a direct consequence of ALR impairment which affects the degradation of autophagic material or *vice versa*. In the study of McGrath et. al 2021 it has been shown that administration of FBS after prolonged starvation stimulates ALR. It provides nutrients necessary for the reactivation of mTORC1 which then triggers ALR initiation. A similar experiment with our KO MEFs might help to understand whether the impairment in the degradative capacity is the primary cause of impaired autophagy.

For a better understanding of the pathophysiology of SPG11 and SPG15, an unbiased mass spectrometry analysis of autofluorescent material isolated from WT, *Spg11* KO and *Zfyve26* KO brains was carried out. Notably, PI4K2A, one of the four kinases involved in the generation of PtdIns(4)P from PtdIns, was found in deposits isolated from SPG11 and SPG15 KO mice but not in WT controls. It has been described that PI4K2A mainly localizes to the TGN under basal conditions and is recruited to autophagosomes under challenged conditions, where it plays an important role in the fusion of autophagosomes with lysosomes (Wang et al. 2015). The increased amount of PI4K2A in *Spg11* KO and *Zfyve26* KO was also confirmed by immunostaining in Purkinje cells. For the first time, we showed that PI4K2A localizes to autolysosomes in neurons and that its abundance is increased upon disruption of either *SPG11* or *ZFYVE26*. High levels of this kinase were also found in KO MEFs. However, qRT-PCR results for *Pi4k2a* mRNA did not show any difference between WT and KOs at the transcript level. These results indicate that the loss of *SPG11* and *ZFYVE26* does not affect the transcription of PI4K2A. Interestingly, we noticed that the turnover of this kinase was impaired in KO samples. In the literature it is described that PI4K2A is ubiquitinated at different sites, which regulates its activity and possibly also its turnover (Mössinger et al. 2012). Thus, we speculate that the impairment of its turnover might be due to an alteration of PI4K2A ubiquitination and a reduced degradative capacity of lysosomes in the absence of SPG11 or

ZFYVE26. This, together with the autophagy impairment described before, might explain the accumulation in autolysosomes upon loss of Spatacsin and Spastizin. Furthermore, we speculate that the retrieval of PI4K2A from autolysosomes could be impaired upon disruption of SPG11 or ZFYVE26. As already observed for SPG48, also the loss of *SPG11* and *ZFYVE26* leads to an altered structure of the TGN (data not shown), which can impair the retrieval of Golgi proteins from late endosomes to the TGN.

Based on our *in vivo* and *in vitro* results and the assumption that Spatacsin and Spastizin are involved in ALR, we decided to overexpress PI4K2A in U2-OS cells to mimic the accumulation observed in MEFs. In cells with PI4K2A overexpression we observed a reduction of reformation tubules similar to our data for KO MEFs. The KD of PI4K2A on the other hand resulted in longer tubules, suggesting a role of this kinase at a late stage of ALR. To evaluate its role, we simultaneously knocked down PI4K2A and treated the cells with Dynasore. This compound is an inhibitor of Dynamin2, a protein involved in the scission of reformation tubules. Surprisingly, no difference in the percentage of lysosomal tubules longer than 5 µm was observed, suggesting a possible role of PI4K2A in the scission of tubules. Similar results were observed after overexpression of PI4K3B, another kinase responsible for the production of PtdIns(4)P (Sridhar et al. 2013). Therefore, we also investigated the role of PtdIns(4)P in ALR. PtdIns(4)P, the product of PI4K2A, was already described to be essential in different processes like exocytosis, membrane trafficking, protein sorting and autolysosome generation (Minogue 2018; Ebner et al. 2019; Wang et al. 2015; Sridhar et al. 2013). Moreover, it has been suggested to play an important role in the maintenance of lysosomal homeostasis. Immunostainings in our *Spg11* KO and *Zfyve26* KO MEFs revealed increased levels of PtdIns(4)P already under basal conditions and even more under starved conditions. Furthermore, after prolonged starvation, levels of PtdIns(4)P were increased on LAMP1-positive vesicles upon disruption of *SPG11* and *ZFYVE26*. These results suggest that increased levels of PI4K2A lead to an increase of its product, supporting the hypothesis that both play a role during ALR. Of note, we were able to show by live cell imaging that PtdIns(4)P is recruited to tubules during ALR. Based on these results, we speculate that the modulation of PI4K2A levels in our KO mice might rescue the process of ALR. In the literature, different inhibitors for this kinase have been described (Sengupta et al. 2019; Pataer et al. 2020). They represent a good strategy to modulate the activity of PI4K2A in our KO mice and to evaluate a possible rescue of the phenotype. Additionally, the use of siRNA against PI4K2A *in vitro* can be used to evaluate the effect on ALR in SPG11 and SPG15.

PtdIns(4)P plays an important role in ALR because it is a precursor of PtdIns(4,5)P$_2$, which is generated upon phosphorylation by PIP5K1A and B (Rong et al. 2012). PtdIns(4,5)P$_2$ is essential for the recruitment of key players of ALR like Clathrin, KIF5B and Dynamin2 (Rong et al. 2012). Thus, we evaluated the recruitment of some of these key players in our KO MEFs. Notably, the recruitment of Clathrin and Dynamin2 on LAMP1-positive structures was increased in KO MEFs. These results could be mimicked by overexpression of PI4K2A in WT MEFs. The data suggest that changes in PI4K2A levels and especially of its product affect the recruitment of important proteins involved in ALR. Recent findings show that mutations in INPP5K, a phosphatase that generates PtdIns(4)P from PtdIns(4,5)P$_2$, cause an abnormal accumulation of PtdIns(4,5)P$_2$ on reformation tubules leading to ALR impairment and muscle skeletal disease (McGrath et al. 2021). These studies support our hypothesis that a finely tuned balance between different phosphoinositides is essential for ALR. For further confirmation, a sensor specific for PtdIns(4,5)P$_2$ could be used in our KO models. This construct would help to confirm that increased levels of PtdIns(4)P result in increased concentrations of PtdIns(4,5)P$_2$, thereby affecting the recruitment of Clathrin, Dynamin2 and KIF5B. Therefore, it could corroborate the finding of this study and give insight into ALR and the pathogenesis of HSP.

Taken together, we confirmed in this study the close relation between SPG48, SPG11 and SPG15. Our mouse models show similar phenotypes and impairments confirming a common role of their respective proteins during autophagy and especially in ALR. We discovered that the loss of these proteins affects not only autophagy but also other compartments like the TGN. We speculate that structural alterations of the TGN together with the retrieval impairment of proteins from late endosomes to the TGN might contribute to the accumulation of PI4K2A in autolysosomes. High levels of PI4K2A promote an increase of PtdIns(4)P and possibly of PtdIns(4,5)P$_2$, thus affecting the recruitment of ALR effectors. This results in an increased recruitment or retention of Clathrin and Dynamin2 on reformation tubules leading to an impairment of ALR. Moreover, it has been shown that mutations of this kinase result in accumulations of undigested material in neurons (Alkhater et al. 2018; Simons et al. 2009). This suggests a close relation between PI4K2A and SPG11, ZFYVE26 and AP-5.

6. Conclusion and future perspectives

This study examined the role of SPG11, ZFYVE26 and AP-5 in the process of autophagy and identified a role of PI4K2A in ALR (Figure 6).

We observed that the absence of these proteins results in an autophagy impairment in our KO mice. In detail, we show that the loss of either SPG11, ZFYVE26 or AP-5 causes autophagic block leading to an increased number of autophagosomes and autolysosomes. This results in the accumulation of undigested material. Analysis of this material revealed increased levels of PI4K2A in *Spg11* KO and *Zfyve26* KO mice. Unfortunately, we could not determine the mechanism behind the increased levels of PI4K2A. Possibly, this kinase is recycled from late endosomes to the TGN in a complex with AP-5, SPG11 and ZFYVE26. Indeed, our data suggest that AP-5 acts as a back-up system of retromer, thus facilitating the transport of proteins from late endosomes back to the TGN. Furthermore, the loss of SPG11, ZFYVE26 and AP-5 leads to structural alterations of the TGN (data not shown for SPG11 and ZFYVE26). We speculate that these alterations together with the retrieval process impairment and a defective turnover might result in an increased amount of PI4K2A in autolysosomes

Further, our analyses demonstrated that increased levels of PI4K2A as well as the absence of SPG11 or ZFYVE26 did not alter the autolysosome formation but resulted in ALR impairment. During ALR, LAMP1-positive tubules elongate from autolysosomes. Interestingly, in our KO models, high levels of PI4K2A and PtdIns(4)P result in ALR impairment due to an excessive recruitment or retention of Clathrin and Dynamin2 on tubules. We propose that PtdIns(4)P generated from PI4K2A on tubules is converted to PtdIns(4,5)P_2 which is necessary for the recruitment of Clathrin, KIF5B and Dynamin2.

Taken together, these data suggest that SPG11, ZFYVE26 and AP-5 are involved in the retrieval of proteins from the TGN back to the endosomes as well as in autophagy and ALR. Further, we propose that PI4K2A and therefore PtdIns(4)P regulate the recruitment of ALR effectors.

As future perspectives, further experiments should be performed to better understand whether a block of autolysosomal degradation impairs ALR or *vice versa*. In the study of McGrath et al. 2021 it has been shown that the administration of FBS after prolonged starvation stimulates robust ALR. It provides nutrients necessary for the reactivation of mTORC1 which then triggers ALR initiation. Thus, a similar experiment with our KO MEFs might help to resolve the primary cause of impaired autophagy in SPG11, SPG15 or SPG48.

Moreover, one should assess whether PtdIns(4)P acts directly on ALR or after its transformation into PtdIns(4,5)P_2. Sensors specific for these phosphoinositides together with antibodies against the main effectors of ALR could be used. Super resolution microscopy combined with a newly described protocol of cell fixation (McGrath et al. 2021), which allows to stabilize the tubules, might help to better characterize this process.

For more mechanistic insights, the Proximity-dependent biotin identification (BioID) may be helpful. It is a relative newly described method for the identification of protein-protein interactions (Varnaitė and MacNeill 2016; Roux et al. 2018). This approach applied to our HSP proteins would help to discover so far unknown AP-5-cargos and give insights into their function. Moreover, AP5-interactors could be analyzed using specific treatments (i.e. 8 h of starvation) which are inducing autophagy.

Additionally, the generation of Knockin (KI) cells for AP-5 as well as SPG11 and ZFYVE26 tagged proteins might help to visualize and evaluate their role by using live cell imaging. Moreover, these cell lines could support the BioID results for the identification of interactors.

Possibly, PI4K2A may be a target for pharmacological intervention. Inhibitors or siRNAs against PI4K2A could be used to analyze whether the modulation of the PI4K2A levels in SPG11 and SPG15 might rescue the process of ALR with an improvement of the phenotype.
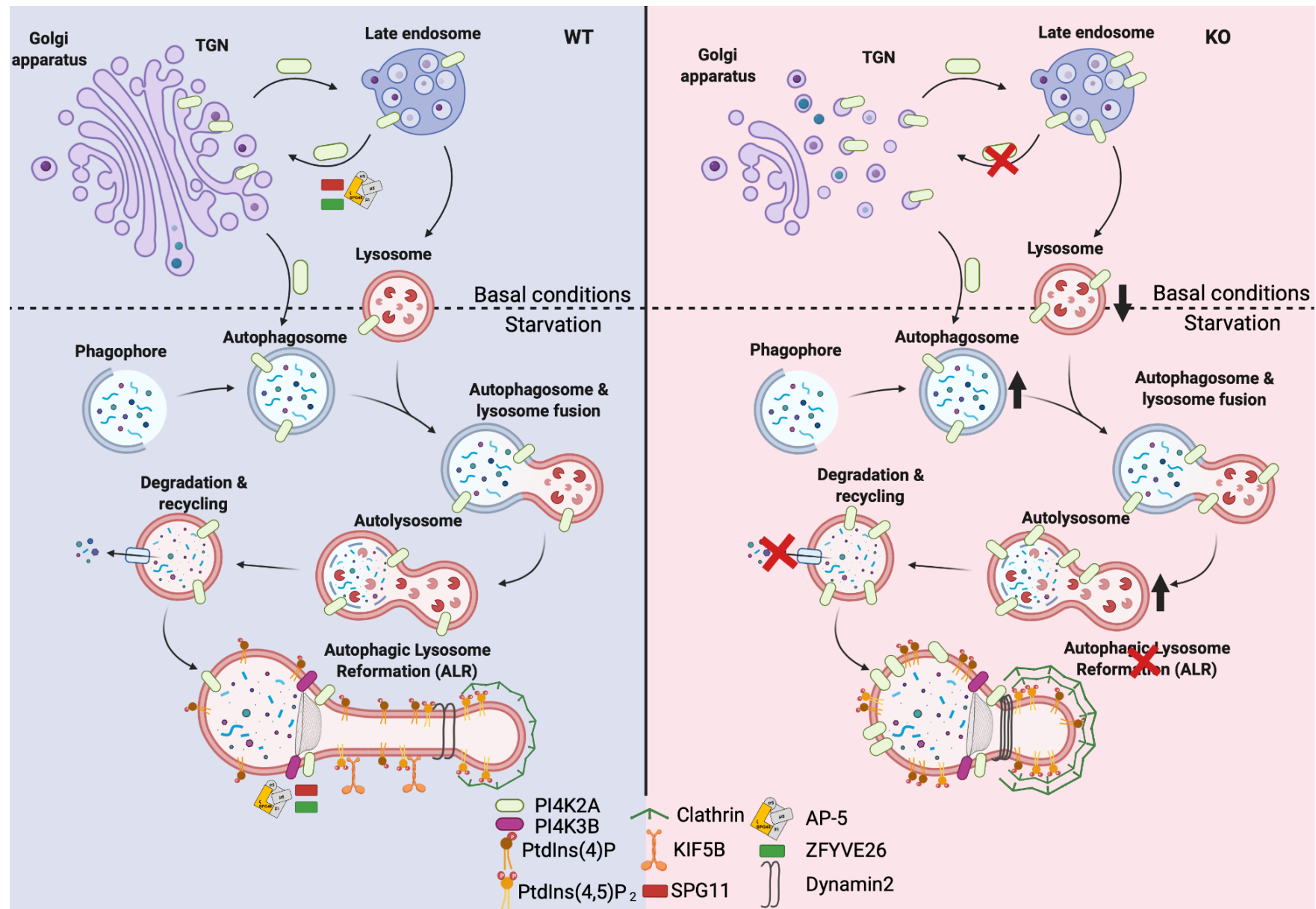
Figure 6. Implication of SPG11, ZFYVE26 and AP-5 role in autophagy. In WT (left panel) SPG11 and ZFYVE26 interact with AP-5, which is involved in the retrieval of proteins from late endosomes to the TGN. PI4K2A localizes under basal conditions mainly in the TGN but also in endosomes and lysosomes. During starvation, the kinase is recruited on autophagosomes where it plays an important role in autophagosome-lysosome fusion. In autolysosomes, the material is degraded and nutrients are released triggering ALR. During ALR, LAMP1-positive tubules elongate from autolysosomes. Proteins are retained in autolysosomes due to the presence of PI4K3B resulting in empty tubules. We propose that the generation of PtdIns(4)P from PI4K2A is converted to PtdIns(4,5)P$_2$ which is necessary for the recruitment of Clathrin, KIF5B and Dynamin2. SPG11, ZFYVE26 and AP-5 are also important players during this process. However, the precise mechanism is still unclear. This current study showed that loss of SPG11 and ZFYVE26 leads to increased levels of PI4K2A (right panel). The loss of SPG11, ZFYVE26 and AP-5 leads to structural alterations of TGN. This, together with the retrieval process impairment would result in an increased amount of PI4K2A in autolysosomes. High levels of PI4K2A and therefore of PtdIns(4)P result in ALR impairment due to an excessive recruitment or retention of Clathrin and Dynamin2 on tubules. This impairment is also suggested by a decreased number of lysosomes and increased autophagosomes and autolysosomes. WT wild type, ALR autophagic lysosome reformation, AP-5 adaptor protein complex-5, TGN *trans*Golgi network, PdtIns(4)P Phosphatidylinositol-4 phosphate, PtdIns(4,5)P$_2$ Phosphatidylinositol-4,5 biphosphate, LAMP1 Lysosome-associated membrane glycoprotein 1 (Created with BioRender.com).

7. Publication bibliography

Abada, Adi; Elazar, Zvulun (2014): Getting ready for building: signaling and autophagosome biogenesis. In *EMBO reports* 15 (8), pp. 839–852. DOI: 10.15252/embr.201439076.

Al-Bari, Md Abdul Alim (2020): A current view of molecular dissection in autophagy machinery. In *Journal of physiology and biochemistry* 76 (3), pp. 357–372. DOI: 10.1007/s13105-020-00746-0.

Al-Bari, Md Abdul Alim; Xu, Pingyong (2020): Molecular regulation of autophagy machinery by mTOR-dependent and -independent pathways. In *Annals of the New York Academy of Sciences* 1467 (1), pp. 3–20. DOI: 10.1111/nyas.14305.

Alkhater, Reem A.; Scherer, Stephen W.; Minassian, Berge A.; Walker, Susan (2018): PI4K2A deficiency in an intellectual disability, epilepsy, myoclonus, akathisia syndrome. In *Annals of clinical and translational neurology* 5 (12), pp. 1617–1621. DOI: 10.1002/acn3.677.

Axe, Elizabeth L.; Walker, Simon A.; Manifava, Maria; Chandra, Priya; Roderick, H. Llewelyn; Habermann, Anja et al. (2008): Autophagosome formation from membrane compartments enriched in phosphatidylinositol 3-phosphate and dynamically connected to the endoplasmic reticulum. In *The Journal of cell biology* 182 (4), pp. 685–701. DOI: 10.1083/jcb.200803137.

Backer, Jonathan M. (2016): The intricate regulation and complex functions of the Class III phosphoinositide 3-kinase Vps34. In *The Biochemical journal* 473 (15), pp. 2251–2271. DOI: 10.1042/BCJ20160170.

Barylko, Barbara; Mao, Yuntao S.; Wlodarski, Pawel; Jung, Gwanghyun; Binns, Derk D.; Sun, Hui-Qiao et al. (2009): Palmitoylation controls the catalytic activity and subcellular distribution of phosphatidylinositol 4-kinase II{alpha}. In *The Journal of biological chemistry* 284 (15), pp. 9994–10003. DOI: 10.1074/jbc.M900724200.

Beetz, C.; Nygren, A. O. H.; Schickel, J.; Auer-Grumbach, M.; Bürk, K.; Heide, G. et al. (2006): High frequency of partial SPAST deletions in autosomal dominant hereditary spastic paraplegia. In *Neurology* 67 (11), pp. 1926–1930. DOI: 10.1212/01.wnl.0000244413.49258.f5.

Blackstone, Craig (2012): Cellular pathways of hereditary spastic paraplegia. In *Annual review of neuroscience* 35, pp. 25–47. DOI: 10.1146/annurev-neuro-062111-150400.

Blackstone, Craig (2018): Hereditary spastic paraplegia. In *Handbook of clinical neurology* 148, pp. 633–652. DOI: 10.1016/B978-0-444-64076-5.00041-7.

Boukhris, A.; Stevanin, G.; Feki, I.; Denora, P.; Elleuch, N.; Miladi, M. I. et al. (2009): Tunisian hereditary spastic paraplegias: clinical variability supported by genetic heterogeneity. In *Clinical genetics* 75 (6), pp. 527–536. DOI: 10.1111/j.1399-0004.2009.01176.x.

Boura, Evzen; Nencka, Radim (2015): Phosphatidylinositol 4-kinases: Function, structure, and inhibition. In *Experimental cell research* 337 (2), pp. 136–145. DOI: 10.1016/j.yexcr.2015.03.028.

Bridges, Dave; Ma, Jing-Tyan; Park, Sujin; Inoki, Ken; Weisman, Lois S.; Saltiel, Alan R. (2012): Phosphatidylinositol 3,5-bisphosphate plays a role in the activation and subcellular localization of mechanistic target of rapamycin 1. In *Molecular biology of the cell* 23 (15), pp. 2955–2962. DOI: 10.1091/mbc.E11-12-1034.

Chang, Jaerak; Lee, Seongju; Blackstone, Craig (2014): Spastic paraplegia proteins spastizin and spatacsin mediate autophagic lysosome reformation. In *The Journal of clinical investigation* 124 (12), pp. 5249–5262. DOI: 10.1172/JCI77598.

Chen, Yang; Yu, Li (2015): Scissors for autolysosome tubules. In *The EMBO journal* 34 (17), pp. 2217–2218. DOI: 10.15252/embj.201592519.

Chen, Yang; Yu, Li (2017): Recent progress in autophagic lysosome reformation. In *Traffic (Copenhagen, Denmark)* 18 (6), pp. 358–361. DOI: 10.1111/tra.12484.

Chen, Yang; Yu, Li (2018): Development of Research into Autophagic Lysosome Reformation. In *Molecules and cells* 41 (1), pp. 45–49. DOI: 10.14348/molcells.2018.2265.

Claude-Taupin, Aurore; Morel, Etienne (2021): Phosphoinositides: Functions in autophagy-related stress responses. In *Biochimica et biophysica acta. Molecular and cell biology of lipids* 1866 (6), p. 158903. DOI: 10.1016/j.bbalip.2021.158903.

Coutinho, P.; Barros, J.; Zemmouri, R.; Guimarães, J.; Alves, C.; Chorão, R. et al. (1999): Clinical heterogeneity of autosomal recessive spastic paraplegias: analysis of 106 patients in 46 families. In *Archives of neurology* 56 (8), pp. 943–949. DOI: 10.1001/archneur.56.8.943.

Coutinho, Paula; Ruano, Luis; Loureiro, José L.; Cruz, Vitor T.; Barros, José; Tuna, Assunção et al. (2013): Hereditary ataxia and spastic paraplegia in Portugal: a population-based prevalence study. In *JAMA neurology* 70 (6), pp. 746–755. DOI: 10.1001/jamaneurol.2013.1707.

Craene, Johan-Owen de; Bertazzi, Dimitri L.; Bär, Séverine; Friant, Sylvie (2017): Phosphoinositides, Major Actors in Membrane Trafficking and Lipid Signaling Pathways. In *International journal of molecular sciences* 18 (3). DOI: 10.3390/ijms18030634.

Deng, Zhiqiang; Purtell, Kerry; Lachance, Veronik; Wold, Mitchell S.; Chen, Shi; Yue, Zhenyu (2017): Autophagy Receptors and Neurodegenerative Diseases. In *Trends in cell biology* 27 (7), pp. 491–504. DOI: 10.1016/j.tcb.2017.01.001.

Denora, Paola S.; Smets, Katrien; Zolfanelli, Federica; Ceuterick-de Groote, Chantal; Casali, Carlo; Deconinck, Tine et al. (2016): Motor neuron degeneration in spastic paraplegia 11 mimics amyotrophic lateral sclerosis lesions. In *Brain : a journal of neurology* 139 (Pt 6), pp. 1723–1734. DOI: 10.1093/brain/aww061.

Dickson, Eamonn J.; Hille, Bertil (2019): Understanding phosphoinositides: rare, dynamic, and essential membrane phospholipids. In *The Biochemical journal* 476 (1), pp. 1–23. DOI: 10.1042/BCJ20180022.

Dikic, Ivan; Elazar, Zvulun (2018): Mechanism and medical implications of mammalian autophagy. In *Nature reviews. Molecular cell biology* 19 (6), pp. 349–364. DOI: 10.1038/s41580-018-0003-4.

Du, Wanqing; Su, Qian Peter; Chen, Yang; Zhu, Yueyao; Jiang, Dong; Rong, Yueguang et al. (2016): Kinesin 1 Drives Autolysosome Tubulation. In *Developmental cell* 37 (4), pp. 326–336. DOI: 10.1016/j.devcel.2016.04.014.

Ebner, Michael; Koch, Philipp Alexander; Haucke, Volker (2019): Phosphoinositides in the control of lysosome function and homeostasis. In *Biochemical Society transactions* 47 (4), pp. 1173–1185. DOI: 10.1042/BST20190158.

Edgar, J. M.; McLaughlin, M.; Barrie, J. A.; McCulloch, M. C.; Garbern, J.; Griffiths, I. R. (2004): Age-related axonal and myelin changes in the rumpshaker mutation of the Plp gene. In *Acta neuropathologica* 107 (4), pp. 331–335. DOI: 10.1007/s00401-003-0808-9.

Erichsen, Anne Kjersti; Koht, Jeanette; Stray-Pedersen, Asbjørg; Abdelnoor, Michael; Tallaksen, Chantal M. E. (2009): Prevalence of hereditary ataxia and spastic paraplegia in southeast Norway: a population-based study. In *Brain : a journal of neurology* 132 (Pt 6), pp. 1577–1588. DOI: 10.1093/brain/awp056.

Falasca, Marco (2012): Phosphoinositides and disease. Dordrecht, London: Springer (Current topics in microbiology and immunology, volume 362). Available online at http://www.springer.com/gb/ BLDSS.

Fernandez-Mosquera, Lorena; Yambire, King Faisal; Couto, Renata; Pereyra, Leonardo; Pabis, Kamil; Ponsford, Amy H. et al. (2019): Mitochondrial respiratory chain deficiency inhibits lysosomal hydrolysis. In *Autophagy* 15 (9), pp. 1572–1591. DOI: 10.1080/15548627.2019.1586256.

Ferreirinha, Fatima; Quattrini, Angelo; Pirozzi, Marinella; Valsecchi, Valentina; Dina, Giorgia; Broccoli, Vania et al. (2004): Axonal degeneration in paraplegin-deficient mice is associated with abnormal mitochondria and impairment of axonal transport. In *The Journal of clinical investigation* 113 (2), pp. 231–242. DOI: 10.1172/JCI20138.

Filimonenko, Maria; Isakson, Pauline; Finley, Kim D.; Anderson, Monique; Jeong, Hyun; Melia, Thomas J. et al. (2010): The selective macroautophagic degradation of aggregated proteins requires the PI3P-binding protein Alfy. In *Molecular cell* 38 (2), pp. 265–279. DOI: 10.1016/j.molcel.2010.04.007.

Fink, John K. (2014): Hereditary spastic paraplegia: clinical principles and genetic advances. In *Seminars in neurology* 34 (3), pp. 293–305. DOI: 10.1055/s-0034-1386767.

Finsterer, Josef; Löscher, Wolfgang; Quasthoff, Stefan; Wanschitz, Julia; Auer-Grumbach, Michaela; Stevanin, Giovanni (2012): Hereditary spastic paraplegias with autosomal dominant, recessive, X-linked, or maternal trait of inheritance. In *Journal of the neurological sciences* 318 (1-2), pp. 1–18. DOI: 10.1016/j.jns.2012.03.025.

Fourtassi, M.; Jacquin-Courtois, S.; Scheiber-Nogueira, M. C.; Hajjioui, A.; Luaute, J.; Charvier, K. et al. (2012): Bladder dysfunction in hereditary spastic paraplegia: a clinical and urodynamic evaluation. In *Spinal cord* 50 (7), pp. 558–562. DOI: 10.1038/sc.2011.193.

Gonatas, N. K.; Stieber, A.; Mourelatos, Z.; Chen, Y.; Gonatas, J. O.; Appel, S. H. et al. (1992): Fragmentation of the Golgi apparatus of motor neurons in amyotrophic lateral sclerosis. In *The American Journal of Pathology* 140 (3), pp. 731–737.

Guidubaldi, Arianna; Piano, Carla; Santorelli, Filippo M.; Silvestri, Gabriella; Petracca, Martina; Tessa, Alessandra; Bentivoglio, Anna Rita (2011): Novel mutations in SPG11 cause hereditary spastic paraplegia associated with early-onset levodopa-responsive Parkinsonism. In

Movement disorders : official journal of the Movement Disorder Society 26 (3), pp. 553–556. DOI: 10.1002/mds.23552.

Guo, Yusong; Sirkis, Daniel W.; Schekman, Randy (2014): Protein sorting at the trans-Golgi network. In *Annual review of cell and developmental biology* 30, pp. 169–206. DOI: 10.1146/annurev-cellbio-100913-013012.

Gwinn, Dana M.; Shackelford, David B.; Egan, Daniel F.; Mihaylova, Maria M.; Mery, Annabelle; Vasquez, Debbie S. et al. (2008): AMPK phosphorylation of raptor mediates a metabolic checkpoint. In *Molecular cell* 30 (2), pp. 214–226. DOI: 10.1016/j.molcel.2008.03.003.

Hammond, Gerald R. V.; Burke, John E. (2020): Novel roles of phosphoinositides in signaling, lipid transport, and disease. In *Current opinion in cell biology* 63, pp. 57–67. DOI: 10.1016/j.ceb.2019.12.007.

Hanein, Sylvain; Martin, Elodie; Boukhris, Amir; Byrne, Paula; Goizet, Cyril; Hamri, Abdelmadjid et al. (2008): Identification of the SPG15 gene, encoding spastizin, as a frequent cause of complicated autosomal-recessive spastic paraplegia, including Kjellin syndrome. In *American journal of human genetics* 82 (4), pp. 992–1002. DOI: 10.1016/j.ajhg.2008.03.004.

Harding, A. E. (1983): CLASSIFICATION OF THE HEREDITARY ATAXIAS AND PARAPLEGIAS. In *The Lancet* 321 (8334), pp. 1151–1155. DOI: 10.1016/s0140-6736(83)92879-9.

Hasegawa, Junya; Iwamoto, Ryo; Otomo, Takanobu; Nezu, Akiko; Hamasaki, Maho; Yoshimori, Tamotsu (2016): Autophagosome-lysosome fusion in neurons requires INPP5E, a protein associated with Joubert syndrome. In *The EMBO journal* 35 (17), pp. 1853–1867. DOI: 10.15252/embj.201593148.

Hazan, J.; Fonknechten, N.; Mavel, D.; Paternotte, C.; Samson, D.; Artiguenave, F. et al. (1999): Spastin, a new AAA protein, is altered in the most frequent form of autosomal dominant spastic paraplegia. In *Nature genetics* 23 (3), pp. 296–303. DOI: 10.1038/15472.

He, Congcong; Klionsky, Daniel J. (2009): Regulation mechanisms and signaling pathways of autophagy. In *Annual review of genetics* 43, pp. 67–93. DOI: 10.1146/annurev-genet-102808-114910.

Hirst, Jennifer; Borner, Georg H. H.; Edgar, James; Hein, Marco Y.; Mann, Matthias; Buchholz, Frank et al. (2013): Interaction between AP-5 and the hereditary spastic paraplegia proteins

SPG11 and SPG15. In *Molecular biology of the cell* 24 (16), pp. 2558–2569. DOI: 10.1091/mbc.E13-03-0170.

Hirst, Jennifer; D. Barlow, Lael; Francisco, Gabriel Casey; Sahlender, Daniela A.; Seaman, Matthew N. J.; Dacks, Joel B.; Robinson, Margaret S. (2012): Correction: The Fifth Adaptor Protein Complex. In *PLoS Biol* 10 (3). DOI: 10.1371/annotation/89dff893-c156-44bb-a731-bfcc91843583.

Hirst, Jennifer; Edgar, James R.; Esteves, Typhaine; Darios, Frédéric; Madeo, Marianna; Chang, Jaerak et al. (2015): Loss of AP-5 results in accumulation of aberrant endolysosomes: defining a new type of lysosomal storage disease. In *Human molecular genetics* 24 (17), pp. 4984–4996. DOI: 10.1093/hmg/ddv220.

Hirst, Jennifer; Itzhak, Daniel N.; Antrobus, Robin; Borner, Georg H. H.; Robinson, Margaret S. (2018): Role of the AP-5 adaptor protein complex in late endosome-to-Golgi retrieval. In *PLoS Biol* 16 (1), e2004411. DOI: 10.1371/journal.pbio.2004411.

Hirst, Jennifer; Madeo, Marianna; Smets, Katrien; Edgar, James R.; Schols, Ludger; Li, Jun et al. (2016): Complicated spastic paraplegia in patients with AP5Z1 mutations (SPG48). In *Neurology. Genetics* 2 (5), e98. DOI: 10.1212/NXG.0000000000000098.

Hosokawa, Nao; Hara, Taichi; Kaizuka, Takeshi; Kishi, Chieko; Takamura, Akito; Miura, Yutaka et al. (2009): Nutrient-dependent mTORC1 association with the ULK1-Atg13-FIP200 complex required for autophagy. In *Molecular biology of the cell* 20 (7), pp. 1981–1991. DOI: 10.1091/mbc.e08-12-1248.

Hurley, James H.; Young, Lindsey N. (2017): Mechanisms of Autophagy Initiation. In *Annual review of biochemistry* 86, pp. 225–244. DOI: 10.1146/annurev-biochem-061516-044820.

Hyttinen, Juha M. T.; Niittykoski, Minna; Salminen, Antero; Kaarniranta, Kai (2013): Maturation of autophagosomes and endosomes: a key role for Rab7. In *Biochimica et biophysica acta* 1833 (3), pp. 503–510. DOI: 10.1016/j.bbamcr.2012.11.018.

Itakura, Eisuke; Kishi, Chieko; Inoue, Kinji; Mizushima, Noboru (2008): Beclin 1 forms two distinct phosphatidylinositol 3-kinase complexes with mammalian Atg14 and UVRAG. In *Molecular biology of the cell* 19 (12), pp. 5360–5372. DOI: 10.1091/mbc.e08-01-0080.

Itakura, Eisuke; Kishi-Itakura, Chieko; Mizushima, Noboru (2012): The hairpin-type tail-anchored SNARE syntaxin 17 targets to autophagosomes for fusion with endosomes/lysosomes. In *Cell* 151 (6), pp. 1256–1269. DOI: 10.1016/j.cell.2012.11.001.

Jin, Meiyan; Klionsky, Daniel J. (2014): Regulation of autophagy: modulation of the size and number of autophagosomes. In *FEBS letters* 588 (15), pp. 2457–2463. DOI: 10.1016/j.febslet.2014.06.015.

Jordens, Ingrid; Fernandez-Borja, Mar; Marsman, Marije; Dusseljee, Simone; Janssen, Lennert; Calafat, Jero et al. (2001): The Rab7 effector protein RILP controls lysosomal transport by inducing the recruitment of dynein-dynactin motors. In *Current Biology* 11 (21), pp. 1680–1685. DOI: 10.1016/s0960-9822(01)00531-0.

Jović, Marko; Kean, Michelle J.; Dubankova, Anna; Boura, Evzen; Gingras, Anne-Claude; Brill, Julie A.; Balla, Tamas (2014): Endosomal sorting of VAMP3 is regulated by PI4K2A. In *Journal of cell science* 127 (Pt 17), pp. 3745–3756. DOI: 10.1242/jcs.148809.

Jović, Marko; Kean, Michelle J.; Szentpetery, Zsofia; Polevoy, Gordon; Gingras, Anne-Claude; Brill, Julie A.; Balla, Tamas (2012): Two phosphatidylinositol 4-kinases control lysosomal delivery of the Gaucher disease enzyme, β-glucocerebrosidase. In *Molecular biology of the cell* 23 (8), pp. 1533–1545. DOI: 10.1091/mbc.E11-06-0553.

Jung, Chang Hwa; Ro, Seung-Hyun; Cao, Jing; Otto, Neil Michael; Kim, Do-Hyung (2010): mTOR regulation of autophagy. In *FEBS letters* 584 (7), pp. 1287–1295. DOI: 10.1016/j.febslet.2010.01.017.

Kara, Eleanna; Tucci, Arianna; Manzoni, Claudia; Lynch, David S.; Elpidorou, Marilena; Bettencourt, Conceicao et al. (2016): Genetic and phenotypic characterization of complex hereditary spastic paraplegia. In *Brain : a journal of neurology* 139 (Pt 7), pp. 1904–1918. DOI: 10.1093/brain/aww111.

Khundadze, Mukhran; Kollmann, Katrin; Koch, Nicole; Biskup, Christoph; Nietzsche, Sandor; Zimmer, Geraldine et al. (2013): A hereditary spastic paraplegia mouse model supports a role of ZFYVE26/SPASTIZIN for the endolysosomal system. In *PLoS genetics* 9 (12), e1003988. DOI: 10.1371/journal.pgen.1003988.

Kim, Eunjung; Goraksha-Hicks, Pankuri; Li, Li; Neufeld, Thomas P.; Guan, Kun-Liang (2008): Regulation of TORC1 by Rag GTPases in nutrient response. In *Nature cell biology* 10 (8), pp. 935–945. DOI: 10.1038/ncb1753.

Kim, Joungmok; Kundu, Mondira; Viollet, Benoit; Guan, Kun-Liang (2011): AMPK and mTOR regulate autophagy through direct phosphorylation of Ulk1. In *Nature cell biology* 13 (2), pp. 132–141. DOI: 10.1038/ncb2152.

Klebe, S.; Stevanin, G.; Depienne, C. (2015): Clinical and genetic heterogeneity in hereditary spastic paraplegias: from SPG1 to SPG72 and still counting. In *Revue neurologique* 171 (6-7), pp. 505–530. DOI: 10.1016/j.neurol.2015.02.017.

Kraft, Lewis J.; Dowler, Jacob; Manral, Pallavi; Kenworthy, Anne K. (2016): Size, organization, and dynamics of soluble SQSTM1 and LC3-SQSTM1 complexes in living cells. In *Autophagy* 12 (9), pp. 1660–1674. DOI: 10.1080/15548627.2016.1199299.

Li, J.; Lu, Y.; Zhang, J.; Kang, H.; Qin, Z.; Chen, C. (2010): PI4KIIalpha is a novel regulator of tumor growth by its action on angiogenesis and HIF-1alpha regulation. In *Oncogene* 29 (17), pp. 2550–2559. DOI: 10.1038/onc.2010.14.

Lundquist, Mark R.; Goncalves, Marcus D.; Loughran, Ryan M.; Possik, Elite; Vijayaraghavan, Tarika; Yang, Annan et al. (2018): Phosphatidylinositol-5-Phosphate 4-Kinases Regulate Cellular Lipid Metabolism By Facilitating Autophagy. In *Molecular cell* 70 (3), 531-544.e9. DOI: 10.1016/j.molcel.2018.03.037.

Magalhaes, Joana; Gegg, Matthew E.; Migdalska-Richards, Anna; Doherty, Mary K.; Whitfield, Phillip D.; Schapira, Anthony H. V. (2016): Autophagic lysosome reformation dysfunction in glucocerebrosidase deficient cells: relevance to Parkinson disease. In *Human molecular genetics* 25 (16), pp. 3432–3445. DOI: 10.1093/hmg/ddw185.

Martin, Elodie; Yanicostas, Constantin; Rastetter, Agnès; Alavi Naini, Seyedeh Maryam; Maouedj, Alissia; Kabashi, Edor et al. (2012): Spatacsin and spastizin act in the same pathway required for proper spinal motor neuron axon outgrowth in zebrafish. In *Neurobiology of disease* 48 (3), pp. 299–308. DOI: 10.1016/j.nbd.2012.07.003.

Martina, Jose A.; Chen, Yong; Gucek, Marjan; Puertollano, Rosa (2012): MTORC1 functions as a transcriptional regulator of autophagy by preventing nuclear transport of TFEB. In *Autophagy* 8 (6), pp. 903–914. DOI: 10.4161/auto.19653.

McGrath, Meagan J.; Eramo, Matthew J.; Gurung, Rajendra; Sriratana, Absorn; Gehrig, Stefan M.; Lynch, Gordon S. et al. (2021): Defective lysosome reformation during autophagy causes skeletal muscle disease. In *The Journal of clinical investigation* 131 (1). DOI: 10.1172/JCI135124.

Mignarri, Andrea; Rubegni, Anna; Tessa, Alessandra; Stefanucci, Stefano; Malandrini, Alessandro; Cardaioli, Elena et al. (2016): Mitochondrial dysfunction in hereditary spastic

paraparesis with mutations in DDHD1/SPG28. In *Journal of the neurological sciences* 362, pp. 287–291. DOI: 10.1016/j.jns.2016.02.007.

Minogue, Shane (2018): The Many Roles of Type II Phosphatidylinositol 4-Kinases in Membrane Trafficking: New Tricks for Old Dogs. In *BioEssays : news and reviews in molecular, cellular and developmental biology* 40 (2). DOI: 10.1002/bies.201700145.

Mizuno, Y.; Hattori, N.; Kitada, T.; Matsumine, H.; Mori, H.; Shimura, H. et al. (2001): Familial Parkinson's disease. Alpha-synuclein and parkin. In *Advances in neurology* 86, pp. 13–21.

Mizushima, N.; Noda, T.; Yoshimori, T.; Tanaka, Y.; Ishii, T.; George, M. D. et al. (1998): A protein conjugation system essential for autophagy. In *Nature* 395 (6700), pp. 395–398. DOI: 10.1038/26506.

Mössinger, Julia; Wieffer, Marnix; Krause, Eberhard; Freund, Christian; Gerth, Fabian; Krauss, Michael; Haucke, Volker (2012): Phosphatidylinositol 4-kinase IIα function at endosomes is regulated by the ubiquitin ligase Itch. In *EMBO reports* 13 (12), pp. 1087–1094. DOI: 10.1038/embor.2012.164.

Munson, Michael J.; Allen, George Fg; Toth, Rachel; Campbell, David G.; Lucocq, John M.; Ganley, Ian G. (2015): mTOR activates the VPS34-UVRAG complex to regulate autolysosomal tubulation and cell survival. In *The EMBO journal* 34 (17), pp. 2272–2290. DOI: 10.15252/embj.201590992.

Murmu, Reena Prity; Martin, Elodie; Rastetter, Agnès; Esteves, Typhaine; Muriel, Marie-Paule; El Hachimi, Khalid Hamid et al. (2011): Cellular distribution and subcellular localization of spatacsin and spastizin, two proteins involved in hereditary spastic paraplegia. In *Molecular and Cellular Neuroscience* 47 (3), pp. 191–202. DOI: 10.1016/j.mcn.2011.04.004.

Nakagomi, Saya; Barsoum, Mark J.; Bossy-Wetzel, Ella; Sütterlin, Christine; Malhotra, Vivek; Lipton, Stuart A. (2008): A Golgi fragmentation pathway in neurodegeneration. In *Neurobiology of disease* 29 (2), pp. 221–231. DOI: 10.1016/j.nbd.2007.08.015.

Nakamura, Shuhei; Yoshimori, Tamotsu (2017): New insights into autophagosome-lysosome fusion. In *Journal of cell science* 130 (7), pp. 1209–1216. DOI: 10.1242/jcs.196352.

Nishimura, Taki; Tooze, Sharon A. (2020): Emerging roles of ATG proteins and membrane lipids in autophagosome formation. In *Cell discovery* 6, p. 32. DOI: 10.1038/s41421-020-0161-3.

Pace, Raffaella de; Skirzewski, Miguel; Damme, Markus; Mattera, Rafael; Mercurio, Jeffrey; Foster, Arianne M. et al. (2018): Altered distribution of ATG9A and accumulation of axonal aggregates in neurons from a mouse model of AP-4 deficiency syndrome. In *PLoS genetics* 14 (4), e1007363. DOI: 10.1371/journal.pgen.1007363.

Pankiv, Serhiy; Alemu, Endalkachew A.; Brech, Andreas; Bruun, Jack-Ansgar; Lamark, Trond; Overvatn, Aud et al. (2010): FYCO1 is a Rab7 effector that binds to LC3 and PI3P to mediate microtubule plus end-directed vesicle transport. In *The Journal of cell biology* 188 (2), pp. 253–269. DOI: 10.1083/jcb.200907015.

Park, Sang Yoon; Guo, Xiaoli (2014): Adaptor protein complexes and intracellular transport. In *Bioscience reports* 34 (4). DOI: 10.1042/BSR20140069.

Parzych, Katherine R.; Klionsky, Daniel J. (2014): An overview of autophagy: morphology, mechanism, and regulation. In *Antioxidants & redox signaling* 20 (3), pp. 460–473. DOI: 10.1089/ars.2013.5371.

Pataer, Apar; Ozpolat, Bulent; Shao, RuPing; Cashman, Neil R.; Plotkin, Steven S.; Samuel, Charles E. et al. (2020): Therapeutic targeting of the PI4K2A/PKR lysosome network is critical for misfolded protein clearance and survival in cancer cells. In *Oncogene* 39 (4), pp. 801–813. DOI: 10.1038/s41388-019-1010-4.

Pendaries, Caroline; Tronchère, Hélène; Plantavid, Monique; Payrastre, Bernard (2003): Phosphoinositide signaling disorders in human diseases. In *FEBS letters* 546 (1), pp. 25–31. DOI: 10.1016/S0014-5793(03)00437-X.

Pensato, Viviana; Castellotti, Barbara; Gellera, Cinzia; Pareyson, Davide; Ciano, Claudia; Nanetti, Lorenzo et al. (2014): Overlapping phenotypes in complex spastic paraplegias SPG11, SPG15, SPG35 and SPG48. In *Brain : a journal of neurology* 137 (Pt 7), pp. 1907–1920. DOI: 10.1093/brain/awu121.

Pozner, Tatyana; Regensburger, Martin; Engelhorn, Tobias; Winkler, Jürgen; Winner, Beate (2020): Janus-faced spatacsin (SPG11): involvement in neurodevelopment and multisystem neurodegeneration. In *Brain : a journal of neurology* 143 (8), pp. 2369–2379. DOI: 10.1093/brain/awaa099.

Proikas-Cezanne, Tassula; Takacs, Zsuzsanna; Dönnes, Pierre; Kohlbacher, Oliver (2015): WIPI proteins: essential PtdIns3P effectors at the nascent autophagosome. In *Journal of cell science* 128 (2), pp. 207–217. DOI: 10.1242/jcs.146258.

Renvoisé, Benoît; Chang, Jaerak; Singh, Rajat; Yonekawa, Sayuri; FitzGibbon, Edmond J.; Mankodi, Ami et al. (2014): Lysosomal abnormalities in hereditary spastic paraplegia types SPG15 and SPG11. In *Annals of clinical and translational neurology* 1 (6), pp. 379–389. DOI: 10.1002/acn3.64.

Rong, Yueguang; Liu, Mei; Ma, Liang; Du, Wanqing; Zhang, Hanshuo; Tian, Yuan et al. (2012): Clathrin and phosphatidylinositol-4,5-bisphosphate regulate autophagic lysosome reformation. In *Nature cell biology* 14 (9), pp. 924–934. DOI: 10.1038/ncb2557.

Rong, Yueguang; McPhee, Christina K.; McPhee, Christina; Deng, Shuangshen; Huang, Lei; Chen, Lilian et al. (2011): Spinster is required for autophagic lysosome reformation and mTOR reactivation following starvation. In *Proceedings of the National Academy of Sciences of the United States of America* 108 (19), pp. 7826–7831. DOI: 10.1073/pnas.1013800108.

Roux, Kyle J.; Kim, Dae in; Burke, Brian; May, Danielle G. (2018): BioID: A Screen for Protein-Protein Interactions. In *Current protocols in protein science* 91, 19.23.1-19.23.15. DOI: 10.1002/cpps.51.

Ruano, Luis; Melo, Claudia; Silva, M. Carolina; Coutinho, Paula (2014): The global epidemiology of hereditary ataxia and spastic paraplegia: a systematic review of prevalence studies. In *Neuroepidemiology* 42 (3), pp. 174–183. DOI: 10.1159/000358801.

Rudge, Simon A.; Anderson, Deborah M.; Emr, Scott D. (2004): Vacuole size control: regulation of PtdIns(3,5)P2 levels by the vacuole-associated Vac14-Fig4 complex, a PtdIns(3,5)P2-specific phosphatase. In *Molecular biology of the cell* 15 (1), pp. 24–36. DOI: 10.1091/mbc.e03-05-0297.

Salazar, Gloria; Zlatic, Stephanie; Craige, Branch; Peden, Andrew A.; Pohl, Jan; Faundez, Victor (2009): Hermansky-Pudlak syndrome protein complexes associate with phosphatidylinositol 4-kinase type II alpha in neuronal and non-neuronal cells. In *The Journal of biological chemistry* 284 (3), pp. 1790–1802. DOI: 10.1074/jbc.M805991200.

Sánchez-Ferrero, Elena; Coto, Eliecer; Corao, Ana I.; Díaz, Marta; Gámez, Josep; Esteban, Jesús et al. (2012): Mitochondrial DNA polymorphisms/haplogroups in hereditary spastic paraplegia. In *Journal of neurology* 259 (2), pp. 246–250. DOI: 10.1007/s00415-011-6155-1.

Sanger, Anneri; Hirst, Jennifer; Davies, Alexandra K.; Robinson, Margaret S. (2019): Adaptor protein complexes and disease at a glance. In *Journal of cell science* 132 (20). DOI: 10.1242/jcs.222992.

Saxton, Robert A.; Sabatini, David M. (2017): mTOR Signaling in Growth, Metabolism, and Disease. In *Cell* 168 (6), pp. 960–976. DOI: 10.1016/j.cell.2017.02.004.

Schulze, Ryan J.; Weller, Shaun G.; Schroeder, Barbara; Krueger, Eugene W.; Chi, Susan; Casey, Carol A.; McNiven, Mark A. (2013): Lipid droplet breakdown requires dynamin 2 for vesiculation of autolysosomal tubules in hepatocytes. In *The Journal of cell biology* 203 (2), pp. 315–326. DOI: 10.1083/jcb.201306140.

Sengupta, Nivedita; Jović, Marko; Barnaeva, Elena; Kim, David W.; Hu, Xin; Southall, Noel et al. (2019): A large scale high-throughput screen identifies chemical inhibitors of phosphatidylinositol 4-kinase type II alpha. In *Journal of lipid research* 60 (3), pp. 683–693. DOI: 10.1194/jlr.D090159.

Shisheva, Assia (2012): PIKfyve and its Lipid products in health and in sickness. In *Current topics in microbiology and immunology* 362, pp. 127–162. DOI: 10.1007/978-94-007-5025-8_7.

Shribman, Samuel; Reid, Evan; Crosby, Andrew H.; Houlden, Henry; Warner, Thomas T. (2019): Hereditary spastic paraplegia: from diagnosis to emerging therapeutic approaches. In *The Lancet Neurology* 18 (12), pp. 1136–1146. DOI: 10.1016/S1474-4422(19)30235-2.

Simons, J. Paul; Al-Shawi, Raya; Minogue, Shane; Waugh, Mark G.; Wiedemann, Claudia; Evangelou, Stylianos et al. (2009): Loss of phosphatidylinositol 4-kinase 2alpha activity causes late onset degeneration of spinal cord axons. In *Proceedings of the National Academy of Sciences of the United States of America* 106 (28), pp. 11535–11539. DOI: 10.1073/pnas.0903011106.

Słabicki, Mikołaj; Theis, Mirko; Krastev, Dragomir B.; Samsonov, Sergey; Mundwiller, Emeline; Junqueira, Magno et al. (2010): A genome-scale DNA repair RNAi screen identifies SPG48 as a novel gene associated with hereditary spastic paraplegia. In *PLoS Biol* 8 (6), e1000408. DOI: 10.1371/journal.pbio.1000408.

Sridhar, Sunandini; Patel, Bindi; Aphkhazava, David; Macian, Fernando; Santambrogio, Laura; Shields, Dennis; Cuervo, Ana Maria (2013): The lipid kinase PI4KIIIβ preserves lysosomal identity. In *The EMBO journal* 32 (3), pp. 324–339. DOI: 10.1038/emboj.2012.341.

Stevanin, Giovanni; Azzedine, Hamid; Denora, Paola; Boukhris, Amir; Tazir, Meriem; Lossos, Alexander et al. (2008): Mutations in SPG11 are frequent in autosomal recessive spastic

paraplegia with thin corpus callosum, cognitive decline and lower motor neuron degeneration. In *Brain : a journal of neurology* 131 (Pt 3), pp. 772–784. DOI: 10.1093/brain/awm293.

Stieber, A.; Mourelatos, Z.; Gonatas, N. K. (1996): In Alzheimer's disease the Golgi apparatus of a population of neurons without neurofibrillary tangles is fragmented and atrophic. In *The American Journal of Pathology* 148 (2), pp. 415–426.

Suzuki, Hironori; Kaizuka, Takeshi; Mizushima, Noboru; Noda, Nobuo N. (2015): Structure of the Atg101-Atg13 complex reveals essential roles of Atg101 in autophagy initiation. In *Nature structural & molecular biology* 22 (7), pp. 572–580. DOI: 10.1038/nsmb.3036.

Takeshige, K.; Baba, M.; Tsuboi, S.; Noda, T.; Ohsumi, Y. (1992): Autophagy in yeast demonstrated with proteinase-deficient mutants and conditions for its induction. In *The Journal of cell biology* 119 (2), pp. 301–311. DOI: 10.1083/jcb.119.2.301.

Tanida, Isei; Ueno, Takashi; Kominami, Eiki (2004): LC3 conjugation system in mammalian autophagy. In *The international journal of biochemistry & cell biology* 36 (12), pp. 2503–2518. DOI: 10.1016/j.biocel.2004.05.009.

Vantaggiato, Chiara; Panzeri, Elena; Castelli, Marianna; Citterio, Andrea; Arnoldi, Alessia; Santorelli, Filippo Maria et al. (2019): ZFYVE26/SPASTIZIN and SPG11/SPATACSIN mutations in hereditary spastic paraplegia types AR-SPG15 and AR-SPG11 have different effects on autophagy and endocytosis. In *Autophagy* 15 (1), pp. 34–57. DOI: 10.1080/15548627.2018.1507438.

Varga, Rita-Eva; Khundadze, Mukhran; Damme, Markus; Nietzsche, Sandor; Hoffmann, Birgit; Stauber, Tobias et al. (2015): In Vivo Evidence for Lysosome Depletion and Impaired Autophagic Clearance in Hereditary Spastic Paraplegia Type SPG11. In *PLoS genetics* 11 (8), e1005454. DOI: 10.1371/journal.pgen.1005454.

Varnaitė, Renata; MacNeill, Stuart A. (2016): Meet the neighbors: Mapping local protein interactomes by proximity-dependent labeling with BioID. In *Proteomics* 16 (19), pp. 2503–2518. DOI: 10.1002/pmic.201600123.

Verny, Christophe; Guegen, Naig; Desquiret, Valerie; Chevrollier, Arnaud; Prundean, Adriana; Dubas, Frederic et al. (2011): Hereditary spastic paraplegia-like disorder due to a mitochondrial ATP6 gene point mutation. In *Mitochondrion* 11 (1), pp. 70–75. DOI: 10.1016/j.mito.2010.07.006.

Vicinanza, Mariella; Korolchuk, Viktor I.; Ashkenazi, Avraham; Puri, Claudia; Menzies, Fiona M.; Clarke, Jonathan H.; Rubinsztein, David C. (2015): PI(5)P regulates autophagosome biogenesis. In *Molecular cell* 57 (2), pp. 219–234. DOI: 10.1016/j.molcel.2014.12.007.

Wang, Hanzhi; Sun, Hui-Qiao; Zhu, Xiaohui; Zhang, Li; Albanesi, Joseph; Levine, Beth; Yin, Helen (2015): GABARAPs regulate PI4P-dependent autophagosome:lysosome fusion. In *Proceedings of the National Academy of Sciences of the United States of America* 112 (22), pp. 7015–7020. DOI: 10.1073/pnas.1507263112.

Wang, Ying Jie; Wang, Jing; Sun, Hui Qiao; Martinez, Manuel; Sun, Yu Xiao; Macia, Eric et al. (2003): Phosphatidylinositol 4 Phosphate Regulates Targeting of Clathrin Adaptor AP-1 Complexes to the Golgi. In *Cell* 114 (3), pp. 299–310. DOI: 10.1016/S0092-8674(03)00603-2.

Yu, Li; McPhee, Christina K.; Zheng, Lixin; Mardones, Gonzalo A.; Rong, Yueguang; Peng, Junya et al. (2010): Termination of autophagy and reformation of lysosomes regulated by mTOR. In *Nature* 465 (7300), pp. 942–946. DOI: 10.1038/nature09076.

Zhang, Jiqian; Zhou, Wei; Lin, Jun; Wei, Pengfei; Zhang, Yunjiao; Jin, Peipei et al. (2016): Autophagic lysosomal reformation depends on mTOR reactivation in H2O2-induced autophagy. In *The international journal of biochemistry & cell biology* 70, pp. 76–81. DOI: 10.1016/j.biocel.2015.11.009.

Zientara-Rytter, Katarzyna; Subramani, Suresh (2018): AIM/LIR-based fluorescent sensors-new tools to monitor mAtg8 functions. In *Autophagy* 14 (6), pp. 1074–1078. DOI: 10.1080/15548627.2018.1454238.

Zolov, Sergey N.; Bridges, Dave; Zhang, Yanling; Lee, Wei-Wei; Riehle, Ellen; Verma, Rakesh et al. (2012): In vivo, Pikfyve generates PI(3,5)P2, which serves as both a signaling lipid and the major precursor for PI5P. In *Proceedings of the National Academy of Sciences of the United States of America* 109 (43), pp. 17472–17477. DOI: 10.1073/pnas.1203106109.

8. Appendix

8.1 Own participation and co-authorship

A mouse model for SPG48 reveals a block of autophagic flux upon disruption of adaptor protein complex five

Mukhran Khundadze*, Federico Ribaudo, Adeela Hussain, Jan Rosentreter, Sandor Nietzsche, Melanie Thelen, Dominic Winter, Birgit Hoffmann, Muhammad Awais Afzal, Tanja Hermann, Cecilia de Heus, Eva-Maria Piskor, Christian Kosan, Patricia Franzka, Lisa von Kleist, Tobias Stauber, Judith Klumperman, Christian Kosan, Markus Damme, Tassula Proikas-Cezanne, Christian A. Hübner. Published in the journal **Neurobiology of Disease** 127 (2019) 419–431 (* first authorship)

Dr. rer. nat. M. Khundadze: western blotting, tissue sample preparation, immunohistochemistry/immunofluorescence, confocal microscope image acquisition and analyses, transfection of primary neurons, preparation of the manuscript (Fig. 1B-C, I-N; Fig. 2A-H, I-M; Fig. 3C-C''; Fig. 4 I-Q; Fig.6 H-J; Fig.7 D-H; Fig. S1 A-B', C-E).

M.Sc. F. Ribaudo: preparation of cells for different experimental procedures, transfection, immunocytochemistry, microscope image optimization and acquisition, live cell imaging establishment and image acquisition, quantification of confocal images and time lapses, data collection, statistical analyses, participation in the preparation of the manuscript (Fig 4 B-D, I-Q; Fig. 5C-H; Fig. 6 A-C, H-J; Fig. S1C-E; Fig. S2 A-D; Video S1 and S2).

M.Sc. A. Hussain: western blotting, beam walking test and statistical analyses (Fig. 1F-H; Fig. 4R; Fig. 5A-B; Fig. 7A-C; Fig. S2E).

M.Sc. J. Rosentreter: transfection, cell culture and samples preparation for FACS analysis (Fig.6E-G).

Dr. rer. nat. S. Nietzsche: Electron microscopy (Fig. 1I-N; Fig. 2I-J; Fig. 3C-C'''; Fig. S1A-B').

Dr. rer. nat. M. Thelen: Mass Spectrometry and support in the preparation of the final manuscript version (Fig. 4A; Table S1).

Dr. rer. nat. Winter: Mass Spectrometry and support in the preparation of the final manuscript version (Fig. 4A; Table S1).

Dr. rer. nat. B. Hoffmann: Confocal microscopy image acquisition and linear unmixing (Fig. 2A-H).

M.Sc. M.A. Afzal: Western blotting and statistical analyses (Fig. 6D).

M.Sc. T. Hermann: Morris water maze test (Fig 1D-E).

Ms. C. de Heus: Electron microscopy and analysis (Fig. 4 E-H).

M.Sc. EM. Piskor: FACS analysis (Fig 6E-G).

PD Dr. Christian Kosan: Providing the opportunity to perform FACS analyses.

Dr. rer. nat. P. Franzka: Contribution to the manuscript.

Dr. Lisa von Kleist: Lysosomal pH measurements, subject area discussions, revision and support in the preparation of the final manuscript version.

Prof. Dr. rer. nat. T. Stauber: Lysosomal pH measurements, subject area discussions, revision and support in the preparation of the final manuscript version.

Prof. Dr. rer. nat. J. Klumperman: Providing the opportunity to perform electron microscopy acquisition and analyses, subject area discussions, revision and support in the preparation of the final manuscript version.

PD Dr. rer. nat. M. Damme: Immunohistochemisty/immunofluorescence and subject area discussions, revision and support in the preparation of the final manuscript version (Fig. 3A-B', D-E'').

Prof. Dr. rer. nat. T. Proikas-Cezanne: Subject area discussions, revision and support in the preparation of the final manuscript version.

Prof. Dr. med. C. A. Hübner: Assignment of the subject area, providing the opportunity to work, providing the materials and equipment, professional supervision and discussions, revision and support in the preparation of the manuscript.

<div align="right">

_____

Prof. Dr. med. C. A. Hübner

</div>

Mouse models for hereditary spastic paraplegia uncover a role of PI4K2A in autophagic lysosome reformation

Khundadze M*, Ribaudo F*, Hussain A, Stahlberg H, Brocke-Ahmadinejad N, Franzka P, Varga RE, Zarkovic M, Pungsrinont T, Kokal M, Ganley IG, Beetz C, Sylvester M, Hübner CA. Published in the journal **Autophagy**, 2021 Mar 9:1-17 8 (* first authorship)

Dr. rer. nat. M. Khundadze: Planning and execution of experimental work in mice, tissue sample preparation, immunohistochemistry/immunofluorescence, confocal microscope images acquisition and analyses, BFP-PI4K2A cloning, preparation of the manuscript (Fig. 1C-R, I-N; Fig. 2A-G; Fig. 3C-M; Fig. 4 C-Eii; Fig. 5; Fig. 6A-Bii; Fig. S1; Fig. S2).

M.Sc. F. Ribaudo: preparation of cells for different experimental procedures, transfection for over-expression and KD, immunocytochemistry, microscope image optimization and acquisition, live cell imaging establishment and image acquisition, quantification of confocal images and time lapses, western blotting, RNA isolation and quantitative RT-PCR, flow cytometry, data collection, statistical analyses as well as participation in the preparation of the manuscript (Fig. 3C-M, N-R; Fig. 4C-Eii; Fig. 6A-I; Fig. 7; Fig. 8; Fig. S3; Fig S4; Fig. S5; Fig S6; Movie S1, S2, S3, S4 and S5).

M.Sc. A. Hussain: western blotting (Fig. 3A-B; Fig. 4F-G).

Bsc. H. Stahlberg: preparation of cells for different experimental procedures, transfection for KD, live cell imaging establishment and image acquisition, quantification of time lapses, western blotting, statistical analyses (Fig. 4F-G; Fig. 6A-Bii, J-N).

Dr. rer. nat. N. Brocke-Ahmadinejad: Mass Spectrometry analysis (Fig. 4 A-B; Table S1-S3).

Dr. rer. nat. P. Franzka: Contribution to the manuscript.

Dr. rer. nat. RE.Varga: Planning and execution of experimental work in mice, beam walking test, western blotting (Fig. 1A-Bi; Fig. 2H-I).

M.Sc. M. Zarkovic: Generation of dKO mouse line, western blotting (Fig. 2H-I).

M.Sc. T. Pungsrinont: Flow cytometry experiment and assistance during analyses (Fig. S4 B-C).

M.Sc. M. Kokal: Preparation of cells for different experimental procedures, transfection for over-expression, immunocytochemistry/immunofluorescence (Fig. 8A-Ci, E-Gi; Fig. S6A-Bii, D-Eii).

Dr. rer. nat. I. G. Ganley: Donation of cells U2-OS LAMP1-GFP, LAMP1-mCherry, LC3-mCherry and LAMP1-GFP, subject area discussions, revision and support in the preparation of the final manuscript version.

Dr. rer. nat. C. Beetz: Subject area discussions, revision and support in the preparation of the final manuscript version.

Dr. rer. nat. M. Sylvester: Mass Spectrometry analyes, subject area discussions, revision and support in the preparation of the final manuscript version (Fig. 4 A-B; Table S1-S3).

Prof. Dr. med. C. A. Hübner: Assignment of the subject area, providing the opportunity to work, providing the materials and equipment, professional supervision and discussions, revision and support in the preparation of the manuscript.

Prof. Dr. med. C. A. Hübner

8.2 Figure index

8.3 Ehrenwörtliche Erklärung

Hiermit erkläre ich, dass mir die Promotionsordnung der Medizinischen Fakultät der Friedrich-Schiller-Universität bekannt ist,

ich die Dissertation selbst angefertigt habe und alle von mir benutzten Hilfsmittel, persönlichen Mitteilungen und Quellen in meiner Arbeit angegeben sind,

mich folgende Personen bei der Auswahl und Auswertung des Materials sowie bei der Herstellung des Manuskripts unterstützt haben: Prof. Dr. med. Christian A. Hübner, M.Sc. Miriam Kokal, M.Sc. Thanakorn Pungsrinont, Dr. rer. nat. Susana Cubillos de Schmeer und alle Autoren, die bei der Publikation der Artikel geholfen haben.

die Hilfe eines Promotionsberaters nicht in Anspruch genommen wurde und dass Dritte weder unmittelbar noch mittelbar geldwerte Leistungen von mir für Arbeiten erhalten haben, die im Zusammenhang mit dem Inhalt der vorgelegten Dissertation stehen,

dass ich die Dissertation noch nicht als Prüfungsarbeit für eine staatliche oder andere wissenschaftliche Prüfung eingereicht habe und

dass ich die gleiche, eine in wesentlichen Teilen ähnliche oder eine andere Abhandlung nicht bei einer anderen Hochschule als Dissertation eingereicht habe.

Jena, 31.05.2021

Federico Ribaudo

8.4 Acknowledgement